Modeling climate change impacts on agricultural water demand and productivity

Modellierung von Klimawandelauswirkungen auf Wasserbedarf und Erträge in der Landwirtschaft

Zur Erlangung des Grades eines Doktors der Naturwissenschaften (Dr. rer. nat.)
Genehmigte Dissertation von Rike Becker, geboren in Duisburg

Tag der mündlichen Prüfung: 11.05.2021

Referent: Prof. Dr. Christoph Schüth
Korreferent: Prof. Dr. Ralf Merz
1. Prüfer: Dr. Stephan Schulz
2. Prüfer: Prof. Dr. Boris Lehmann
3. Prüfer: Prof. Dr. Andreas Henk

Darmstadt 2021 – D17

TECHNISCHE UNIVERSITÄT DARMSTADT

IAG Institut für Angewandte Geowissenschaften

Rike Becker

Dissertation
Modeling climate change impacts on agricultural water demand and productivity
Modellierung von Klimawandelauswirkungen auf Wasserbedarf und Erträge in der Landwirtschaft

Verteidigt am 11.05.2021

Veröffentlichungsjahr der Dissertation auf TUprints: 2021
URN der Dissertation: urn:nbn:de:tuda-tuprints-185864

Referent: Prof. Dr. Christoph Schüth
Korreferent: Prof. Dr. Ralf Merz
1. Prüfer: Dr. Stephan Schulz
2. Prüfer: Prof. Dr. Boris Lehmann
3. Prüfer: Prof. Dr. Andreas Henk

Dissertationsort: Technische Universität Darmstadt (D17)

Erklärung laut Promotionsordnung (Declaration of authorship)

§8 Abs. 1 lit. c PromO
Ich versichere hiermit, dass die elektronische Version meiner Dissertation mit der schriftlichen Version übereinstimmt.

§8 Abs. 1 lit. d PromO
Ich versichere hiermit, dass zu einem vorherigen Zeitpunkt noch keine Promotion versucht wurde. In diesem Fall sind nähere Angaben über Zeitpunkt, Hochschule, Dissertationsthema und Ergebnis dieses Versuchs mitzuteilen.

§9 Abs. 1 PromO
Ich versichere hiermit, dass die vorliegende Dissertation selbstständig und nur unter Verwendung der angegebenen Quellen verfasst wurde.

§9 Abs. 2 PromO
Die Arbeit hat bisher noch nicht zu Prüfungszwecken gedient.

Darmstadt, 25.03.2021

R. Becker

Short CV

Since 2020 — **Employee at the Water Management Association Emschergenossenschaft & Lippeverband, Essen**

Hydrometeorology and Flood Information System Group

2017 to 2020 — **Research scientist at IWW-Water Centre and PhD Student at Technical University of Darmstadt**

Department: Material and Earth Sciences, Institute of Applied Geosciences

PhD-thesis title: "Modeling climate change impacts on agricultural water demand and productivity"

2014 to 2017 — **Master student and teaching assistant at University of California, Los Angeles (UCLA)**

Studies: Civil & Environmental Engineering / Water Resources Engineering

Teaching: Field methods in hydrology and hydrological modeling

2013 to 2014 — **Scientific researcher at the Institute for Natural Resources and Development (ITT), Cologne University of Applied Sciences**

Research focus: Water resources management, capacity building in water sciences, water use efficiency in agricultural irrigation systems

2005 to 2012 — **Student at Eberhard Karls University of Tübingen**

Studies: Geography (Diplom)

Diploma-thesis title: "Water balance modeling to estimate the impact of land use changes on hydrological processes in the semi-arid central Chile"

Foreword

This thesis compiles the research I conducted during my time as a PhD candidate at the Technical University of Darmstadt and at the research institute IWW-Water Centre. During this time, I was a member of the "InoCottonGROW" research team, which was funded by the German Ministry of Education and Research (BMBF) and constituted of a project consortium of Universities, private companies and research institutions from Pakistan, Turkey and Germany. The overall project aim was the development of a tool to assess and to reduce the water footprint of the cotton-textile production chain, with regional focus on cotton production in Pakistan. My specific part in this project was the set-up of an agro-hydrological model to calculate local crop water demand, water consumption and water availability and assess climate change impacts on agricultural water demand and productivity. The particularities of our study region made this task more challenging than first anticipated, but the problems I was facing helped to derive interesting research questions which, step by step, formed the basis of my PhD research outlined in this manuscript.

All this work would not have been possible without the people who helped me throughout the course of my PhD with the computational and programming part, the development of my research questions, with understanding the local scientific and non-scientific peculiarities during the trips to Pakistan, and, finally and most importantly, with the moral support.

For the friendly help and support I got during the time in Pakistan I want to thank my Pakistani friends Muhammad Usman, Talha Mahmood and the academic staff and students at the University of Agriculture Faisalabad. I won't forget their welcoming attitudes. Furthermore, I particularly want to thank Stephan Schulz for his close guidance. His excellent scientific and moral support was a tremendous help throughout the entire PhD process. I also thank my supervisors and mentors Dr. Tim aus der Beek, Prof. Ralf Merz, and especially Prof. Christoph Schüth for the continuous support and the constructive and motivating comments on my work. Their time and willingness to give support whenever I needed their help and their readiness to hold regular online-meetings made it possible to finish the work even during the Corona-pandemic and under timely pressure. Furthermore, I thank the entire InoCottonGROW-Team, and especially Natalia Mikosh, Muhammad Usman, Lennart Schelter, Bernhard Tischbein and Frank-Andreas Weber for the close collaboration, the numerous discussions about our work, the exchange of research results and knowledge, and the adventurous trips to Pakistan we made together.

Finally, I want to thank my family, friends, and Akash who supported me throughout the PhD and always showed interest in my work. Even if they might have lost interest during my long explanations about what I was working on, they never let me feel it. Thank you all for listening!

Summary

Climate change and variability threatens the sustainability of future food production as well as the sustainability of water availability, especially in semi-arid regions where water resources are limited, and irrigated agriculture is widespread. Increasing temperatures will exacerbate evaporative losses and increase plant water needs. Consequently, higher irrigation intensities would be a logical measure to mitigate climate change impacts in these regions. But are increasing irrigation intensities truly the right adaption measure and can they help to reduce climate change induced agricultural production losses?

To address this question, this PhD thesis investigates climate change impacts on agricultural productivity as well as changes in agricultural water demand. The study area, where the research is conducted, encompasses the intensively irrigated region of the Lower Chenab Canal System in Pakistan (15 000 km^2), which is part of the Indus River irrigation system, the largest irrigation system in the world; and covers economically important crop growing areas.

Two processed-based numerical models are used to simulate the effects of potential future climate scenarios on the agricultural system – the agro-hydrological Soil & Water Assessment tool (SWAT) and the biophysical Agricultural Production Systems Simulator (APSIM). The unique characteristics of the study area, with complex and highly diverse agricultural practices, as well as a nearly entirely human controlled hydrology require alternative ways of model calibration, validation, and uncertainty analysis. A central part of this thesis is therefore devoted to the complex procedure of setting up and calibrating an agro-hydrological model in this heterogeneous environment, which is done using satellite evaporation data. Furthermore, it is shown, how a framework can be developed which combines field observations and numerical modeling to acquire data of important water balance parameters, without the need of detailed input data set. This framework could be used to generate data for validating hydrological models in data-scarce regions and for highly managed environments, like the one selected for this research.

Finally, the calibrated and validated models are used to answer the central question of future climate change impacts. The results of this thesis reveal that agricultural productivity is highly affected by climate change and productivity levels are projected to decrease significantly. It could furthermore be shown that an intensification of irrigation might fail as a measure to counteract climate change, due to severe negative impacts of temperature stress on plant growth. To mitigate climate change impacts, the reductions of crop heat stress should therefore be prioritized in near future, while a more sustainable water management is unquestionable to continue to fulfill the high water demands in the long-term future.

Table of contents

List of figures

List of tables

Abbreviations

APSIM	Agricultural Production Systems Simulator
°C	Degree centigrade
CMORPH	Climate Prediction Centre morphing technique (= satellite precipitation product)
CORDEX	Coordinated Downscaling Experiment
DDS	Dynamically Dimensioned Search Algorithm
ET	Evapotranspiration
ET_{act}	Actual Evapotranspiration
ET_c	Crop specific Evaporanspiration (= ET_{ref} x K_c)
ET_p	Potential Evapotranspiration
ET_{ref}	Reference Evapotranspiration
Fig.	Figure
GCM	Global Climate Model
GWR	Ground water recharge
HRU	Hydrological Response Unit
IPCC	Intergovernmental Panel on Climate Change
K_c	Crop coefficient
KGE	Kling-Gupta Efficiency
LAI	Leaf Area Index
LCC	Lower Chenab Canal (Study area in Punjab, Pakistan)
RCM	Regional Climate Model
RCP	Representative Concentration Pathway (Climate change scenario)
SEBAL	Surface Energy Balance Algorithm
SWAT	Soil & Water Assessment Tool
Tab.	Table
TRMM	Tropical Rainfall Measuring Mission (satellite precipitation data)

1 Introduction

1.1 Background and relevance of the study

In recent years, climate change and its impact on the environment have become one of the main concerns worldwide. Especially, its effect on agricultural systems has become a major problem, considering the alarming global developments regarding water and food security (Hanjra and Qureshi, 2010; Schewe et al., 2014). The latest special report of the UN Intergovernmental Panel on Climate Change (IPCC 2019) predicts, with high confidence, that future changes in climatic conditions will exacerbate existing water and food shortages for billions of people. One of the main reasons considered responsible for the expected food shortage is the inability to meet future agricultural water demands (Fader et al., 2016). Globally, irrigation volumes have more than doubled since the 1960s (IPCC 2019) and are likely to increase further due to climate change in regions with already limited water supply (Wada et al., 2013; Wang et al., 2016).

In semi-arid and developing regions like Pakistan, agriculture is the most important economic sector, employing nearly half of the population (Qureshi, 2011). A large part of agricultural workers are small scale farmers, highly dependent on maintaining their productivity levels and becoming increasingly vulnerable to climate change impacts and potential losses of income (Oxfam, 2009). At the same time agricultural activities demand over 90% of the country's fresh water resources (Fischer et al., 2007). The projected increase in water scarcity, due to climate change along with the increasing demand of the fast-growing population, poses a severe threat to the national food supply and to the productivity of economically important cash crops such cotton, maize and rice (Khan et al., 2016; Qureshi, 2011; Schewe et al., 2014).

The Long-Term Climate Risk Index 2019 (Eckstein et al., 2018), which indicates a level of exposure and vulnerability to extreme climate events, ranks Pakistan amongst the 10 most affected countries (Fig. 1-1). In addition, as part of the Indus river basin irrigation system, which is primarily fed by glacier and snow melt from the Himalayan mountains, the study area is considered a hot spot for the impact of climate change on water availability and agricultural productivity, as it constitutes one of the world's largest irrigation areas highly dependent on water resources from outside the area (i.e. from the upper Indus basin). Climate change impacts in the Himalaya mountains, the head waters of the Indus river and its main tributaries like the Chenab river, will therefore be amongst the main controlling factor of the downstream water availability (Immerzeel et al., 2010) (Fig. 2-1). Yet, it is still highly uncertain in how far climate change will affect water availability and demand.

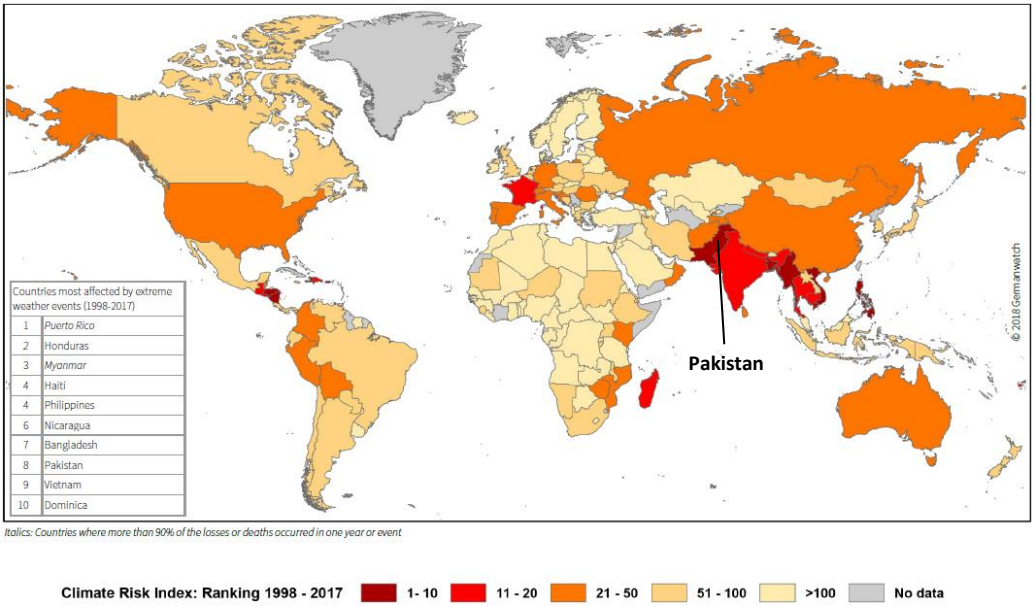

Fig. 1-1: Global climate risk index ranking (Source: Germanwatch e.V.; Eckstein et al., 2018)

Studies on the current behavior of Himalayan glaciers, show on average a glacier retreat and a loss in glacier mass balances (Bolch, 2019; Kulkarni and Karyakarte, 2014). Even though there is still a high uncertainty about future glacier dynamics in the upper Indus basin, modeling studies project a reduction in ice volume of 40% to more than 60% by 2100 (Bolch, 2019). Increasing glacier melt is expected to lead to increasing runoff rates, until their “peak water” is reached by approx. 2050 - 2070 (Huss and Hock, 2018; Lutz et al., 2014), and later to a subsequent decrease. The extreme glacier-melt-dependency of the entire LCC irrigation system depicts its high vulnerability to future hydrometeorological dynamics in the upper catchments, which will have long term impacts on the downstream hydrology.

Next to the uncertainty of water availability, climate change is significantly impacting local temperatures in the study area. The research done in the scope of this thesis (chapter 6), as well as Saeed and Athar (2018) estimate a mean increase in temperature of approx. + 1.6 °C until 2050. Extreme temperatures, especially during the already hot summer months (> 35 °C Jun/Jul, Fig. 1-2) which coincide with the main growing period of cash crops, will pose a severe stress on plant productivity in this region (Ullah, 2017). Lobell and Burke (2008) point out that sensitivities of crops to changes in temperature can be higher than their sensitivities to changes in water availability. Temperature induced stress on agricultural productivity might therefore be the crucial factor in limiting future agricultural yields in the study region.

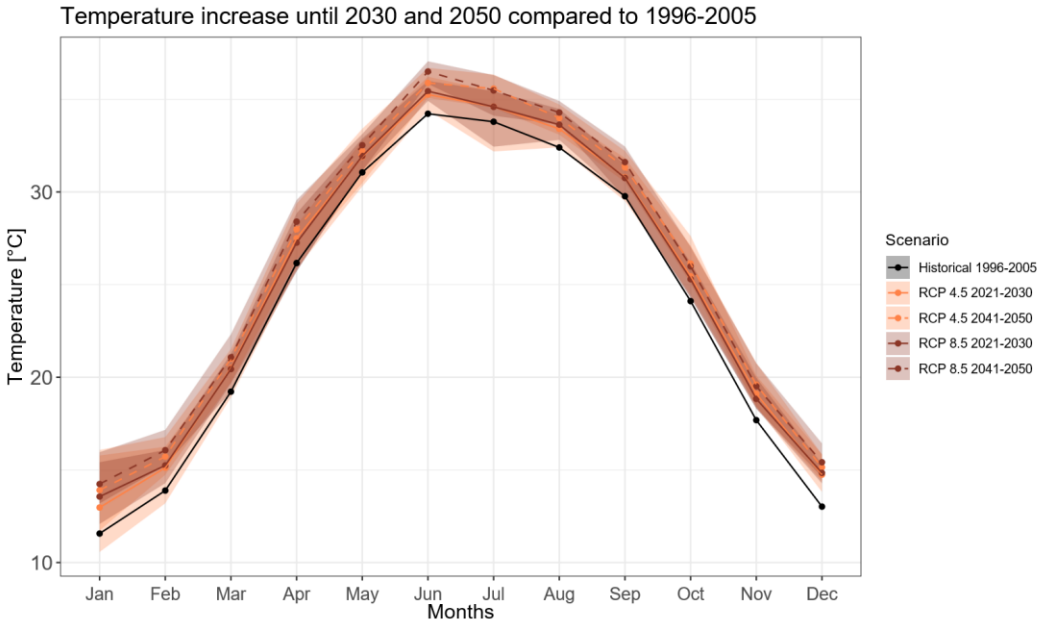

Fig. 1-2: Projected average monthly temperature increases under RCP 4.5 and RCP 8.5 for 2021-2030 and 2041-2050 for the study region. Black line represents the historical period 1996-2006.

Considering these developments regarding water resources availability and temperature trends, it is therefore imperative to understand the role of environmental stresses on crop growth and resulting plant water demand, in connection to water stress. Furthermore, improved knowledge about possible impacts of temperature and water stress as well as their interlinkages on future crop growth will help defining adequate adaptation strategies. In terms of adequate water availability for crop growths, especially in semi-arid regions, previous studies highlight that there is still very limited understanding of the potentials and limits of irrigation related climate change adaptation (Tack et al., 2017; Taraz, 2018); and that more research is needed to disentangle the effects of temperature and water stress related climate change impacts on agricultural yields (Carter *et al* 2016).

The overarching aim of this thesis is therefore to investigate the impact of climate change induced heat and water stress on agricultural water demand and productivity in the study area of the Lower Chenab Irrigation System.

1.2 Research objective & research questions

Under the above-described circumstances the quantification of future water resources and the potential impact of climate change becomes more and more important. Local and detailed quantitative information on water demand and availability as well as information about future changes of the

hydrological system could help to better understand potential future risks related to water demand and agricultural productivity. Yet, the more complex a system is, the bigger the challenge to get reliable estimates of single process variables such as inflow, soil water storage, evapotranspiration, percolation rates, surface runoff or groundwater recharge. In this context, hydrological models can be useful tools to simulate multi-faceted systems and the complex interactions of various water balance parameters.

The assurance of a reliable model performance in the study area of the Lower Chenab Canal System is a difficult task, as the region is characterized by complex and highly diverse agricultural practices, as well as a nearly entirely human controlled hydrology (i.e., intensive irrigated agriculture without any natural river network; Awan et al., 2016). In combination with sparse data availability for model calibration and validation, it becomes a challenging undertaking to adequately implement hydrological and bio-physical models in this region. Common methods of model calibration, validation, and uncertainty analysis, where natural hydrological response variables are used to assess model performance, cannot be applied and alternative approaches must be found.

Furthermore, focusing on climate change impacts and especially on the effects of temperature and water stress on agricultural productivity, reveals the importance of model uncertainty, not only with respect to model parameterization but also with respect to model structure. As (Jin et al., 2016) show in a model comparison study for maize crops, model structural differences show significantly different results in the response of plant productivity to stress factors such as heat and water stress.

To assure a sound modeling study, which accounts for the described difficulties in model parametrization in a complex agricultural area and model structural uncertainty with respect to heat and water stress, a strong focus is laid on the methodological part of the modelling process. The first research objective of this thesis is therefore a careful model set-up, calibration, and validation of the applied SWAT (Soil & Water Assessment Tool) model.

Research questions which are directing this first research objective are:

- How can an agro-hydrological model be set-up, calibrated and validated, ensuring the representation of the small-scale heterogeneity and physical correctness of hydrological processes, in a highly human impacted environment?
- Can a framework be developed which can help to acquire data of important water balance parameters without the need of detailed input data set and which can be used to validate the set-up of hydrological models?

The first question is addressed in chapter 4, which deals with the challenging set-up and complex calibration of the SWAT (Soil & Water Assessment Tool)-model in the entirely human controlled

irrigation system of the LCC study area. It presents an alternative way of calibrating a hydrological model using remotely sensed evapotranspiration (ET) data. Advantages and challenges of this approach are discussed.

The second question is tackled in chapter 5, which presents how the collection of field data combined with a modeling approach using the model Hydrus 1-D, can help to get reliable ET estimates. Evapotranspiration data obtained by this approach can be used as validation data in ungauged sites, such as the one selected for this thesis. Here it should be mentioned that the work for this part of the thesis was undertaken with substantial support from Dr. Stephan Schulz. He assisted in the process of the field campaign and took the lead for the work described in chapter 5 and for the publication, which resulted from this work (see Schulz et al., 2021).

Only after this careful model set-up, calibration and validation the second research objective can be addressed, which is the application of two models to assess climate change impacts on future agricultural water demand and productivity as well as the evaluation of their different results with respect to model structural differences.

Central research questions directing the second objective are:

- How are agricultural water demand and productivity expected to change in future? Which conclusion can be drawn for a more sustainable future water management and productivity in this region?
- How are structural model differences impacting the simulated yield response to changes in climate variables?

In chapter 6, the SWAT model as well as the Agricultural Production System Model (APSIM) are applied to get answers to the question how climate change will impact future agricultural water demand and agricultural productivity.

2 Study Area

2.1 The Lower Chenab Canal System (LCC-System) in Punjab, Pakistan

The study area is located in the Lower Chenab Canal System Area (LCC) in Pakistan, which comprises about 15,000 km^2 of agricultural land and which is located on the floodplains between the rivers Chenab in the north and river Ravi in the south of the study area (Fig. 2-1).

According to Köppen-Geiger, the climate in the Punjab region is classified as hot arid (Kottek et al., 2006). Annual potential evaporation, more than three times larger than annual precipitation (approx. 1800 mm potential evaporation vs. approx. 500 mm rainfall), show a strong demand for additional water supply for irrigation. The annual distribution of precipitation is characterized by monsoonal rain events during summer months (July-August), accounting for approx. 75% of the annual total rainfall (Awan and Ismaeel, 2014) and leaving the remaining months of the year with limited water resources for rain-fed irrigation.

River Chenab is the main source for irrigation water supply in this area, receiving its waters from the glacierized headwaters in the Himalaya mountains. This makes the region highly dependent on water resources extracted from sources outside of the study area as well as highly vulnerable with respect to climate change (see introduction section and Immerzeel et al., 2010).

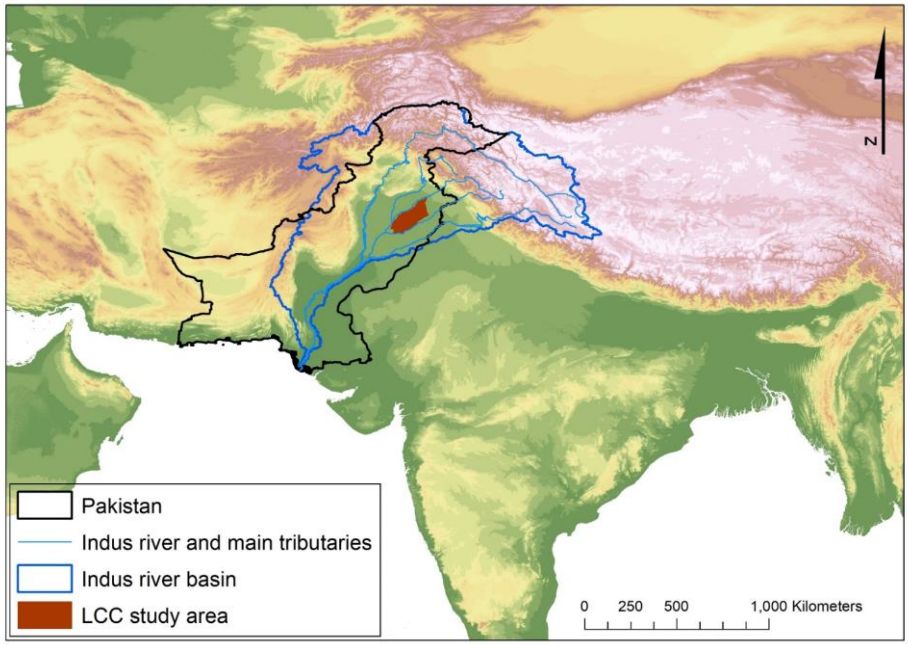

Fig. 2-1: Study Area: Lower Chenab Canal Area (LCC, in red) within the Indus river basin in Pakistan

To guarantee irrigation water supply throughout the year, the study area receives water through the Indus Basin Irrigation System (IBIS), the world largest irrigation system. The entire hydrological system of the LCC area is artificially built and managed to supply the necessary irrigation water (Fig. 2-2). Irrigation channels are the only water courses in the study area and no further natural streams exist. The channel discharge is exclusively determined by management decisions, following formal local policies as well as informal local agreements. These sometimes subjective and therefore often unpredictable decisions on water channel flows might interfere with, or even supersede, the natural behavior of the hydrological system. This makes it extremely challenging to set up a hydrological model, which is usually driven by the "natural" responses and interplay of water balance components (e.g., the reaction of discharge to changes in precipitation).

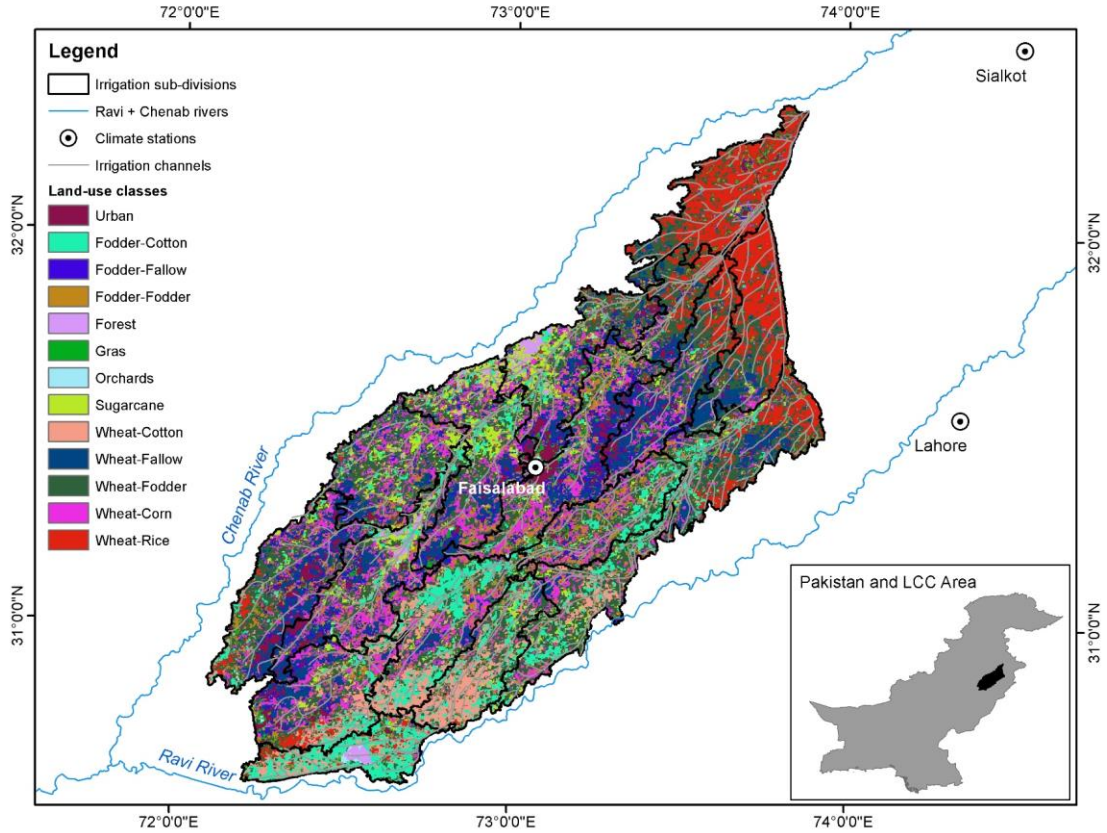

Fig. 2-2: Spatial distribution of land-use classes and crop rotation patterns in the study area. The dense irrigation channel network is displayed in light grey.

In theory, the scheduling of irrigation in the LCC area, follows the stringent local "Warabandi" irrigation scheme with fixed water allocation schedules (Qureshi and Hussain, 1994). However, this stringent system is sometimes relaxed by using alternative sources such as groundwater pumping and on-site irrigation water storage (Qureshi et al., 2010), which helps to achieve a more plant demand-oriented

irrigation. On the other hand this also leads to an increasing exploitation of local groundwater resources (Habib, 2004).

During dry winter season (Rabi) the dominating crop type grown in the study area is winter wheat while during the wetter summer (Kharif) the crop pattern diversifies and mainly cotton, maize, rice and fodder are grown on small scale farm plots (Fig. 2-3). In the first part of the paper the entire ensemble of land-use classes shown in figure 2-2 is used to parameterize the agro-hydrological model, while the second part of the study focusses on climate change impacts on cotton, maize, and rice crops, as these are central cash crop types in this region. Knowing about potential negative impacts on the productivity of these crop types is therefore of paramount economic importance for this region.

Fig. 2-3: Typical small scale farm plots in the study region (close to Faisalabad city) on the plains between river Chenab and river Ravi, in Punjab, Pakistan (picture R. Becker).

3 Methods and Data

Detailed descriptions of the specific methods applied for the three main research fields of this thesis can be found in the separate method sections in the respective chapters (chapters 4, 5 and 6). The method section in chapter 4 outlines in detail the setup of the hydrological model and the complex process of model calibration using remote sensing evapotranspiration data. Chapter 5 elaborates on the establishment of a framework to acquire data for important water balance components for model validation, and chapter 6 describes the methods of applying an ensemble of a hydrological model (SWAT) and a biophysical crop model (APSIM) and the assessment of model structural differences.

The principal methods, models and data sets used for the studies are briefly outlined below.

3.1 SWAT model

General overview

In the first part of this research, the physically-based and spatially distributed agro-hydrological SWAT model (Soil & Water Assessment Tool, Arnold et al., 2012) is setup and thoroughly calibrated. The hydrological model SWAT simulates the quantity and quality of water flow within catchments, incorporates detailed management strategies (e.g. irrigation schedule, planting schedule) and basic plant physiognomic stages, e.g. root development, leaf area development, biomass change (Arnold et al., 2012; Gassman et al., 2014). The main underlying principle for the simulation of water fluxes is the water balance equation (Neitsch et al., 2009). By accounting for spatially distributed environmental changes, it simulates their effects on individual water balance components. Its strengths are therefore the closing of the hydrological cycle and the detection of spatially distributed changes in water availability and demand.

Main reasons for the selection of SWAT for this study are its capabilities to incorporate detailed management strategies such as irrigation scheduling and efficiency, planting schedule and plant physiognomy, and to account for spatially distributed land-use and management changes and their effects on single water balance components. Principal processes simulated by SWAT and APSIM are displayed in figure 3-1. Processes which are studied in more detail in the scope of this thesis are highlighted in bold and italic letters.

To adequately calibrate the SWAT model, an automated and spatially distributed model calibration approach is applied, implementing the global Dynamically Dimensioned Search Algorithm (DDS, Tolson and Shoemaker, 2007). To account for the spatio-temporal heterogeneity of water balance

fluxes in the calibration process, remote sensing-derived evapotranspiration (ET) estimates are used as observational data set. The remote sensing ET data is taken from (Usman et al., 2015a), who derived monthly ET data for the study area based on the Surface Energy Balance Algorithm (SEBAL), developed by (Bastiaanssen et al., 1998a). Model parameters are adjusted based on the fit between SWAT and SEBAL ET values using Kling-Gupta Efficiency (KGE) as objective function. Reasons for the limitations and challenges of this approach are discussed in chapter 4.

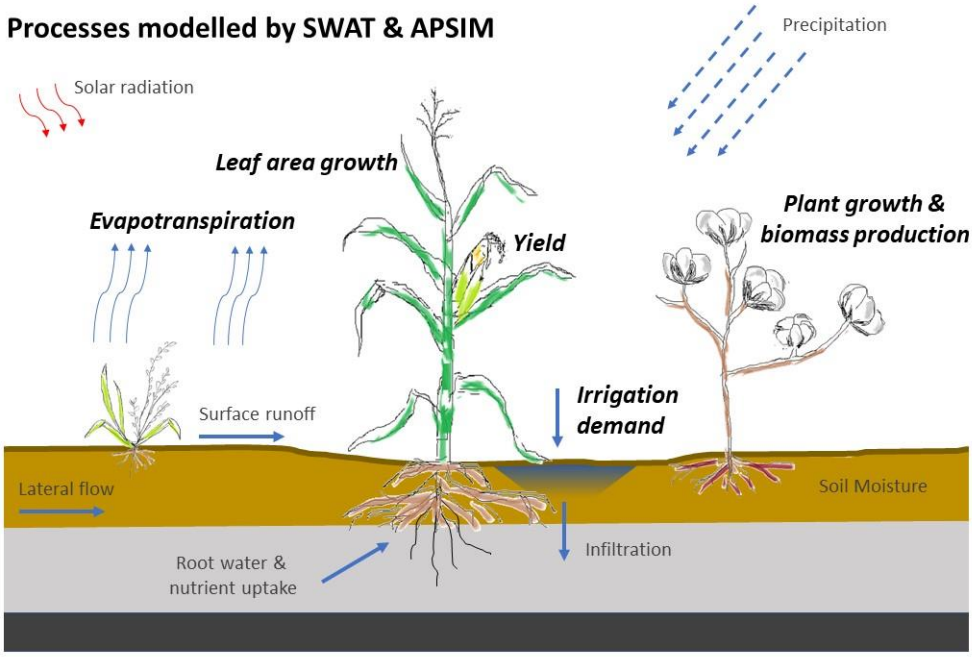

Fig. 3-1: Schematic representation of principal processes modelled with SWAT and APSIM. Processes which are evaluated in more detail in this thesis are highlighted in bold and italic letters.

Model structural characteristics

To better understand the differences between the two models (i.e., SWAT and APSIM) which are discussed in detail in chapter 6, structural characteristics of central variable estimations are outlined here (for APSIM see the next subchapter). In the following an example of important model equations is shown, which reveal discrepancies in their reaction to environmental stress variables (e.g., heat and water stress). Differences in the results of the two models with respect to climatic changes (e.g., increasing temperatures = increasing heat stress), can therefore be ascribed, to the following structural model inconsistencies.

Potential biomass production (biom) calculated in SWAT is based on plant specific radiation-use efficiency (RUE), which defines the conversion of intercepted light at the leaf surface into biomass, and the amount of intercepted light available for photosythesis ($H_{photosyn}$).

$$\Delta biom = RUE * H_{photosyn} \quad (1)$$

While the radiation-use efficiency itself is assumed to be independent of the plant growth stage, the amount of intercepted light depends on the plant leaf area development (Neitsch et al 2009).

$$H_{photosyn} = 0.5 * H_{day} * (1 - \exp(-k_l * LAI_{act}) \quad (2)$$

With H_{day} being the incident total solar radiation, k_l being the light extinction coefficient and LAI being the leaf area index.

The leaf area index, which controls the amount of intercepted light, is simulated dynamically based on the concept of potential heat units (PHUs). The heat unit theory assumes plant specific temperature requirements for the different phenological stages of plant maturation, denominated as “heat units”, or more commonly known as “growing degree days”. Heat units are accumulated over time and control the leaf and plant growth until a maximum LAI and plant maturity is reached, after which leaf senescence begins and LAI declines.

To estimate the actual plant growth, the actual LAI (LAI_{act}) and the actual biomass growth ($biom_{act}$) are reduced according to the stress experienced by plants due to extreme temperature stress (tstrs). Water stress (wstrs) and nutrient stresses (nstrs and pstrs) are reduced to a minimum in the study by assuring constant irrigation and sufficient fertilization.

$$\Delta LAI_{act} = \Delta LAI * \sqrt{(1 - \max(wstrs, tstrs, nstrs, pstrs))} \quad (3)$$

$$\Delta biom_{act} = \Delta biom * (1 - \max(wstrs, tstrs, nstrs, pstrs)) \quad (4)$$

Finally, yield is estimated in SWAT by multiplying the actual biomass, produced at the time of harvest, by a plant specific harvest index (HI).

$$Yield = biom_{act} * HI_{act} \quad (5)$$

The harvest index depends on the fraction of accumulated potential heat units (fr_{PHU}) and is defined as

$$HI = HI_{opt} \left(\frac{100 * fr_{PHU}}{100 * fr_{PHU} + \exp[11.1 - 10 * fr_{PHU}]} \right). \quad (6)$$

The actual harvest index (HI_{act} in eqn. 5) is a reduced HI, depending on the impact of water deficit stresses. In this study water deficit is close to zero and HI = HI_{act}, due to constant and demand-based irrigation. Optimal harvest indices (HI_{opt}) used in this study are 40% for cotton and 50% for maize and rice, according to Awan et al., (2016).

This procedure shows that SWAT simulations of leaf area development, biomass and ultimately yield production are highly dependent on one single dominating environmental stress factor. In this study this results in a strong sensitivity of plant productivity to temperature stress, which leads to significant reductions of LAI, biomass and yield with increasing temperatures.

3.2 APSIM model

General overview

The Agricultural Production System Simulator (APSIM; Holzworth et al., 2014) is a biophysical crop modelling framework which simulates agricultural crop dynamics with respect to varying climatic and environmental conditions. It has been used extensively to assess climate change impacts on agricultural productivity (e.g. Deihimfard et al., 2018; Liu et al., 2013; Williams et al., 2015). Model performance and applications are studied in depths within the scope of the Agricultural Modelling Intercomparison and Improvement Project (AgMIP; Rosenzweig et al., 2014), in which the APSIM model was applied in the same study region of southern Punjab to assess climate change impact on crop production. Focus and strength of the APSIM framework is the plant-specific simulation of biophysical dynamics with respect to changes in the environment. Due to its modular approach, with individual sub-models for each crop type, it can account for plant specific reactions to climate change. It uses the Ozcot Model for cotton simulations (Hearn, 1994), the CERES-based maize model for maize simulations (Jones and Kiniry, 1986) and the Oryza2000 model for rice simulations (Bouman et al., 2001). Each model accounts for crop specific physiologies such as plant phenology, photosynthesis, plant stresses, nutrient cycling and carbon allocation.

Model structural characteristics

The main difference to SWAT is the strength in accounting for detailed bio-physical processes. The cotton model for example, includes a plant respiration factor (Resp) in the photosynthesis calculation (adopted from Hearn 1994).

$$H_{photosyn} = 2.391 + H_{day}\left(1.374 - \left(0.0005415 H_{day}\right)\right) * (1 - \exp(-k_l * LAI)) - Resp \quad (7)$$

The respiration factor is affected by temperature and water stress. Thus, the photosynthesis and carbon assimilation part already account for the direct impact of stress factors and not only indirectly through LAI (eqn. 2). The maize model uses a similar concept to SWAT for the estimation of the light driven biomass production but directly includes temperature, phosphorus, and nitrogen stresses into the calculation (adopted from Jin et al 2016).

$$\Delta biom = H_{day} * RUE * \min\{wstrs, tstrs, nstrs, pstr\} \quad (8)$$

Accounting for all stresses (i.e., water, temperature, and nutrients) in different phenological stages, makes the APSIM models less sensitive to one single dominating stress (= temperature stress in SWAT). Yet, some stages are lacking the impact of temperature stress, which might lead to an overestimation of plant productivity in environments, where temperature stress is high while the remaining stresses are low. The cotton model for example does not account for heat stress in the initial parts of leaf area development. In the leaf area formation, temperature stress is not considered until the first square event. After the first square event, it is indirectly included through vapor pressure deficit (VPD).

$$\Delta LAI_{act} = \sqrt{0.1847} - 0.1165 * SMI - 1.514 * VPD + 1.984 * SMI * VPD \quad (9)$$

When the soil moisture index (SMI) and VPD are low (as in the case of the intensively irrigated and from monsoon rainfall impacted region), LAI development will hardly be affected by environmental stresses. This is one reason for the strong differences between SWAT and APSIM results regarding their LAI estimations.

Yield estimations of the APSIM models are based on crop specific fruiting dynamics rather than on the more stringent harvest index (HI) method used in SWAT. Yield is estimated based on grain number and grain filling (maize and rice) or ball growth rates (cotton), which makes it less dependent on LAI and dry matter production. This explains, why yield declines are projected even under strengthening leaf area development.

By comparing both models, model strengths and weaknesses as well as the effect of main structural differences between the two models are analyzed (see chapter 6).

3.3 Climate data - data sources and pre-processing steps

Historical climate data

For the assessment of past and future climate condition CFSR data (Climate Forecast System Reanalysis; Saha et al., 2010) is taken as historical reference climate data for a baseline period, from 1996-2005. The product offers historical climate data on a 0.25° x 0.25° grid. To ensure the accuracy of the baseline data set, the CFSR data is bias-corrected using climate records of three available local climate stations, located in and in close proximity to the study area (namely: Faisalabad, Lahore and Sialkot, see Fig. 2-2). Non-parametric quantile mapping is used as statistical fitting method between observed and simulated data over the entire available period 1979-2014. The bias correction is conducted using the R-package "Qmap" (Gudmundsson et al., 2012).

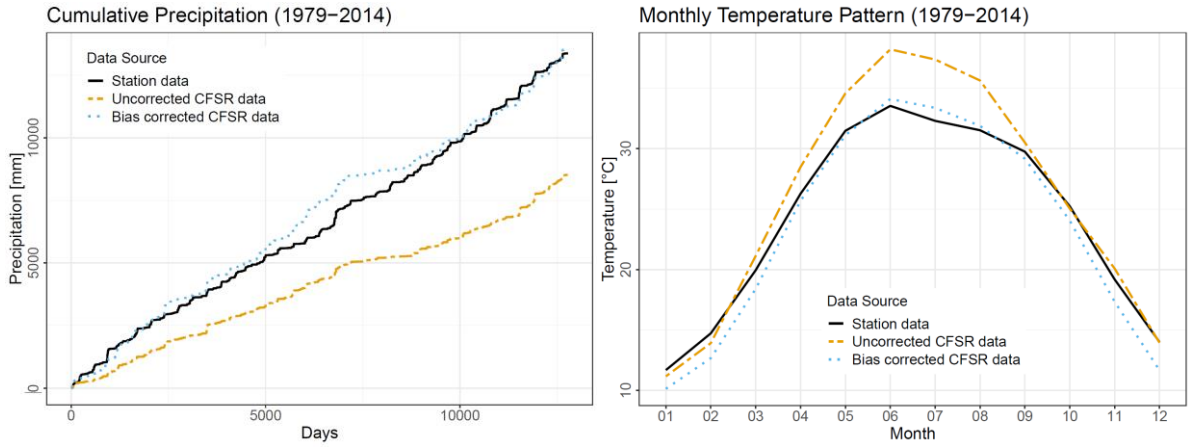

Fig. 3-2: Results of bias correction procedure. Station data vs. uncorrected and bias-corrected CFSR data

Figure 3-2 shows the fit of the reanalysis data before and after the bias correction, for precipitation and mean temperature. It shows that the bias correction procedure was successful in removing the negative bias of original CFSR precipitation data as well as the positive bias of summer temperatures. Winter temperatures are "over corrected" and are now slightly underestimating temperatures from November until March. As the study focuses on climate impacts during the summer period (May-October), where a clear improvement of the fit between observed and bias corrected CFSR data can be achieved, these results are accepted as such, despite the winter-deviation from the observed data.

The same correction procedure (i.e., quantile mapping) is used to correct the remaining climate variables, namely relative humidity, solar radiation and windspeed, which are used by SWAT to calculate evapotranspiration rates according to Penman-Monteith (results not shown).

Data of future climate projections

Data for the climate change assessment is taken from the Coordinated Regional Climate Downscaling Experiment (CORDEX; www.cordex.org), which provides a suite of regional climate projections based on Global Climate Models of the Coupled Model Intercomparison Project, Phase 5 (CMIP5; Taylor et al., 2012). The scenarios are based on the IPCC RCP scenarios 4.5 and 8.5 and are used to assess possible climate trends until 2050.

First, daily CORDEX climate projections, of 15 climate models of the South-Asian CORDEX domain, at a resolution of 0.44° x 0.44° are selected (for specific model names see Fig. 3-3). CORDEX hindcast data of the same 15 GCM-RCM model combinations, is used to test the fit of CORDEX model outputs with the chosen baseline climate data from the CFSR-data set. Here, the maximum overlapping period of the data products (1979-2005) is used to test their agreement. The performance of single CORDEX GCM-RCM combinations with respect to the baseline climate data is displayed in Figure 3-3, which shows their goodness of fit in terms of standard deviation, correlation and RMSE, with respect to each climate variable (i.e., precipitation, temperature, solar radiation, relative humidity, and wind speed).

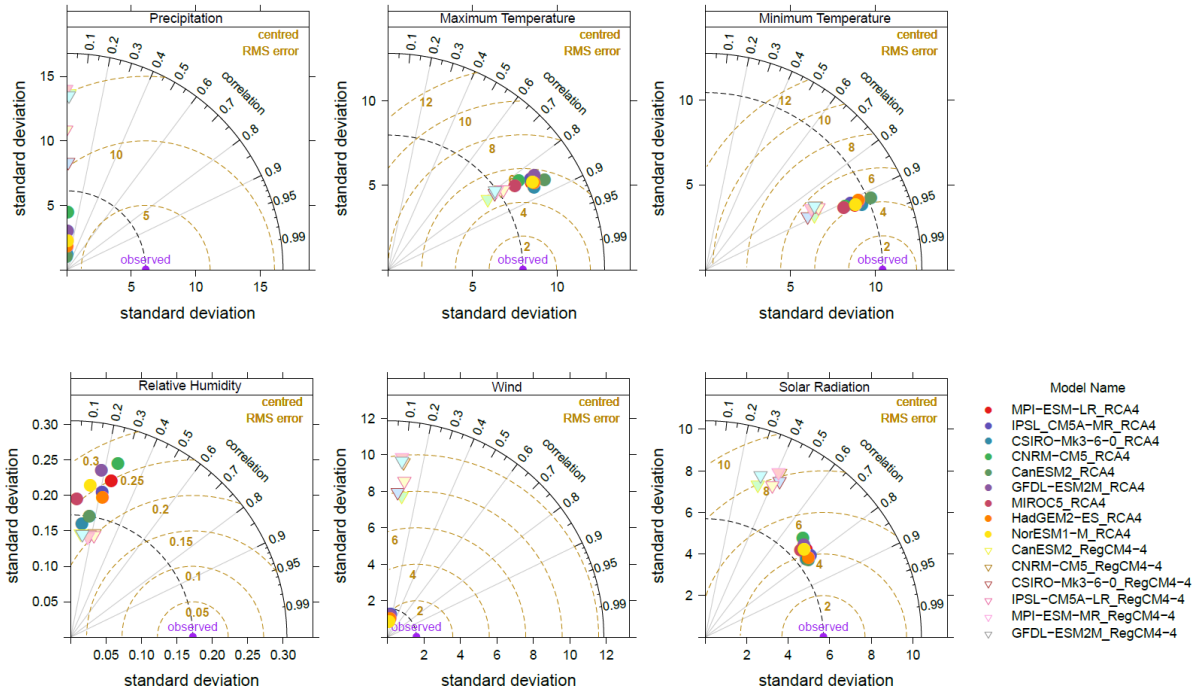

Fig. 3-3: Goodness-of-Fit between CFSR Reanalysis Data (observed) and CORDEX GCM-RCM models (triangles and points), showing correlation, RMSE and standard deviation as goodness-of-fit measures.

The unsatisfactory performance of all models which employ the Regional Climate Model "RegCM4-4" for downscaling purposes (Figure 3-3, triangles), leads to the exclusion of these models. Based on the

goodness of fit between CORDEX and CFSR data, the data sets of all 9 models which use "RCA4" Regional Climate Models for downscaling (Figure 3-3, points) are selected.

To minimize any further bias, which the data sets of 9 selected RCMs still present, a commonly used linear scaling correction approach (Teutschbein and Seibert, 2012) is applied to each ensemble member and to each climate variable. Here, the relative changes, based on 10-year monthly mean difference between CORDEX hindcasts (1996-2005) and CORDEX future forecasts (2021-2030 and 2041-2050) are used as correction factors to create new daily future climate times series. The final future climate time series consist of the daily CFSR baseline data plus the added difference between CORDEX hindcasts and CORDEX future data, defined by the respective monthly correction factors.

3.4 Additional model input data: Land use, soil & agricultural management data

Further datasets needed to set up the SWAT and the APSIM model are information on land cover data, topography, soil characteristics, agricultural management rules and the above-mentioned meteorological time series. Sources, as well as temporal and spatial resolution for each dataset used in this study are summarized in table 3-1.

Tab. 3-1: Model input data sets

Variable	Spatial Resolution	Temporal Resolution	Source
DEM	90 m	-	SRTM, NASA
Soil Map	500 m	-	Water and Soil Investigation Division (WASID), Pakistan
Soil characteristics (lab analysis)	Point data	-	Field campaign conducted in the scope of this thesis. (https://doi.pangaea.de/10.1594/PANGAEA. 921389 (Schulz, 2020).
Land-use map	250 m	annual	Awan and Ismaeel (2014)
Agricultural Management	-	-	Local observations & communications (see table 3-2)
Meteorological Data	Point data (3 stations)	daily	Pakistan Meteorological Department (PMD)
CFSR reanalysis data	0.25° x 0.25°	daily	Saha et al. (2010)
CORDEX	0.44° x 0.44°	daily	www.cordex.org

Land use data

The land use map which is used in this study is displayed in figure 2-2. Detailed information in the generation and quality control of the land use data can be found in Awan et al. (2016) and Awan and Ismaeel (2014). In the last part of this thesis, the focus is laid on climate change impact on cotton, maize, and rice crops. Their spatial distribution in the study area can be seen in figure 6-1.

Soil data

Information on the spatial distribution of soil classes were derived from the Pakistani Water and Soil Investigation Division (WASID), which as kindly provided by Dr. Awan (see Awan et al., 2016). Detailed physical soil characteristics were obtained from soil samples, taken and during a field campaign and analysed in the soil laboratory at the Technical University of Darmstadt (see also chapter 5 for more details on the field campaign). The soil data is available on the openly accessible data repository https://doi.pangaea.de/10.1594/PANGAEA.921389 (Schulz et al., 2020).

Agricultural management data

Data on agricultural management strategies such as irrigation rules, and irrigation scheduling, as well as irrigation efficiency, plant types and fertilizer rules are based on local communications and observations during the visits to Pakistan. Principal management parameters which were integrated into the SWAT and APSIM models are listed in table 3-2.

Tab. 3-2: Agricultural management strategies in the study area

Parameter	***APSIM***	***SWAT***
Irrigation frequency	demand based	demand based
Irrigation efficiency	0.7	0.7
Irrigation trigger	soil water deficit	soil water deficit
Fraction of available soil water below which irrigation is applied	0.9	0.9
Fertilizer application	on sowing date and each 14 days	with irrigation
Fertilizer type	Urea_N	Urea
Sowing rule	fixed date	fixed date
Cultivar type - cotton	S71BR	not specified (from SWAT data base)
Optimal temperature cotton	25	30
Base temperature cotton	8	15
Cultivar type - maize	Pioneer_3153	not specified (from SWAT data base)
Optimal temperature maize	15	25
Base temperature maize	8	8
Cultivar type - rice	BR3	not specified (from SWAT data base)
Optimal temperature rice	30	25
Base temperature rice	8	10
Row spacing, density of plants	according to local practices	not specified in SWAT model

4 Spatially distributed model calibration of a highly managed hydrological system using remote sensing-derived ET data

As outlined above, the specific characteristics in the study area of the Lower Chenab Canal System, in Pakistan, made the setup of a hydrological model particular challenging. The following chapter describes, how the setup and the complex calibration was undertaken in order to ensure the representation of the small-scale heterogeneity and physical correctness of hydrological processes, in this highly human impacted environment.

4.1 Introduction

The importance of calibrating and validating hydrological models and thereby assessing their uncertainties before using them for predictions and decision making is unquestionable. However, with increasing model complexity the calibration procedure has become increasingly difficult. For example, problems with unique parameter identification of large unknown model parameter sets (i.e. model equifinality) and issues of model and data uncertainties become more severe (Abbaspour et al., 2017; Gupta et al., 1998; Zhang et al., 2008), especially in highly managed systems with small scale agricultural practices, and spatially as well as temporarily diverse hydrological processes (Bastiaanssen and Bandara, 2001). Furthermore, due to intensive human actions as well as due to climate change, hydrological systems became statistically non-stationary (Fatichi et al., 2016), which makes the calibration of physically based water balance models for such impacted systems very challenging.

To capture the interdependency of various water fluxes and the spatio-temporal heterogeneity of hydrological processes, calibration should preferably be done with process-based variables, which reflect the relevant interactions of the numerous water balance components (Arnold et al., 2012). Streamflow is therefore most often taken as calibration variable as its dynamic can be closely related to variations in water balance components such as evapotranspiration (ET), surface runoff, interflow, and infiltration or percolation rates. Hence, observed and simulated hydrographs are commonly compared, and discharge-based objective functions serve as evaluation criteria for model performance. However, using streamflow data for calibration is difficult in areas, which lack run-off information or even the presence of a natural river network.

To tackle the calibration challenge, ET data have gained importance in the calibration process of hydrological models, and have been used for calibration in various studies (Legates and McCabe, 1999; Lopez Lopez et al., 2017; Rajib et al., 2018; Rientjes et al., 2013; Tobin and Bennett, 2017). One advantage is that ET data can be derived from remote sensing platforms, making spatio-temporally distributed calibration data available. Moreover, ET serves as an overall indicator for surface water

availability, independent of the cause of its availability, i.e. if water allocation was human or naturally induced. Hence, from ET, principal changes in hydrological processes can still be inferred even if surface water availability is controlled by often unknown human decisions.

Examples for such controlled systems are entirely managed irrigation schemes, where irrigation channels are the only water courses in the study area and no further natural streams exist. As outlined in the study area section (chapter 2), in the LCC region the channel discharge is exclusively determined by management decisions, following formal local policies as well as informal local agreements. These sometimes subjective and therefore often unpredictable decisions on water channel flows might interfere with, or even supersede, the natural behavior of the hydrological system. Thus, streamflow becomes inappropriate as fitting variable during calibration (Immerzeel and Droogers, 2008). A successful inverse estimation of spatially distributed model parameters through calibration based on these entirely managed runoff values is therefore highly unlikely. In this case, an alternative way of model calibration has to be applied. This approach has to account for the spatial heterogeneity of water balance fluxes and at the same time, it has to be independent from unforeseeable water management decisions.

In addition, to be able to address research questions on changing hydrological fluxes with respect to changing land use or small-scale agricultural management strategies, an evaluation of the distributed behavior of the model beyond just catchment integrated performance is needed (Zink et al., 2018). The implementation of such a spatial evaluation into the calibration procedure, as well as the high number of model parameters, which need to be parameterized, make a trial and error calibration of complex distributed models unfeasible (Usman et al., 2018). For this reason, automated calibration strategies, which use optimization algorithms to find the best parameter values, are increasingly used for parameter estimation. Several studies exist on the application of automated calibration procedures for lumped models (Sorooshian et al., 1993; Vrugt et al., 2003), and since the past decade these approaches have also been used for spatially distributed models (Campo et al., 2006; Immerzeel and Droogers, 2008; Li et al., 2018; Zink et al., 2018). Immerzeel and Droogers (2008) used remotely sensed ET data to calibrate a spatially distributed SWAT (Soil & Water Assessment Tool) model in an automated calibration approach. A comparable methodology, using the same model and ET estimation procedure, will be presented here. In this study, however, a stronger focus is laid on the challenges of using remote sensing-derived ET data for model calibration in a highly diverse agricultural setting.

Past studies outline the complexity of spatially distributed hydrological model applications in irrigation systems and intensively used agricultural areas (Droogers et al., 2000; Jiang et al., 2015) and also specifically of SWAT model applications in such managed regions (Awan et al., 2016; Dechmi et al.,

2012). Yet, the application of automated calibration strategies using remote sensing-derived ET data for models of entirely managed irrigation system has not yet been studied in depth.

Key subjects this study addresses are therefore (i) the calibration of a spatially distributed hydrological model of an entirely managed irrigation system using satellite ET measurements, and (ii) to evaluate the suitability of ET data, derived from a Surface Energy Balance Algorithm (SEBAL), for calibrating a SWAT model in such a complex agricultural setting. Finally, the potential and limitations of this calibration approach is examined to assess the importance of spatial information in the observation data set used for calibration.

4.2 Materials and Methods

SWAT Model

The Soil & Water Assessment Tool (SWAT) model software (Arnold et al., 1998) is used for this study (see also chapter 3 for a more detailed model description). Basic datasets needed to set up a SWAT model are topography, soil characteristics, land cover data and meteorological time series. Sources, as well as temporal and spatial resolution for each dataset used in this study are listed in chapter 3, table 3-1. In addition, crop rotation patterns are considered and specific planting and harvesting times are defined for each major crop type according to Figure 4-1.

Season	Rabi				Kharif						Rabi	
Crop type - (Rabi-Kharif)	Jan	Feb	Mar	Apr	May	Jun	Jul	Aug	Sep	Oct	Nov	Dec
WHFO – Wheat-Fodder												
WHCO – Wheat-Cotton												
WHMZ – Wheat-Maize												
WHFA – Wheat-Fallow												
WHRI – Wheat-Rice												
FOCO – Fodder-Cotton												
FOFO – Fodder-Fodder												
FOFA – Fodder-Fallow												
SUGR – Sugarcane												

Fig. 4-1: Agricultural land-use classes in the study area and their planting (green/hatched), irrigation (blue) and harvesting (orange/crosshatched) times. White color indicates fallow land/no irrigation. Kharif = wet, summer season. Rabi = dry, winter season.

The spatial discretization is represented in SWAT by hydrological response units (HRUs), each representing specific soil, land-cover, and topographic characteristics. Their extent in the study area varies from approx. 0.008 km^2 to 340 km^2, with a mean extent of approx. 20 km^2. The size of an HRU

depends on the homogeneity of the underlying soil, and land-use characteristics, with larger sizes for homogeneous and smaller sizes for heterogeneous landscape patterns, respectively.

Irrigation is assumed to be demand-based, i.e., an irrigation supply function is automatically activated every time water availability falls below a water demand threshold. Even though the irrigation schedule in the study area is supposed to follow the stringent local "Warabandi" irrigation scheme with fixed water allocation schedules (Qureshi and Hussain, 1994), irrigation according to plant water demand better represents the actual local irrigation practice, where groundwater pumping and on-site irrigation water storage are leading to a more flexible and demand-based irrigation (Qureshi et al., 2010). Administrative boundaries of the so called "irrigation sub-divisions" (Fig. 2-2) are used to delineate pre-defined artificial sub-catchments. The reason for this artificial catchment delineation is the local surface water allocation system. Apart from precipitation, surface water availability for agricultural purposes is entirely human controlled and its allocation strictly follows the administrative rules of irrigation canal command areas. This, however, implies that sub-catchments are purely administratively defined and are not bounded by topography. This again infers that a model based on these artificial sub-catchment delineations can only calculate water balance components correctly, if surface and subsurface flows between these "catchments" are negligible – an assumption, which seems very plausible considering the entirely flat nature of the study area (Fig. 2-3), the restricted surface runoff due to dams surrounding the fields to enable furrow and flood irrigation, as well as the high plant water demand which leads to negligible horizontal water movement.

Hence, to ensure a suitable SWAT model application in the study area with its specific local characteristics, the following assumptions are made: (i) irrigation is driven by plant water demand; (ii) no lateral flow exists between HRUs; (iii) streamflow is ignored as a valid response variable due to the fact that water availability in the channels is entirely human-controlled and no natural streams exist, which could indicate a natural response to changes in hydrological fluxes. Consequentially, routing routines are disabled, and the entire analysis of the model outputs is based only on HRU level and no further spatial aggregation (e.g., basin or sub-basin scale) is made. Therefore, SWAT is used for this study rather like a land-surface model than a conventional surface-runoff model.

This unconventional SWAT model set up adds to the fact that discharge cannot be used for calibration. Hence, a spatially distributed calibration on HRU level becomes necessary to guarantee a sound evaluation of the model performance. In this study we take actual ET (ET_{act}) as fitting variable, as it can be used to derive spatially distributed information on surface water fluxes.

Actual ET (ET_{act}) is calculated in SWAT as the sum of the potential evaporation from the intercept storage (rainwater trapped in the plant canopy), actual soil water evaporation and actual plant

transpiration. Potential soil water evaporation and potential plant transpiration are calculated in SWAT using the Penman-Monteith ET equation (Eq. 10)

$$ET = \frac{1}{\lambda}\frac{\Delta(R_n - G_o) + \rho_a c_a \frac{(e_s - e_a)}{r_a}}{\Delta + \gamma(1 + \frac{r_s}{r_a})} \quad (10)$$

Where ET is the potential evapotranspiration [mm day^{-1}], R_n is the daily net radiation [MJ m^{-2} day^{-1}], G_o is the soil heat flux [MJ m^{-2} day^{-1}], ρ_a is the mean density of air at constant pressure [kg m^{-3}], c_a is the specific heat of air [MJ kg^{-1} °C^{-1}], $(e_s - e_a)$ is the vapor pressure deficit of the air [kPa], r_a and r_s are aerodynamic and bulk surface resistances [s m^{-1}], Δ is the slope of the saturation vapor pressure curve [kPa °C^{-1}], γ is the psychrometric constant [kPa °C^{-1}] and λ is the latent heat of vaporization [MJ kg^{-1}].

SWAT calculates reference ET (ET_{ref}) with fixed resistance factors for a reference alfalfa crop, as well as a plant type specific potential ET (ET_p), with varying plant specific r_a and r_s parameters. Meteorological data from local climate stations is used to retrieve the climate parameters. Leaf area indices as well as crop heights are used to determine aerodynamic and surface resistances of specific crop types for estimating ET_p. Following, ET_{ref} is used to estimate the potential soil water evaporation, where ET_{ref} is adjusted for evaporation of free water in the canopy and is then related to the degree of soil shading, to account for ET reducing effects due to soil cover by plants.

Actual soil water evaporation is then calculated using a biomass dependent soil cover index and information on available water storage capacity (AWC-coefficient) in the soil. The AWC-coefficient, controlling the available water storage capacity, was found to be highly sensitive with respect to ET variations and is therefore used as one of the calibration parameters. ET_p is taken as the maximum possible plant transpiration and is adjusted according to the available water in the soil profile to estimate actual plant water uptake which equals the actual plant transpiration. Using the plant uptake compensation factor (EPCO-coefficient) the depths from where water is allowed to be used for plant uptake can be adjusted. This parameter was likewise found to be highly sensitive in controlling ET in the study and is therefore also included into the calibration parameter set (Table 4-2).

Finally, the SWAT model is run on a monthly basis to generate a monthly ET time series with a spatial resolution identical to the resolution of the model HRUs. This means, that the SWAT ET output is not a gridded product, but holds HRU discretization and therefore land-use, soil and topography dependent ET information.

SEBAL

Remote sensing data provide spatially distributed information on actual ET and thus enables the possibility for a spatially distributed calibration procedure. In this study, ET_{act} estimates from Usman et al. (2015a) are used, who derived spatio-temporal ET_{act} estimates from MODIS satellite data using the Surface Energy Balance Algorithm (SEBAL) approach, briefly described below.

The SEBAL (Surface Energy Balance Algorithm) approach (Bastiaanssen et al., 1998a, 1998b), was developed to estimate spatially distributed information on surface energy balances. It is based on the land surface energy balance theory, which relates the single incoming and outgoing energy components through the energy balance equation

$$R_n = G_0 + H + LE \quad (11)$$

where R_n = net radiation, G_0 = ground heat flux, H = sensible heat flux and LE = latent heat of vaporization (all in W m^{-2}). The energy required for ET (= latent heat of vaporization (LE)) can therefore be calculated as the residual term of the equation

$$LE = R_n - G_0 - H. \quad (12)$$

SEBAL solves this equation by retrieving surface characteristics such as surface albedo, normalized differenced vegetation indices (NDVIs), surface temperature, and emissivity based on remotely sensed information of spectral radiances in the visible, near infrared, and thermal infrared spectrum. Using these derived surface characteristics, SEBAL converts the spectral information into the surface energy fluxes R_n, G_0 and H to estimate LE. The computation of sensible heat flux (H) is hereby the most challenging part. H is calculated by

$$H = (\rho_a + c_a + \Delta T) / r_a \quad (13)$$

where all constants are as listed above (Eq. 10) and ΔT is the vertical temperature difference between two heights. The unknown ΔT is calculated by using the hottest and the coldest pixels of the remote sensing image as anchor pixels where maximum and minimum LE is sensed. It is assumed that H of all other pixels relate linearly to the derived slope of ΔT. The aerodynamic resistance factor r_a, depends amongst other parameters on land cover (i.e., plant type) dependent parameters, such as plant height to define the roughness length for heat transfer. This information is derived from land use maps or using the derived albedo and NDVI data.

Once R_n, *and H* are computed (G_0 is neglected due to daily calculation of ET), LE can be calculated and is then used to define the instantaneous evaporative fraction (EF_{ins}), by

$$EF_{(ins)} = LE/(LE + H) \quad (14)$$

to finally calculate daily ET by

$$ET_{(day)} = (86400*10^3)*(EF_{(ins)})*(R_{nday}/(\lambda*\rho_w) \quad (15)$$

where R_{nday} *is daily net radiation (W* m^{-2}*),* λ *is latent heat of vaporization (J* kg^{-1}*) and* ρ_w *is the density of water (kg* m^{-3}*).*

To average daily ET to a monthly value, daily ET is related to a reference ET (ET_{ref}), which can be calculated on a daily basis using the Penman-Monteith equation and daily meteorological data. Subsequently, the cumulative ET_{ref} of all days of a respective months is used to derive the ratio of the cumulative to a monthly average ET value. This ratio is finally used to convert daily ET to monthly ET.

Usman et al. (2015b) derived monthly ET data using MODIS (level 1-B) data for the study area and developed a time series of monthly ET for 2005-2012, with a spatial resolution of 1 km x 1 km grid cells. The product was validated using the advection aridity method (Usman et al., 2015b, 2015a), resulting in Nash-Sutcliffe efficiencies of 0.92 and 0.71 for dry (Rabi) season and wet (*Kharif)* season, respectively. A validation using observed data from lysimeters or other point estimates, like Bowen energy balance and eddy covariance estimates, was not feasible due to the lack of this information for the study area. Noteworthy, Usman et al. (2015b) also reported difficulties in retrieving accurate ET data during wet season, especially during the monsoon months, due to the lack of cloud free satellite images. For this reason, the months July and August are excluded from the ET time series used for calibration. For the remaining months the images of the two years 2009 and 2010 show the highest data quality (i.e. lowest cloud cover, least data gaps) and are therefore chosen as calibration data set for this study.

To be able to compare the pixel based SEBAL ET data set with the HRU based SWAT ET data set, which differ in spatial resolution, a new SEBAL based ET data set is created which projects SEBAL ET information to the HRUs. In cases where the HRU areas exceeded the extent of a SEBAL pixel, the mean of all SEBAL pixels within one HRU was calculated for the respective HRU area. To assure a good correspondence of the SWAT HRUs and the respective SEBAL ET data, only HRUs representing the most dominant land-use classes (each covering more than 10% of the catchment area) are selected for calibration. Thus, small areas with higher uncertainties in the land-use class estimation and therefore with higher uncertainties in ET estimates are excluded from calibration. Following these selection criteria, 293 out of 780 HRUs are finally chosen and the respective “observed” ET time series were extracted from the original SEBAL data set. Hereafter, the term “SEBAL ET data” refers to the extracted

and HRU based SEBAL data set and has to be distinguished from the original, pixel based SEBAL data set, which we will denote as “original SEBAL data”.

A third and modified SEBAL ET product is created (referred to as “modified SEBAL”), which is based on the SEBAL ET product but includes plant specific ET information. To account for the land-use dependent ET variations, a modification of the SEBAL data set was designed by multiplying each monthly SEBAL ET value with a land-use class specific correction factor for each HRU. The correction factor is derived from crop specific temporal ET patterns (ET_c). ET_c is estimated for each land-use class using the FAO CROPWAT model approach, which simply multiplies a reference ET with a crop specific coefficient (K_c; Allen et al., 1998a). The monthly correction factor for each crop type is given by the monthly ratio of each land-use specific ET_c to the mean ET_c of all land-use classes, estimated by CROPWAT (Tab. A 4-1, Annex). The monthly SEBAL ET value of each HRU is then multiplied by this monthly land-use class specific correction factor. The characteristics of the different SEBAL and SWAT ET products are summarized in Table 4-1.

Tab. 4-1: Different ET data sets and their spatial resolution

Name of ET data set	**Spatial resolution**	
SWAT ET	HRU extent	on average 20 km²
Original SEBAL ET	Gridded / MODIS based	1 km x 1 km
Unmodified SEBAL ET / SEBAL ET	HRU extent / A mean ET value of the original SEBAL ET is extracted for each SWAT HRU	on average 20 km²
Modified SEBAL ET	HRU extent / Each HRU of the unmodified SEBAL data set is corrected with a crop specific ET correction factor	on average 20 km²

Calibration procedure

The calibration procedure, applied in this study follows the workflow summarized in Figure 4-3: After the initial SWAT model setup, the model is calibrated using SWAT simulated ET as calibration variable and the unmodified SEBAL ET data set as “observed” data. A set of 44 parameters is adjusted during calibration to optimize the Kling-Gupta efficiency criteria (KGE) between SWAT and SEBAL ET values. Non-satisfactory initial calibration results make a second calibration necessary. In the second approach, the modified SEBAL ET data set is used, which better accounts for detailed crop specific ET. Finally, the calibration outputs are validated to assess the calibration success and transferability of the results.

DDS - Optimization algorithm

The optimization algorithm used in calibration is a crucial factor in parameter estimation (Singh Vijay P. and Woolhiser David A., 2002). In this study we apply the Dynamically Dimensioned Search

Algorithm (DDS) which was developed by Tolson and Shoemaker (2007), to efficiently solve complex calibration problems with a high number of fitting parameters. It has been applied in the calibration of spatially distributed hydrological models (Lin et al., 2017; Tolson and Shoemaker, 2007) and its performance has been discussed by (Behrangi et al., 2008). The difference of DDS compared to other commonly applied global search algorithms (e.g. shuffled complex evolution algorithm (SCE) (Duan et al., 1994, 1993)), is the way the search space is dynamically adjusted by successively decreasing the parameter dimension until the number of iterations reaches its user defined limit. For this study, the DDS was set up with 44 parameters (Tab. A 4-2, Annex) and 10,000 iterations using the software Ostrich (Matott, 2017).

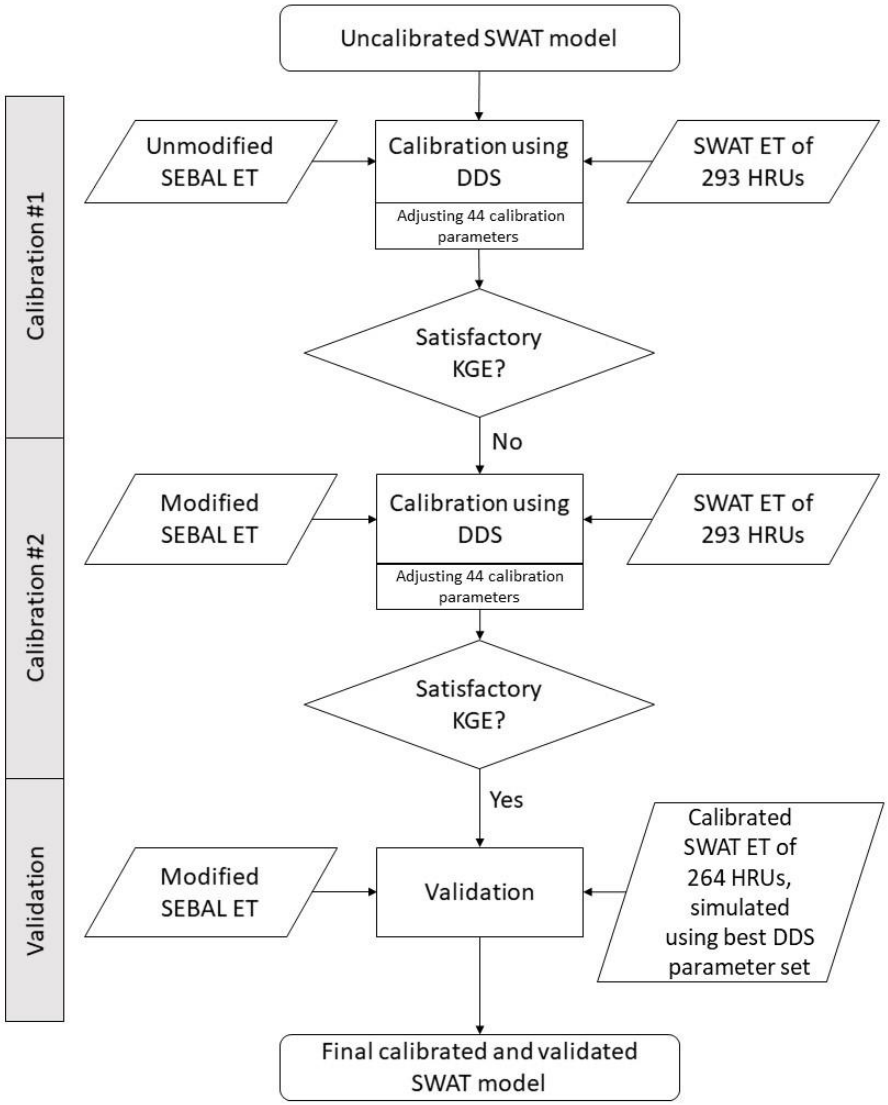

Fig. 4-2: Workflow of the calibration procedure

Calibration parameters

A first selection of 12 calibration parameters (Tab. 4-2) was made based on most commonly selected SWAT calibration parameters used in previous SWAT-calibration studies (Abbaspour et al., 2015; Zambrano-Bigiarini and Rojas, 2013; Zhang et al., 2008), as well as parameters, which were found to be most sensitive with respect to changes in ET according to a manual trial and error tests. The pre-selection of these 12 parameters was then tested for sensitivity using the Latin-Hypercube One-factor-at-a-time (LH-OAT) sampling strategy (van Griensven et al., 2006). As a result, the five most sensitive parameters for the SWAT model of the study area with respect to changes in evapotranspiration could be identified. Only these parameters (highlighted with * in Tab. 4-2) were used in the calibration process. Subsequently, these five model parameters were further differentiated based on their dependency on individual soil or land-use classes as well as on soil depth, resulting in 44 parameters to calibrate. Initial values are within the range of the given maximum and minimum values but vary with land-use class, soil class, and soil depth, respectively. The parameter ranges were defined based on SWAT suggested minimum and maximum values for "unmeasurable" model parameters (e.g. EPCO, ESCO, CN II) and on estimates used in previous studies in this region (Awan et al., 2016).

Tab. 4-2: SWAT parameters selected for initial sensitivity analysis (all) and for final model calibration (*)

#	Parameter	Parameter name	Unit	Range	
				min	max
1*	Plant uptake compensation factor	EPCO	-	0	1
2*	Initial SCS CN II value	CN2	-	35	85
3*	Available water capacity	SOL_AWC	mm H_2O/mm soil	0.01	0.20
4*	Ground water delay time	GW_DELAY	days	0	500
5*	Saturated hydraulic conductivity	SOL_K	mm/h	0	500
6	Soil evaporation compensation factor	ESCO	-	0	1
7	Organic carbon content	SOL_CBN	% soil weight	0	10
8	Maximum rooting depth	SOL_ZMX	mm	600	2000
9	Moist bulk density	SOL_BD	g/cm^3	0.95	1.90
10	Base flow alpha factor	Alpha_BF	days	0	1
11	Deep aquifer percolation fraction	RCHG_DP	-	0	1
12	Maximum canopy storage	CANMX	mm H_2O	0	20

Objective function

It is widely suggested to treat the calibration problem of hydrological models as a multi-objective problem (Gupta et al., 2009, 1998; van Griensven and Bauwens, 2003) , i.e. using either multi-variable measurements, multi-site measurements or multi-response functions in the calibration process (Madsen, 2003). The method used in this study can be seen as a "multi-site calibration" as it uses individual ET time series from 293 "sites" (i.e. HRUs). Moreover, to account for multiple hydrological responses, hence to estimate temporal as well as total volumetric error behavior we chose the Kling-Gupta-Efficiency (KGE) as objective function (Kling et al., 2012). This goodness-of-fit criterion includes

measures of correlation (r), variability (α), and bias error (β) (Gupta et al., 1998; Kling et al., 2012). It assesses the fit between modelled and observed values on a scale of –infinity to 1, with 1 indicating a perfect match and decreasing KGEs indicating decreasing fits between model results and observations.

Finally, the optimization problem becomes a single-criterion maximization problem, which combines multiple criteria into the single goal function of maximizing the mean KGE of all selected sites. The objective function is given as:

$$\max KGE_{mean} = \sum_{j=1}^{k} \frac{1}{k}\left(1 - \sqrt{((r-1)^2 + (\alpha-1)^2 + (\beta-1)^2)_j}\right) \quad (16)$$

where k is the total number of HRUs, r is the regression coefficient, α is a measure of relative variability (ratio of simulated and observed standard deviation), and β is the bias (ratio of simulated and observed means).

Validation

To validate the calibrated SWAT model, a cross-validation approach is applied. A new set of 264 HRUs is selected. These HRUs were not used during calibration but represent the same land-use classes of the previously used HRUs. This way it is tested if parameter adjustments, which were done during calibration, can be transferred to other SWAT HRUs. The SWAT model is run with the best parameter set obtained by the DDS algorithm and finally SWAT ET values of the new 264 HRUs are compared to SEBAL ET values for the same locations. The calibration success is then evaluated based on the goodness-of-fit between SWAT and SEBAL ET.

4.3 Results

Despite the underestimation of SWAT ET values compared to SEBAL ET throughout the dry months and overestimation during monsoon months, the temporal pattern as well as the corresponding efficiency criteria (e.g., KGE = 0.51, r^2 = 0.81 and RMSE = 20 mm/month) show, that the uncalibrated SWAT ET data fit reasonably well to the SEBAL data (Fig. 4-3). Both ET time series capture the same temporal variation with respect to growing and harvesting seasons and except for the two wettest summer months, deviations of SWAT *vs*. SEBAL ET are small. SEBAL is therefore considered to be an adequate “observed” data set to be used for parameter estimation in the SWAT calibration procedure.

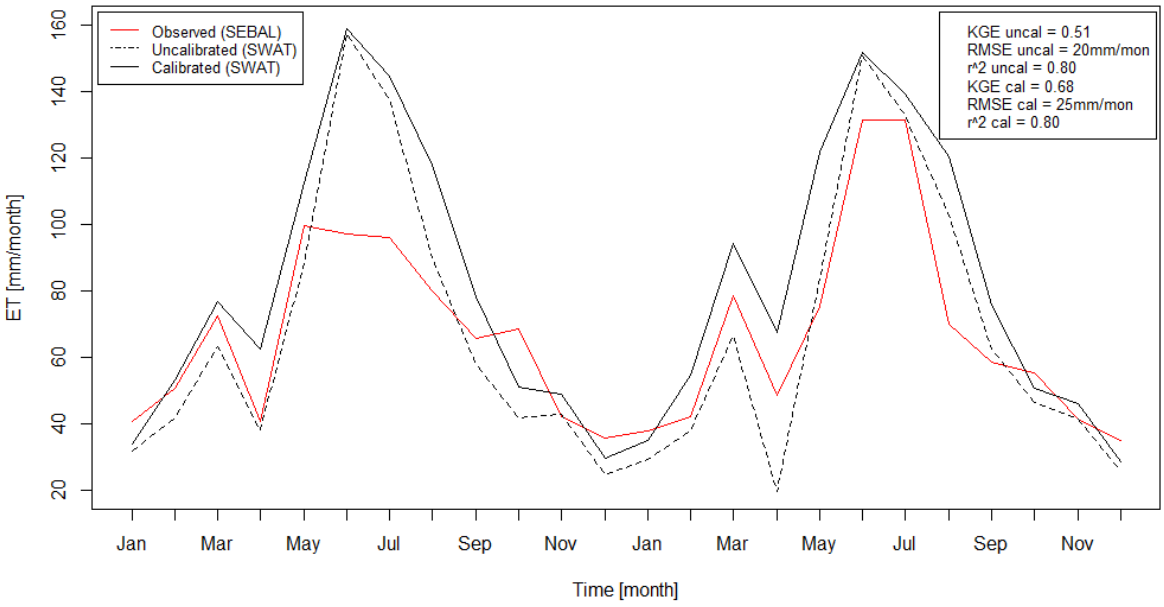

Fig. 4-3: SEBAL (red) and SWAT (black ET time series before and after calibration, for the period of 24 months (years 2009-2010). Efficiency criteria (KGE, RMSE and r^2) show the fit between unmodified SEBAL ET and uncalibrated SWAT ET.

Calibration Results

The spatially distributed SWAT calibration using a SEBAL data set seems promising but also reveals limitations. The initial KGE of 0.04 is calculated by averaging the individual KGEs of all 293 HRUs and represents the fit between SWAT ET and SEBAL ET before calibration (Tab. 4-3). Calibrating the SWAT model using the DDS algorithm yielded the following results: the automated calibration procedure improved the mean KGE by 0.23, from initially 0.04 to 0.27, within the first 5,000 calibration runs. The best KGE of 0.28 was achieved after approx. 10,000 DDS runs, showing that a fast convergence within the first 5,000 runs was reached, while the following 5,000 runs were only leading to a further improvement of about 0.01 [KGE].

Tab. 4-3: Calibration results of calibration with unmodified SEBAL ET data. Percentiles are indicating the spread of KGE values among the selected 293 HRUs

	Initial fit (uncalibrated model)	**Calibration results**		
Evaluation Criteria	*Mean (all HRUs)*	*Mean (all HRUs)*	*5th percentile*	*95th percentile*
KGE	0.04	0.27	-0.15	0.56
R^2	0.54	0.51	0.001	0.81
RMSE [mm/month]	40.20	44.70	32.70	57.70

Even though a KGE of 0.27 is clearly not showing a satisfying model performance, an overall improvement of 0.23 [KGE] seems promising for a spatially distributed model calibration. While in a traditional calibration procedure time series of spatially integrated data (Fig. 4-3) would be fitted, in a spatially distributed calibration all HRUs are treated as separate time series. Thus, spatially dependent misfits are not averaged out. Comparing the lumped initial KGE of mean SEBAL ET and mean SWAT ET of 0.51 with the spatially distributed initial KGE values (mean KGE of all HRUs) of 0.04, already points towards the complexity of calibrating a model using a spatially distributed approach.

A closer look into the detailed results of this calibration process shows that the results have to be examined with respect to seasonal patterns as well as spatial variations in the goodness-of-fit. Calibration results differ clearly between single HRUs. Best HRUs reach KGE values of up to 0.6 after calibration, whereas some areas show values as low as -0.60. In the following, the reasons for the low calibration performance and for the temporal and spatial error variations are presented in detail.

Seasonal differences of goodness-of-fit

Mean ET time series for all HRUs of the uncalibrated (dotted black line) as well as for the calibrated (solid black line) SWAT model are presented in Figure 4-3. Furthermore, it shows the SEBAL data (mean of all HRUs, solid red line) which was used as observation data for calibration. While this figure does not reveal much about the spatial fit, it shows the improvement of temporal model performance during the calibration process.

It can be observed that the calibration helped to reduce the underestimation of ET by the SWAT model during the drier winter months. Yet, the seasonal variation in the goodness-of-fit remains. While during most of the year a good fit of SWAT *vs.* SEBAL values can be observed, during summer months SWAT values (uncalibrated and calibrated) still clearly exceed the SEBAL estimates. These months coincide with the wet season (Kharif) in the study area, where cloud cover is high and remote sensing estimates of surface energy balances calculations exhibit higher uncertainties (Usman et al., 2015a). This hypothesis is also supported by the spread of the model performance on HRU scale (Fig. 4-4).

Dry winter months show very low differences between SEBAL and SWAT data sets, whereas wet summer months show differences in ET of over +/- 100 mm/month (Fig. 4-4). For this reason, some studies have excluded the monsoon months from calibration (Immerzeel and Droogers, 2008). For study areas, however, where each season has entirely different cropping characteristics, neglecting all wet months would exclude an entire cropping cycle with its unique temporal and spatial land-use characteristics. Accordingly, the parameterization would be biased by only one cropping and climate

pattern. Therefore, methods of separating wet and dry seasons in the calibration process have been applied in other studies (Gao et al., 2018). Yet, the parameters selected for calibration in this study, namely EPCO, CN2, SOL_AWC, GW_DELAY, and SOL_K are not expected to significantly change from wet to dry months, as these coefficients are depending mainly on characteristics of soil structure, grain size distribution, geological factors etc. which are changing on long-term time scales but not by season. To be physically consistent, this study therefore does not separate wet and dry seasons for calibration.

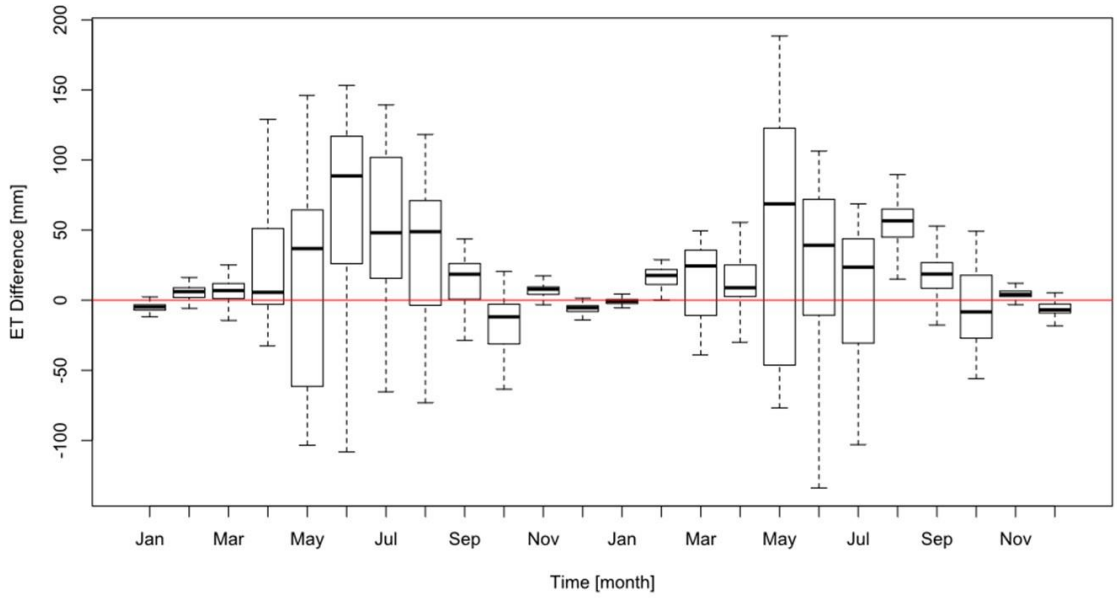

Fig. 4-4: Differences of calibrated SWAT model ET values and unmodified SEBAL ET values of all 293 HRUs used for calibration. Positive values = SWAT overestimates SEBAL ET. Negative values = SWAT underestimates SEBAL ET.

Examining the distributions of monthly ET values separately for SEBAL and SWAT (Fig. 4-5) reveals that the reason for the mismatch of ET during summer months could lay in the low variance of SEBAL ET values (Fig. 4-5a). In contrast to the expectation that SEBAL would reflect high ET variances during monsoon months due to higher diversity in the agricultural cultivation as well as higher uncertainties in the remote sensing data, it shows a surprisingly low data spread compared to SWAT ET (Fig. 4-5b). Assessing the dependency of ET with respect to each land-use class shows a high variance of SWAT ET. This seems quite plausible as different land-use types have specific plant physiognomies and growing patterns, and hence unique ET time series (Fig. 4-5d). Consequently, SWAT results show a clear distinction of different land-use class ET estimates, while the SEBAL data entirely lack any land-use class dependent ET characteristics, and show nearly identical ET patterns for all HRUs (Fig. 4-5c).

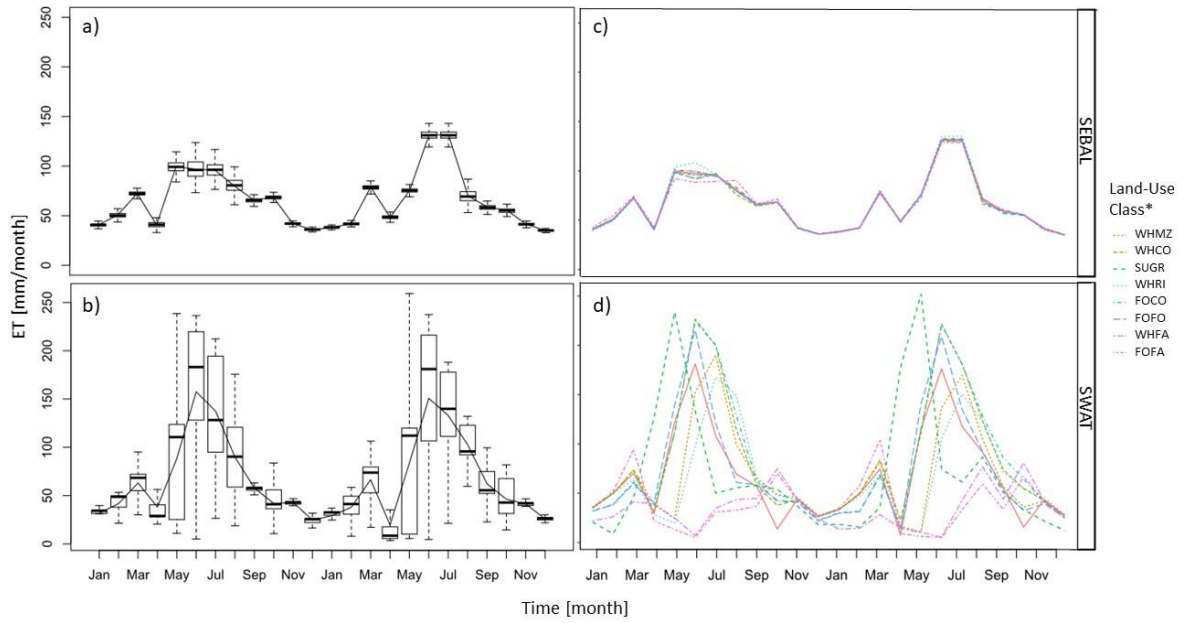

Fig. 4-5: Differences in the spread of (a) unmodified SEBAL ET and (b) calibrated SWAT ET of all 293 HRUs. Land-use class specific ET patterns are shown separately for (c) unmodified SEBAL ET data and (d) calibrated SWAT ET data. *For land-use class description see Fig. 4-1.

The limitations of using this SEBAL data set for a spatially distributed calibration of a small-scale farming system are further reflected by the spatial differences of the calibration results.

Spatial differences of goodness-of-fit

A closer look into the spatial distribution of the calibration results shows that the error between observed and simulated ET is highly land-use dependent, i.e., KGEs vary significantly between land-use classes (Fig. 4-6). While HRUs of the land-use class Wheat-Rice show a mean KGE of over 0.3, with a maximum KGE of 0.69, Fodder-Fallow only yields a mean KGE of less than -0.50. This shows a discrepancy of over 0.8 KGE between “best” and “worst” mean fit (see Fig. 2-2 for spatial distribution of land-use classes and Fig. 4-9 for mean KGEs of each individual land-use class).

The clear land-use dependency of the calibration results reveals again that the best goodness-of-fits occur for land-use classes with ET characteristics closest to the average temporal ET pattern of all land-use types. This underlines the hypothesis that the extracted SEBAL data represents only a mean ET value of all land-use classes. At the same time, land-use types, which vary significantly from the mean show lowest goodness-of-fits. Hence, to improve the overall calibration result an alternative ET data set, which better accounts for differences due to land-use characteristics, is needed.

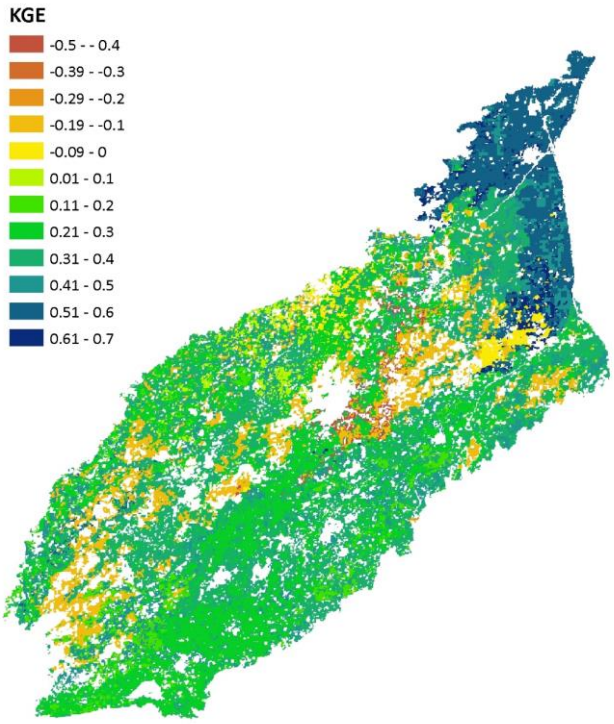

Fig. 4-6: Spatial distribution of KGE values after calibration using unmodified SEBAL ET values as observed data.

Calibration results using a modified SEBAL ET data set

As mentioned, the main reason for the low calibration performance might lay in the missing reproduction of land-use dependent ET patterns by the SEBAL data during the wet season. The modified SEBAL data set, which better accounts for land-use dependent ET variation, is therefore used for a second calibration trial.

The resulting mean ET time series of each land-use class from the modified SEBAL data set are shown in Figure 4-7. Now, land-use class dependent ET variations better reflect expected differences between different crop types. The initial fit between SWAT ET and the modified SEBAL ET yields a KGE of 0.22 (compared to 0.04 in the previous case) and thus, already presents an improved starting point for a spatial calibration (Tab. 4-4).

Tab. 4-4: Calibration results using the modified SEBAL data set

	Initial fit (uncalibrated model)	**Calibration results with modified SEBAL data**		
Evaluation Criteria	*Mean (all HRUs)*	*Mean (all HRUs)*	*5th percentile*	*95th percentile*
KGE	0.22	0.40	0.14	0.60
R^2	0.36	0.39	0.24	0.68
RMSE [mm/month]	45.50	46.90	26.70	66.10

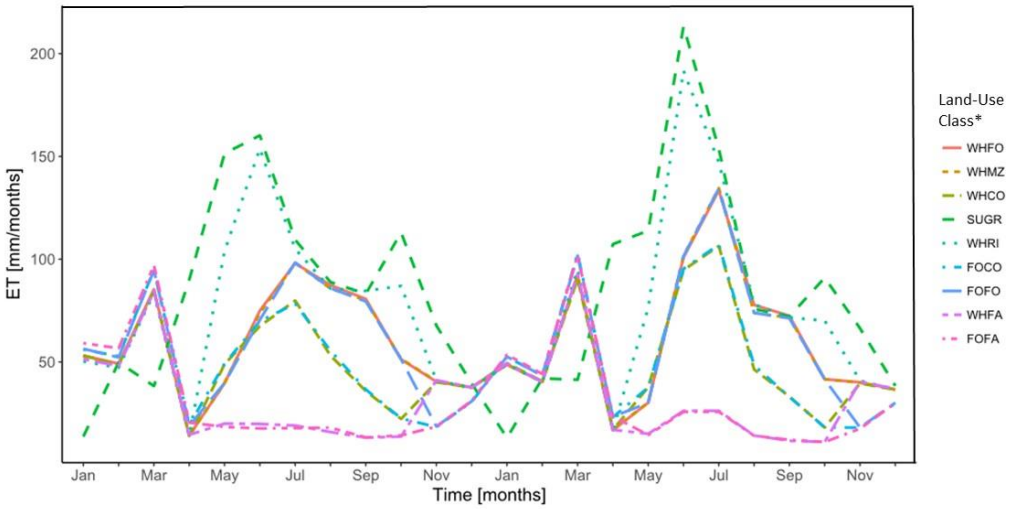

Fig. 4-7: Modified SEBAL data after multiplying each land-use class with a correction factor based on the deviation of the crop specific ET (ET_c) from the mean of al ET_c; *For land-use class descriptions see Fig. 4-1.

As expected, the results show that a consideration of the land-use dependent ET characteristics clearly improves the calibration performance. A final mean KGE of 0.40 could be achieved, with a 5th and 95th percentile of 0.14 and 0.60 KGE, respectively (Tab. 4-4). Furthermore, the results show that except for two land-use classes (Fodder-Cotton (FOCO) and Wheat-Cotton (WHCO)) the calibration could reach comparable KGEs for all land-use classes as opposed to the previous attempt, where mean KGEs varied from approx. -0.50 to 0.40 depending on the respective land cover type (Fig. 4-9b and 4-9d). As mentioned above, during calibration with unmodified SEBAL ET data, KGEs were high for land-use classes with ET estimates close to the average SEBAL ET and low for land-use classes for which ET deviated strongly from this mean. It can be assumed that the reason for a less successful calibration of single land-use classes (i.e., FOCO and WHCO) is no longer the strong general difference from the mean SEBAL ET estimate compared to the simulated mean ET, as it was the case during the first calibration attempt. Both, FOCO and WHCO for example, show relatively low KGEs (Fig. 4-9d) but closer proximity to the average modified SEBAL ET estimates (mean absolute difference = approx. 30 mm/month) than land-use classes, which reached highest KGEs. SUGR (Sugarcane) for example, shows a higher deviation from the mean SEBAL data (mean absolute difference = 40 mm/month), but shows a much better match with its respective SEBAL time series and a mean KGE above 0.60. A low KGE can therefore now be attributed to land-use specific performance of SWAT ET estimation.

The spatial distribution of the model performance (Fig. 4-8) as well as land-use class specific KGE improvement (Fig. 4-9) illustrate once more that the second calibration procedure leads to a study area wide improvement of the model performance. Hence, the calibration results using the modified

SEBAL data set enable a spatially distributed assessment of the model performance. This helps to achieve the initially stated aim of examining and improving the model set-up without losing spatially distributed information.

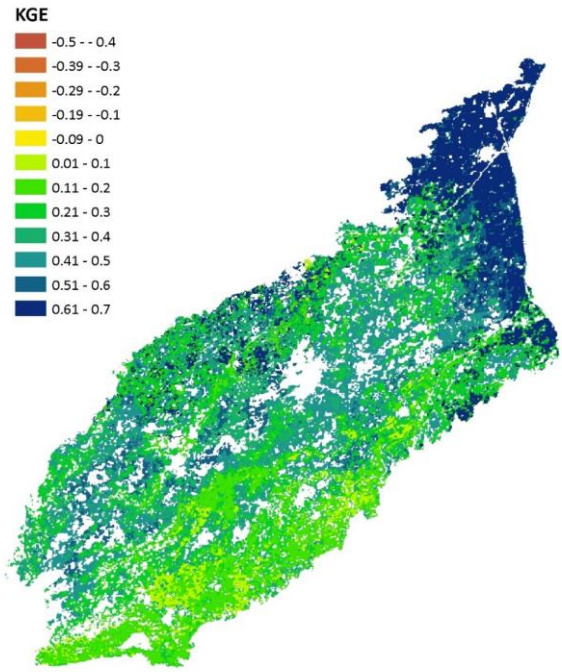

Fig. 4-8: Spatial distribution of KGE values after calibration using a modified SEBAL ET data set as observed data.

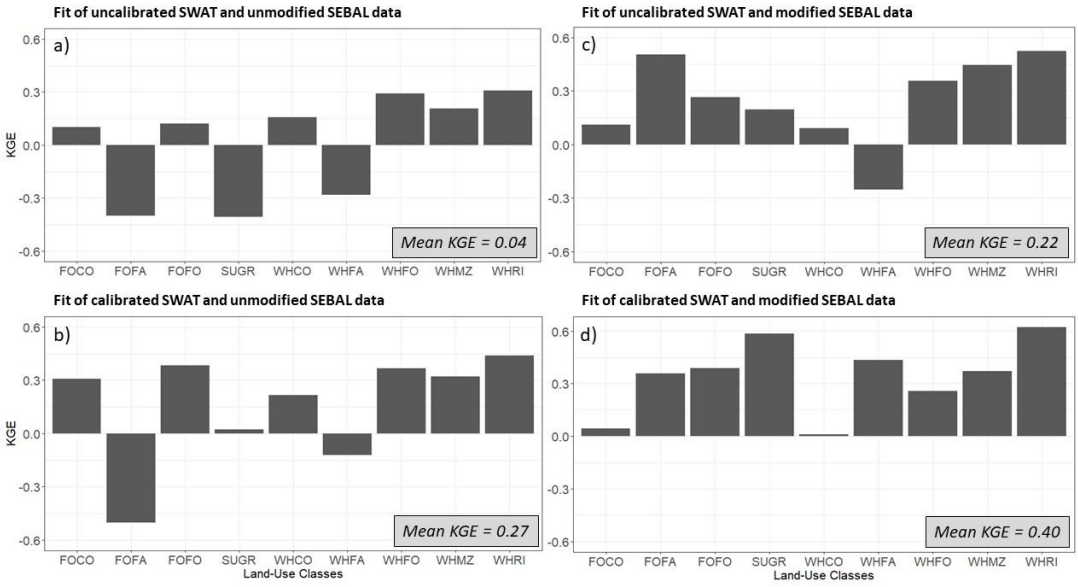

Fig. 4-9: Fit between SEBAL and SWAT ET, measured in KGEs for each land-use class. Using the unmodified SEBAL data set: (a) fit before calibration and (b) fit after calibration. Using the modified SEBAL data set: (c) fit before calibration and (d) after calibration; for land-use class descriptions see Fig. 4-1.

Validation

The validity of the best parameter set, derived by the above-described calibration procedure, is tested using a cross-validation approach. Due to the quality of the observation data described above, the same time period (2009-2010) has to be used for validation. Therefore, the verification is done using a new HRU set of 264 HRUs, which were not used during calibration but represent the same land-use classes. The validation results show a mean KGE of 0.57 with best KGEs of up to 0.74 (Tab. 4-5), which is on average even slightly higher than during calibration. This shows that the calibrated parameters are transferable to other areas (HRUs) in the study region and hence ascertains a valid calibration. The KGE-distribution with respect to each land-use (except for Wheat-Rice) shows similar or even higher values compared to the calibration output.

Tab. 4-5: Validation results using the modified SEBAL data set

Evaluation Criteria	***Mean (all HRUs)***	***5th percentile***	***95th percentile***
KGE	0.57	0.02	0.63
R^2	0.39	0.14	0.64
RMSE [mm/month]	41.60	26.50	65.30

4.4 Discussion

The remote sensing derived SEBAL data set enables a spatially distributed calibration of the hydrological SWAT model. Yet, the study shows that the calibration results of the first trial are unsatisfactory and show a high seasonal variation in the goodness-of-fit between SEBAL and SWAT ET. Especially during months with heterogeneous cropping patterns, land-use type specific ET information differs significantly between both data sets and a decent parameterization and hence a satisfactory calibration is not possible using the original SEBAL ET data. However, the result can be improved using the modified SEBAL product, which accounts for plant type specific ET characteristics. The resulting improved calibration performance hints towards the importance of using a plant type dependent ET data set for model calibration of small scale and heterogeneous agricultural areas. Still remaining differences of modified SEBAL and SWAT ET can be explained by (i) differences in the ET calculation methods of SEBAL and SWAT, (ii) differences in input data sets, (iii) differences in spatial scales of SWAT HRUs and the initial SEBAL grid, and (iv) by differences in model assumptions, regarding parameters controlling ET.

Differences in ET calculation methods of SEBAL and SWAT

As mentioned in the introduction section, SEBAL ET is based on the surface energy balance, with visible near infrared and thermal infrared images being the input data for the retrieval of radiation and relevant land surface characteristics (e.g NDVI). Hence, energy balance components are the main factors controlling the ET estimation. While this sparse input data requirement is an advantage for the large-scale application in this work, it also poses a potential source of ET uncertainty. For example, all plant dependent information needed for the ET calculation, such as leave area or plant height to define the roughness length for heat transfer, are estimated from the spectral information of the remote sensing product. Hence, if the spectral data cannot resolve the spatial variability of the respective plant information, such as vegetation height, roughness length, and displacement height, it will not be able to give plant specific spatially distributed ET estimates (Ershadi et al., 2013). This can be seen in Figure 4-5c, which shows the weak performance of the SEBAL data set in separating the single land-use dependent ET patterns.

In SWAT on the other hand, ET calculation is embedded into the overall water balance equation, which relates ET estimates to the entire hydrological cycle. SWAT includes detailed information about the different land use types, such as rooting depth, plant height, leaf area index etc. and thus enables a plant type specific ET estimation, at the model unit scale (i.e., HRU-level), as can be seen in Figure 4-5d. However, similar to the uncertainties of the SEBAL product, also the SWAT ET calculation is based on parameter assumption which induce uncertainty. Embedding the ET estimation into the overall water balance calculation and therefore linking it to other water fluxes, such as soil moisture availability, which again depends on percolation rates, lateral flow, surface runoff, etc. increases the number of model parameters responsible for the final ET rate and hence increases uncertainty. Therefore, the selection of SWAT parameters to be included into the calibration procedure is crucial. Rajib et al. (2018), found that for a successful SWAT calibration using ET data, biophysical parameters should be considered, as they are representing vegetation dynamics and energy utilization mechanisms and thus enable a better model accuracy regarding ET. However, an accurate “observed” data set, which reflects the same detail in spatial and temporal variation in ET as the model output, is still required for a successful calibration, as further discussed in the following sections.

Differences in input data sets

Another reason for the discrepancy between SEBAL and SWAT ET might be a general mismatch due to differences in input data for ET calculations. While the SEBAL product applied in this study uses plant information (NDVI and LAI) derived from MODIS products, SWAT uses Landsat derived land-use classification as well as soil information from the Water and Soil Investigation Division of Pakistan to

estimate ET. Input data sets are therefore entirely independent and might lead to temporal and spatial differences in the final ET estimation.

However, as illustrated in Figure 4-4 and Figure 4-5, the ET mismatch is only apparent for the wet summer season, which shows a high variety of crop types. Dry winter months, with mainly one crop type (winter wheat) show a nearly perfect fit of SEBAL and SWAT ET estimates. Thus, it seems reasonable to assume that the main difficulty does not lay in the general mismatch of ET values due to differences in ET calculation methods or discrepancies in the input data sets but rather in a spatial discrepancy.

Differences of spatial scales

A spatial mismatch between SEBAL and SWAT due to scaling and averaging procedures is one more reason for the hampered calibration success. Similar discrepancies of observed and simulated ET due to scaling problems were reported by Liaqat et al. (2015), who compared Surface Energy Balance System (SEBS) results with advection-aridity derived ET. Also, Bastiaanssen et al. (2012) compared ET based on remote sensing data with lysimeter values and reported differences in ET estimates due to scaling discrepancies. While agricultural fields in the study area have an average size of about 150 x 150 m, SEBAL calculates ET only on a 1 km x 1 km scale and hence, delivers an average ET of several different fields within one SEBAL pixel. SWAT averages the SEBAL ET estimates over HRUs with areas of approx. 20 km^2. Taking the mean of all SEBAL pixels, which fall within one HRU polygon, all spatial differences in SEBAL ET characteristics are lost. Consequently, this method leads to smoothed "observed" SEBAL ET time series for all HRUs and hence, wrongly implies equal ET characteristics for each land-use class (Fig. 4-5c). Moreover, it is known that MODIS-based ET estimates are able to correctly reproduce basin average ET patterns, as it is also shown in this study, but that they fail to distinguish variation in ET fluxes between crop types at smaller scales (McCabe and Wood, 2006; Y. Q. Wang et al., 2016). This explains the spatial distribution of KGEs (Fig. 4-8) and the findings that KGEs are highest for land-use classes which show ET patterns closest to the basin average ET values. In areas, which show a larger extent of homogeneous crop types, like rice growing areas in the northern part of the catchment, a better fit of the MODIS-based SEBAL estimates and SWAT can be observed. This means, that a higher spatial resolution of the input data set, used for remote sensing-derived ET calculation, would be necessary to get more reliable ET information for smaller scales. Only then, SEBAL would yield ET information, which would be sufficiently spatially discretized to be used for a successful SWAT model calibration procedure as described in this study. The improvement of the calibration results, using the modified SEBAL data set, which accounts for a higher spatial variability of crop-specific ET patterns, shows the potential for a successful calibration using such a higher spatially resolved data product.

Differences in model parameter assumptions

So far, the discussion mainly dealt with the difficulties of the calibration approach due to limitations of the remotely sensed ET product. However, given the local conditions of the study area the SEBAL data set used in this study still offers valuable information, which is very useful for a basin wide SWAT model calibration. For example, SEBAL serves well as calibration data for temporal variations of ET. It gives good ET approximations in dry winter months and due to its initially gridded information, it accounts for detailed spatially distributed temperature and precipitation variations in the region. In addition, considering the local characteristics of the study area, where surface water content is nearly entirely determined by irrigation water supply, SEBAL ET data provides the advantage that they inherently account for the information of surface water availability. In this semi-arid and extensively irrigated area, energy partitioning between sensible and latent heat flux is strongly varying with surface water availability. As SEBAL derives ET from the amount of energy available for latent heat flux, it indirectly accounts for the surface water content which controls ET. In turn, SWAT needs detailed irrigation management information as well as crop planting and harvesting times, to guarantee a correct estimation of surface water availability and hence actual ET rates. These management strategies are often unknown, and approximations are taken as initial model parameters. Consequently, this yields a high degree of model parameter and hence ET uncertainty. SEBAL can therefore help to calibrate the SWAT model with respect to management parameter settings. The final calibration results (Fig. 4-9d) show, that if the SEBAL data set contains crop-type dependent ET pattern (i.e., modified SEBAL ET data set), variations in the goodness-of-fit between SEBAL and SWAT are still noticeable. However, in this case a less satisfying goodness-of-fit can be attributed to single crop types (Fig. 4-9d, e.g., WHCO and FOCO) and thus to a land-use specific performance of SWAT ET estimation. To account for this, the model can be calibrated accordingly.

4.5 Conclusions

This part of the thesis assessed the potential as well as shortcomings of using remote sensing-derived ET data in a spatially distributed model calibration approach. A SEBAL data set was used to obtain ET time series, which were subsequently applied in a spatially distributed calibration procedure. The work could demonstrate that the extraction of spatial ET data from a 1 km x 1 km MODIS-based SEBAL data set, using the extent of SWAT model HRU areas, leads to averaged and nearly equal remote sensing-derived ET data for all HRUs. The extracted time series from SEBAL data are therefore insufficiently representing spatial differences in ET patterns and are inhibiting satisfactory calibration results. In order to use remote sensing-derived ET data for model calibration, which is often the only spatially

distributed data set available, a detailed assessment of the spatial variability of SEBAL ET data is necessary. For a small scale and highly diverse agricultural setting the preservation of the spatial heterogeneity of the "observed" (i.e., remote sensing) data set remains one of the main challenges. For an improved model calibration in such an environment, a higher resolution or a modified "observed" ET data set, which accounts for land-use class specific ET pattern is therefore desirable. The final calibration of SWAT using a modified SEBAL ET data set, which captures the spatial ET variability, showed the potential of this calibration approach for a complex spatially distributed hydrological model.

In line with the findings of this study the following should be considered for a successful spatially distributed calibration using remote sensing-derived ET data:

- Temporal variability of ET is captured well by SEBAL data but shows lower accuracies during wet seasons when cloud cover reduces the reliability of remote sensing-derived ET data.
- During seasons with homogeneous crop types, i.e., low spatial heterogeneity, SEBAL and SWAT ET estimates show a satisfactory match. During seasons when crop patterns are highly diverse, the remote sensing product is biased towards specific land-use patterns, which results in the same trend in the calibration results.
- Especially for small-scale agricultural areas, the averaging of remote sensing-derived data to a mean ET value per HRU cannot resolve the spatial ET variability during seasons when crop patterns are highly diverse. A correction of the "observed" data set is therefore suggested to account for the characteristics of each specific land-use class and to remove the bias mentioned above.

5 Estimating water balance components in irrigated agriculture using a combined approach of soil moisture and energy balance monitoring, and numerical modeling

The previous chapter showed the importance of data availability for model calibration and validation. The method of using remote sensing derived ET data showed its advantages for the calibration of a large-scale hydrological model but at the same time it showed significant limitations in resolving small scale heterogeneity. In addition, factors such as cloud cover, parameter assumption and uncertainties of additional input data of the retrieval algorithms, as well as differences in spatial resolution seemed to significantly affect the quality of the remotely sensed data (see discussion section in chapter 4).

Considering these challenges, the question arose: can a framework be developed which can help to acquire data of important water balance parameters without the need of detailed input data set and which can then be used to validate the set-up of hydrological models?

A framework was developed to estimate water balance components using a combined approach of in-situ data of soil moisture and energy balance parameters and numerical modeling. The following chapter outlines in detail the development of this framework and is based on Schulz et al. (2021). The data acquired through this approach as well as the collected in-situ data helped to get a better estimate of hydrological dynamics in the study area. It furthermore helped in improving the model parameterization of the APSIM model (see chapter 6).

5.1 Introduction

Information on water balance components is essential in hydrological sciences and related disciplines. It is needed to quantify the replenishment of natural resources and thus forms the basis for sustainable water resources management. For irrigated agricultural systems it helps in irrigation and drainage planning and in distinguishing between blue and green water footprints of crops.

Unfortunately, the possibilities for direct measurements of some balance components such as actual evapotranspiration (Allen et al., 2011; Wang and Dickinson, 2012) and groundwater recharge (Healy, 2010) are quite limited. Therefore, indirect approaches that require less own measurement effort are more frequently applied. Very common for the approximation of actual evapotranspiration (ET_{act}) is, for example, the Penman-Monteith equation, which uses routine weather data and information on plant physiology, usually extracted from readily accessible databases (Allen et al., 1998b). Indirect methods for estimating groundwater recharge (GWR) include for instance hydrograph analysis, various tracer methods and modeling. Hydrological models are particularly interesting because they usually provide estimates of all water balance components. However, the reliability of their results depends

strongly on the availability and quality of the input data, which therefore constitute the principal source for uncertainties, particularly in data scarce regions.

In addition to ET_{act} and GWR, natural water inflow, i.e. precipitation, can also be subject to uncertainties, for instance if there are no precipitation measuring stations in the vicinity or if only spatially integrated data from satellite data (e.g. TRMM, CMORPH) or reanalysis (e.g. ERA5) are available. If imprecise precipitation estimates are then used in models, incorrect parameter estimates and model results may occur (Fraga et al., 2019; Peters-Lidard et al., 2008; Troutman, 1983). For irrigated agricultural systems, irrigation water is also an important but often insufficiently known inflow component (Brocca et al., 2018; Lankford, 2006; Wisser et al., 2008). The degree of uncertainty depends on the type of irrigation. In systems where the water is distributed by a piping system, equipped with flow meters, fairly accurate application rates are available. In many parts of the world, however, there are more rudimentary systems. For example, simple, hand-dug channels for water distribution are common. Here, flow rates and transmission losses are often only roughly estimated, based on visual observations, irrigation schedules, and experience (Forkutsa et al., 2009). Irrigation rates become even more uncertain in case of excess irrigation. Here, in addition to inflow rates, drainage rates are required to calculate the net water input into the soil.

Motivated by the problem of inaccurate or unavailable precipitation measurements, Brocca et al. (2013) developed an approach to estimate precipitation amounts by analyzing soil moisture changes. To do this, they inverted the soil water balance equation. Water balance components required in addition to soil moisture change were either neglected (evapotranspiration and surface runoff) or estimated using empirical methods (drainage). Soil moisture changes can be derived from in situ observations (Brocca et al., 2015) or from satellite-based radar data (Brocca et al., 2014). Later, this approach was also used to estimate irrigation volumes (Brocca et al., 2018; Dari et al., 2020; Filippucci et al., 2020).

The aim of the present study is to present a method that allows a reliable estimation of the water balance components ET_{act}, GWR, and water inflow (precipitation and irrigation) with moderate measurement efforts. This approach is particular suitable for irrigated areas, where irrigation water inflows are insufficiently known and difficult to measure. For this purpose, a combined approach of soil moisture and radiation balance monitoring, remote sensing data analysis, and numerical modeling is applied. Unknown irrigation amounts are estimated based on soil moisture data and an inversion of the soil water balance equation. This is accompanied by an iterative process in which other required water balance components are estimated stepwise by numerical modeling using Hydrus (Šimůnek et al., 2008).

5.2 Study site

The approach is applied to an agricultural test field of the University of Agriculture Faisalabad in Punjab, Pakistan, which is part of the Lower Chenab Canal (LCC) system (Fig. 2-1, Becker et al. 2019). The test field has a dimension of 110 m x 30 m and the crop cycle during the investigation period from July 2018 to June 2019 is cotton (Kharif season, monsoon) and wheat (Rabi season, inter-monsoon). The water allocation is realized with the Warabandi system (Narain, 2008) and applied to the plants by flood irrigation. While for the total LCC system and its larger irrigation subdivisions fairly precise canal supplies are known, on the field-scale only sparse data are available on irrigation operations and irrigation volumes (Ahmad et al., 2009). For a more detailed description of the study area see chapter 2.

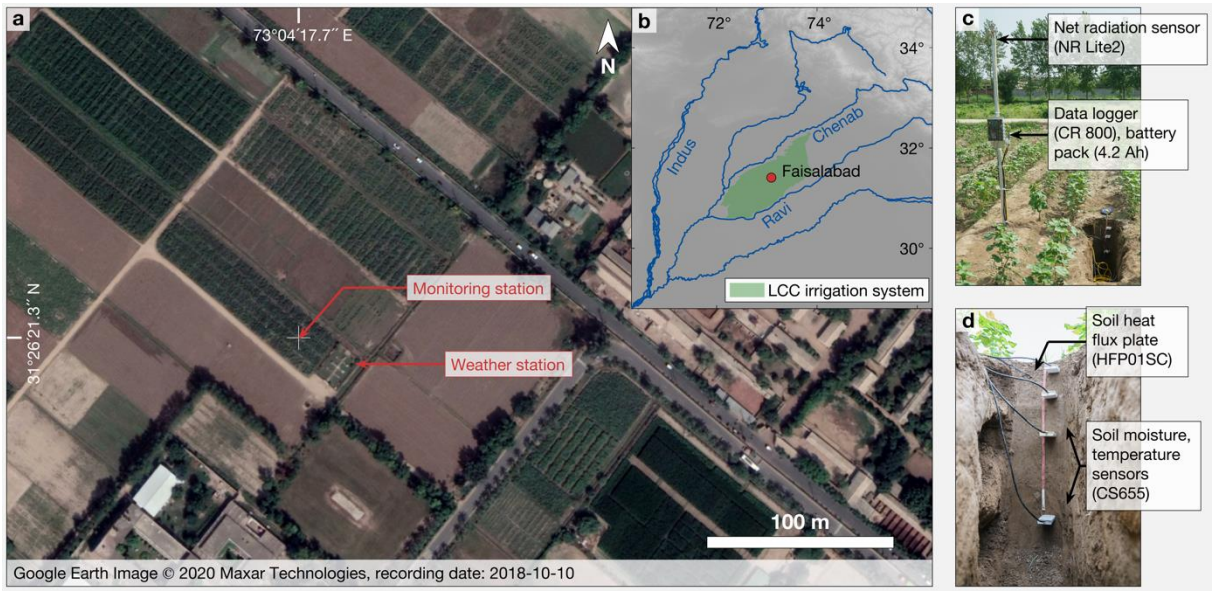

Fig. 5-1: (a) True color satellite image from 2018-10-10 of the test site. (b) Overview map with the Lower Chenab Canal (LCC) system. (c) Monitoring station on the test field with young cotton plants. (d) Subsurface part of the monitoring station with soil heat flux plate and four soil moisture and temperature sensors.

5.3 Methods

Monitoring and soil sampling

A monitoring station was installed in July 2018 on a test field of the University of Agriculture Faisalabad (UAF) in Pakistan (Figure 5-1). The station is located at 73°04'17.7'' N, 31°26''21.3'' E and is equipped with the following devices:

(i) one net radiometer (NR-Lite2, Kipp & Zonen), mounted at a height of 2.5 m to a vertical pipe;

(ii) one self-calibrating soil heat flux plate (HFP01SC, Hukseflux), installed in a depth of 8 cm below ground level (b.g.l.);

(iii) four soil moisture and temperature sensors (CS650, Campbell Scientific), installed in a depth of 10, 20, 40 and 80 cm b.g.l., respectively;

(iv) one data logger (CR800, Campbell Scientific), mounted to the vertical pipe of the net radiometer and set to a 1-minute recording interval;

(v) one 12 V battery with a capacity of 4.2 Ah.

This station was in operation from 2018-07-03 to 2019-06-01. Due to empty batteries or full memory storage the records show some gaps. The cumulative gap length is 51 days, and the number of full days with records is 281. This database is available via https://doi.pangaea.de/10.1594/PANGAEA.921389 (Schulz, 2020).

Additionally, routine weather data such as air temperature (minimum, maximum and mean), relative humidity, precipitation, class A pan evaporation, sunshine duration, and wind speed are available from a nearby (< 100 m) weather station.

During the installation of the monitoring station, three undisturbed soil samples were taken using 250 ml soil sample rings in depths of 10, 40 and 80 cm b.g.l., respectively. The samples were oven-dried at 105°C for 24 hours and weighted to derive the bulk density. Subsequently, the three sub-samples per layer were combined and wet sieved with various mesh sizes to quantify the mass fractions for particle diameters larger than 63 µm. For particle diameters smaller than 63 µm, a sedimentation analysis was carried out. Results are given in the Tab. A 5-1 (Annex).

Overview of data processing methodology

To estimate the water balance components ET_{act}, GWR, and water inflow an approach was applied, which comprises a series of data processing steps (Figure 5-2). First, reference crop evapotranspiration (ET_0) was estimated using energy balance data from the installed monitoring station and routine weather data. Subsequently, surface reflectance data from satellite images (Sentinel-2) are used to derive time-variable plant-specific information such as leaf area index (LAI), which then serves to partition ET_0 into energy limited evaporation (E_{max}) and transpiration (T_{max}). The next step is a first approximation of the inflow (sum of precipitation and irrigation) by inverting the soil water balance equation. Required changes in soil moisture storage are derived from interpolation and integration of the observed soil moisture data. To account for uncertainties, resulting from interpolation, a range of soil moisture changes are calculated by applying different interpolation schemes. Moreover, at this stage, drainage is neglected and the sum of E_{max} and T_{max} serves as a first guess of ET_{act}.

Afterwards, a first series of forward simulations of the water flow in the unsaturated zone and the root water uptake using Hydrus are performed. The upper boundary conditions for this model are first approximations of the water inflow, E_{max}, and T_{max}. To further account for soil parameter uncertainties, simulations are run with a quite wide range of a priori estimates of van Genuchten parameters, derived from a soil texture analysis. This first modeling step yields a range of estimates for ET_{act} and drainage (flux at 1 m b.g.l.), which are then used to better estimate the inflow from the inverted soil water balance equation. The final step is to incorporate these improved inflow estimates into the model and calibrate the soil parameters by inverse modeling. Here, the observed soil moisture data form the reference figure for calibration. Forward simulations with calibrated soil parameters and improved inflow estimates result in final estimates for ET_{act} and GWR. A detailed description of all processing steps is given in the following sections.

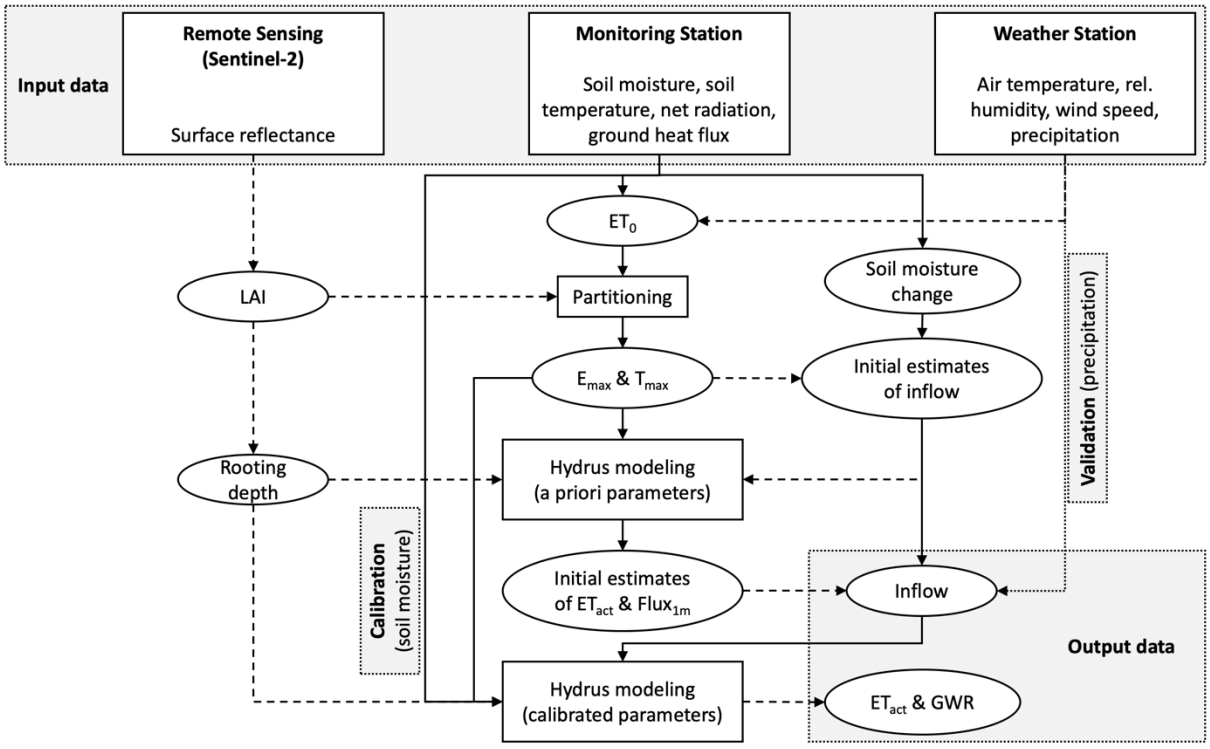

Fig. 5-2: Overview of data processing methodology

Evapotranspiration – Radiation balance

Similar to the above described SEBAL-method, the amount of energy, which is available for the latent heat (LE) and the sensible heat (H), is defined by the one-dimensional surface energy balance (equation 1, Hartmann, 2016).

$$LE + H = Rn - G \tag{17}$$

While the net radiation (Rn) is directly measured by the net radiometer, the estimation of the ground heat flux (G) requires some computation. The heat flux, which is measured with the installed

monitoring station, is the flux in a depth of 8 cm (G_{8cm}). To derive the ground heat flux, a storage term (S_{heat}) needs to be accounted for, which describes the change of heat stored in the layer above the heat flux plate (Eq. 18).

$$G = G_{8cm} + S_{heat} \tag{18}$$

The storage term depends on the volumetric heat capacity of the moist soil (C_s) and is defined in equation 19 (Hartmann, 2016).

$$S_{heat} = dT_s \cdot \frac{dz}{dt} \cdot C_s \quad \text{with} \quad C_s = \rho_s \cdot c_s \cdot f_s + \rho_w \cdot c_w \cdot f_w \tag{19}$$

Estimates for the soil temperature change (dT_s) over the time period (dt) as well as the volume fraction of water (f_s) of the upper soil layer with a thickness (dz) of 8 cm base on records from the uppermost (10 cm b.g.l.) soil moisture and temperature sensor. The product of the soil density (ρ_s) and the volume fraction of soil (f_s) is the previously determined bulk density. The specific heat capacity of most dry mineral soils (c_s) and of water (c_w) are 837 $Jkg^{-1}K^{-1}$ and 4190 $Jkg^{-1}K^{-1}$, respectively, and the density of water (ρ_w) is assumed to be 1.00 gcm^{-3} (Hanks, 1992).

Evapotranspiration – Leaf area index and rooting depth

Leaf area index (LAI) and rooting depth are plant characteristics, which are required to quantify transpiration, i.e. LAI serves for partitioning of evapotranspiration (Allen et al., 1998b) and rooting depth defines the soil depth from which plants can take up water (Feddes et al., 1976).

Leaf area indices (LAI) for the test site are estimated using red and near-infrared reflectance data. This approach was introduced by Clevers (1989) and bases on an empirically derived linear relationship (Eq. 20) between LAI [m^2m^{-2}] and the weighted difference vegetation index (WDVI).

$$LAI = 0.109 \cdot WDVI - 0.3233 \tag{20}$$

Furthermore, Clevers (1989) suggests to calculate the WDVI using red (R_{670}) and near-infrared (R_{870}) reflectance data of the plant canopy and the soil ($R_{670,soil}$ and $R_{870,soil}$), respectively (Eq. 21).

$$WDVI = R_{870} - C \cdot R_{670} \quad \text{with} \quad C = \frac{R_{870,soil}}{R_{670,soil}} \tag{21}$$

Given the availability of high-resolution satellite data, Clevers et al. (2017) revisited this approach and proofed its usability with space-borne multispectral reflectance data from the Sentinel-2 satellite mission. An advantage of this approach, especially for small-scale applications such as in the presented case, is the relatively high spatial resolution of 10 m of the required spectral information, i.e. band 4 (665 nm) and band 8 (842 nm).

For this study, 65 sets of satellite images are analyzed, covering the monitoring period from 2018-07-10 to 2019-06-01. To allow for the further use of these scenes, the data are converted from top-of-atmosphere into top-of-canopy reflectance using the atmospheric correction procedure sen2cor (Louis et al., 2016). Afterwards, images with haze or clouds covering the test field are excluded. For the remaining images, reflectance values of band 4 and 8 are extracted from the pixel at the location of the monitoring station. To calculate the slope of the soil line (C in Eq. 21) averages of the band values are used at the same location of images at times between cropping periods, i.e., with bare soil.

Rooting depth (r_d) is assumed to be proportional to the soil cover fraction (SCF) (equation 6; e.g. Wongkaew et al., 2018).

$$\frac{r_d}{SCF} = constant \tag{22}$$

The value for the constant in equation 21 can be determined by dividing the maximum rooting depth by the maximum SCF. While maximum rooting depths are tabulated for various crop types in the FAO Irrigation and Drainage Paper No. 56 (Allen et al., 1998b), SCF is calculated according to equation 23 (Campbell and Norman, 1998).

$$SCF = 1 - e^{(-K_b \cdot LAI)} \tag{23}$$

Plant-specific canopy extinction coefficients (K_b) are also available from Allen et al. (1998b). The extinction coefficients for cotton and wheat are 0.65 and 0.55, and the maximum rooting depths are 1.35 m and 1.65 m, respectively.

Evaporation – Energy-limited ET

Estimates of energy-limited (soil) evaporation and energy-limited transpiration, i.e. not limited by the availability of water, are derived from methods suggested in the FAO Irrigation and Drainage Paper No. 56 (Allen et al., 1998b). Parts of these methods are slightly adapted to better meet the requirements of the numerical simulation tool Hydrus. First, reference crop evapotranspiration (ET_0) is calculated based on the FAO Penman-Monteith method, thoroughly described by Allen et al. (1998b), using data from the monitoring station (Rn and G) and routine weather data from the nearby weather station. In order to separate ET_0 into a plant-specific and energy-limited transpiration and evaporation component, the dual crop coefficient approach is appplied. Here, transpiration is calculated without considering limitations in soil water availability and thus, constitutes maximum possible transpiration (T_{max}), equation 24.

$$T_{max} = ET_0 \cdot K_{cb} \tag{24}$$

The basal crop coefficient (K_{cb}) characterizes the growth stage of the plant and can be derived from the time-variable LAI (Eq. 25).

$$K_{cb} = K_{c\,min} + \left(K_{cb\,full} - K_{c\,min}\right) \cdot \left(1 - e^{-0.7 \cdot LAI}\right) \tag{25}$$

$K_{c\ min}$ is the minimum crop coefficient for bare soil (K_c = 0.15) and $K_{cb\ full}$ is the plant-specific K_{cb} during the mid-season at peak plant height. $K_{cb\ full}$ for cotton and wheat are 1.15 and 1.1, respectively (Allen et al., 1998b).

Evaporation from the soil (E) depends strongly on the growth stage of the plant, i.e. the more of the soil surface is covered by plants, the lower the evaporation. In contrast to the previous calculation of transpiration, evaporation additionally bases on the availability of soil water for evaporation, described by the evaporation reduction coefficient (K_r, Eq. 26). However, for further use in Hydrus we are only interested in the energy-limited (maximum possible) evaporation (E_{max}). Therefore, we set K_r to its maximum value of 1, which results in equation 27.

$$E = ET_0 \cdot K_r \cdot (K_{c\,max} - K_{cb}) \tag{26}$$

$$E_{max} = ET_0 \cdot (K_{c\,max} - K_{cb}) \tag{27}$$

The maximum crop coefficient ($K_{c\ max}$) represents the upper limit for the actual evapotranspiration, considering the constraints of the available energy (Eq. 28).

$$K_{c\,max} = max\left(\left\{1.2 + [0.04 \cdot (u_2 - 2) - 0.004(RH_{min} - 45)] \cdot \left(\frac{h}{3}\right)^{0.3}\right\}, \{K_{cb} + 0.05\}\right) \tag{28}$$

Wind speed at 2 m height (u_2) and daily minimum relative humidity (RH_{min}) are obtained from the nearby weather station. The mean plant heights during mid or late season stages (h) for cotton and wheat are 1.2 m and 1.0 m, respectively (Allen et al., 1998b).

Crop coefficients and evapotranspiration rates are initially calculated on a daily basis. However, hourly values are required for the model. To downscale daily values to hourly values, daily rates of E_{max} and T_{max} are multiplied by the hourly relative diurnal variations of the theoretically maximum available energy for evapotranspiration (LE + H), exemplified for E_{max} in equation 29 (indices 1-24 represent the hours of a day).

$$\begin{pmatrix} E_{max,1} \\ E_{max,2} \\ \vdots \\ E_{max,24} \end{pmatrix} = E_{max} \cdot \begin{pmatrix} LE_1 + H_1 \\ LE_2 + H_2 \\ \vdots \\ LE_{24} + H_{24} \end{pmatrix} \Big/ \sum_{h=1}^{24} LE_h + H_h \tag{29}$$

To allow a comparative analysis to the estimation of energy-limited evaporation and transpiration described above, which bases on energy balance data from the monitoring station and routine weather data from the nearby weather station, two alternative methods are applied. First, same procedure as

described above is followed, but for the estimation of ET_0 only data from the nearby weather station is used, i.e. air temperature, relative humidity, wind speed and sunshine hours (Allen et al., 1998b). Second, the theoretical maximum available energy for evapotranspiration (LE + H) is calculated, using only data from the monitoring station, i.e. Rn and G. Here, the temperature-dependent latent heat of vaporization was calculated using the temperature recordings of the upper CS650 sensor and an approach proposed by Henderson-Sellers (1984). These two alternative methods are evaluated by comparing them to the previously presented approach and may serve as an alternative when not all required data are available.

First approximation of inflow

For days with observed positive changes in soil water storage, it is assume that either precipitation or irrigation must have taken place. For these days the amount of water inflow (sum of irrigation and precipitation) is calculated, using the water balance of the first meter of the unsaturated zone (Eq. 30).

$$Inflow = dS_{1m} + flux_{1m} + ET_{act} \quad (30)$$

Daily changes of soil moisture storage in the upper 1 m (dS_{1m}) result from the water volume stored at the end of the day (t) minus the water volume stored at the end of the previous day (t-1). To estimate these water volumes, first, temperature corrected (Campbell Scientific, 2018) measurements of volumetric water content (θ) at 10, 20, 40 and 80 cm b.g.l. are extrapolated, yielding continuous values every 10 cm. Subsequently, extrapolated soil moistures are integrated over the first 1 m (dz, Eq. 31).

$$dS_{1m} = \int_0^{1\ m\ b.g.l.} \theta_t(z)\ dz - \int_0^{1\ m\ b.g.l.} \theta_{t-1}(z)\ dz \quad (31)$$

This approach introduces some uncertainty as the application of different extrapolation schemes result in different daily changes of soil moisture storage. To quantify this uncertainty, the extrapolation is run with the five standard interpolation methods that are available in Matlab 2020a: “linear”, “nearest”, “makina”, “pchip” and “spline”. The lowest and the highest estimate for dS_{1m} constitute the lower and upper bound of the uncertainty range, respectively. Since it is not known too much about the variables $flux_{1m}$ (flux at 1 m depth, previously referred to as drainage) and ET_{act}, for now, the initial assumption $flux_{1m} = 0$ and $ET_{act} = E_{max} + T_{max}$ is applied. This step serves only for a first estimation of the inflow. At the second step better estimates of $flux_{1m}$ and ET_{act} will be available. Nevertheless, it is expected that this assumption is not too far from reality. On a daily basis, the expected $flux_{1m}$ is quite low compared to the relatively large, periodically applied inflow quantities that are common in flood irrigation. Moreover, irrigation contributes to a constant water supply for evaporation, which allows the assumption that evapotranspiration is mostly energy limited.

Numerical modeling

Modeling of water flow and root water uptake are performed with the numerical simulation tool Hydrus (Šimůnek et al., 2008). The model set up for this study represents a one-dimensional vertical soil profile, divided into three layers of 0-15 cm b.g.l., 15-60 cm b.g.l. and 60-200 cm b.g.l., and it covers a period from 2018-08-16 to 2019-05-04. The vertical spatial resolution, i.e., the distance between two neighboring nodes, is 1 cm and the temporal resolution is 1 hour. Time variable energy-limited evaporation and transpiration, and water inflow (sum of irrigation and precipitation) constitute the upper boundary. As the simulated soil profile is quite deep (2 m b.g.l.) and still far away from the groundwater table (approximately at 10 m b.g.l.), a significant capillary rise from deeper layers into the profile is not expected and thus, lower boundary is set to free drainage. The hydraulic properties of the soil are described by the van Genuchten-Mualem model (van Genuchten, 1980). To account for temperature changes and their effects on the soil hydraulic properties, the heat flow is also simulated and the temperature correction function in Hydrus is activated. Thermal conductivity parameters of loam are derived from the internal database of Hydrus (Chung and Horton, 1987). The time-variable upper and lower Dirichlet boundary conditions of the heat flow model are linearly extrapolated temperatures of the soil surface and 2 m b.g.l., respectively. Parallel to the flow modeling, root water uptake is simulated using the Feddes model (Feddes et al., 1976). Parameter of the Feddes model for cotton and wheat base on values provided by Taylor & Ashcroft (1972), cited in Forkutsa et al. (2009) and Wesseling (1991), respectively.

Final estimation of inflow

Final estimates of inflow are derived from a first model application. The van Genuchten parameters (VGP) and the saturated hydraulic conductivity (Ks) of the model are not yet calibrated and only a priori estimates based on the particle size distribution and the bulk density are available. These estimations are predicted by pedotransfer functions implemented in the Rosetta model (Schaap et al., 2001; Zhang and Schaap, 2017). This is an elegant and frequently used approach. However, due to its empirical nature (pedotransfer functions are derived from a neural network analysis of a soil database), it is associated with uncertainties that are quantified with the standard deviations (σ) resulting from a bootstrap-resampling method (Zhang and Schaap, 2017). In this study, except for the saturated water content (θ_s), the range of the a priori estimation of the hydraulic parameters is defined as their mean predicted value $\pm\ 2 \cdot \sigma$. Due to intense irrigation, i.e., high availability of water, we assume that the highest observed volumetric water content is a good estimate for θ_s.

Now we perform a series of forward simulations with all possible parameter configurations for all three soil layers and the five initial estimates of the inflow. The resulting sets of simulations of $flux_{1m}$ and

ET_{act} are used to improve the calculation of the inflow (equation 30). Maximum and minimum estimates represent the uncertainty range of the inflow.

Parameter optimization

With an estimation of the inflow boundary condition and a quantification of its uncertainty, an optimization of the hydraulic parameters can be carried out. For this purpose, an inverse modeling approach using the PEST (Model-Independent Parameter Estimation and Uncertainty Analysis) tool (Doherty, 2015) is applied. Here the global optimization tool CMA-ES (Covariance Matrix Adaptation Evolution Strategy) is employed to minimize the objective function, i.e. the sum of squared residuals of simulated and observed volumetric soil moisture (Hansen, 2006). In analogy to the estimation of the inflow uncertainty, the mean predicted value $\pm\ 2 \cdot \sigma$ from the Rosetta model as the parameter range for the VGPs and K_s is used during optimization. θ_s is an exception here as well. This parameter is kept constant on its a priori estimated value, i.e., the highest observed volumetric water content. The optimization procedure is applied for the minimum, mean and maximum inflow estimations, resulting in three sets of calibrated hydraulic parameters.

5.4 Results and Discussions

Evapotranspiration – Radiation balance

The observed average energy flux at the surface (top of canopy or ground) of the test site is 119 Wm^{-2} and 0.2 Wm^{-2} from net radiation (Rn) and ground heat flux (G), respectively (Figure 5-3a). With this, ground heat flux contributes on average less than one percent to the total energy budget (Rn-G). However, looking at the daily values, the share of ground heat flux ranges approximately between -50% to 10% with negative values referring to an energy flow from the soil into the atmosphere and positive values vice versa. The mean absolute value of the daily fraction is 16%. Typically, it is assumed that the magnitude of the ground heat flux in day periods is very small and may therefore be neglected (Allen et al., 1998b). However, this seems to be too much of a simplification for the system studied here. A possible explanation can be found in the specific conditions for the test site. Due to the intensive irrigation, the soil is almost always moist, which results in a rather high heat capacity of the soil, since the specific heat capacity of water is more than four times higher than that of mineral soil (Hanks, 1992). Combined with a high but variable energy input due to climatic conditions, this can result in a high energy storage in the soil, which does not allow for quick heat equalization.

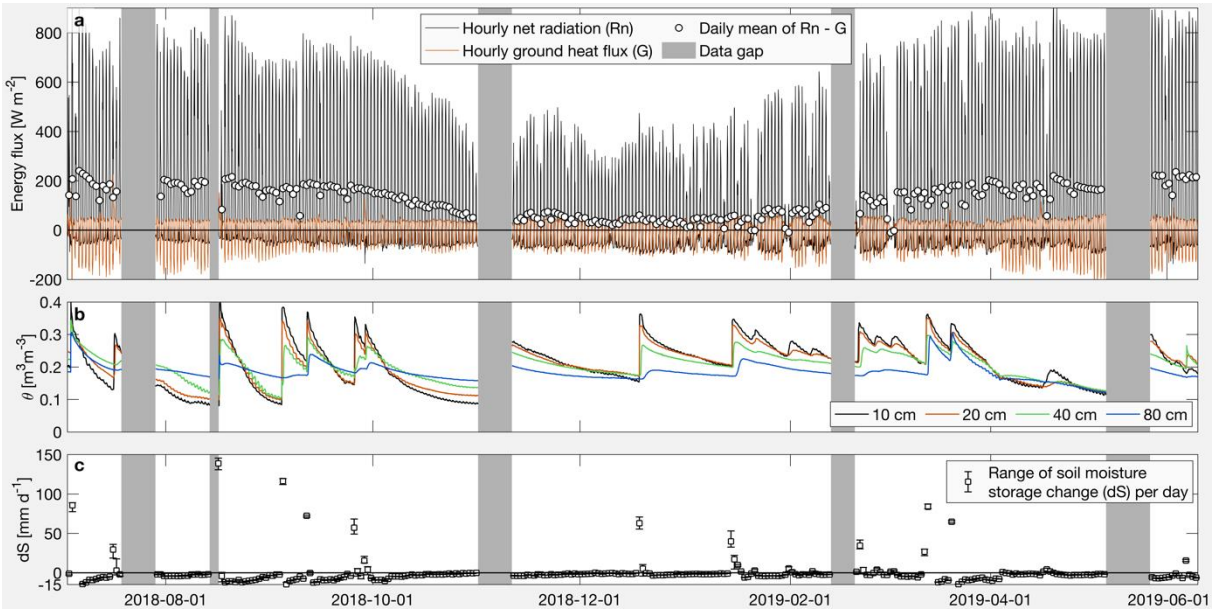

Fig. 5-3: (a) Records of net radiation and ground heat flux. (b) Records of volumetric water content. (c) Daily changes in soil moisture storage.

Leaf area index and rooting depth

The basis for estimating LAI and rooting depth is the canopy or soil reflection data from the Sentinel 2 satellite mission. After sorting out the images with haze or cloud cover over the test field, 11 images for cotton, 9 images for wheat and 7 images for bare soil remained for the observation period. From the images showing bare soil, we calculated a value of 1.39 for the slope of the soil line (C in equation 21). For both cotton and wheat, the temporal development of the LAI clearly shows the different growth stages from early plant development to harvest (Fig. 5-4a). Observed values for cotton and wheat range from 0.1 to 1.7 and from 0.4 to 3.2, respectively. The rooting depth depends on the constant canopy extinction coefficients and the time-dependent LAI and thus shows a similar temporal pattern as the LAI.

Energy-limited evapotranspiration

Energy-limited evapotranspiration (E_{max} + T_{max}) show pronounced inter-annual variabilities with higher rates during the hot summer months (up to almost 10 mmd^{-1}) and significantly lower rates during the temperate winter months (Fig. 5-4b). The partitioning of evapotranspiration is based on the dual crop coefficient concept. Like the rooting depth, crop coefficients highly depend on the LAI. The more photosynthetically active leaves the plant has, the larger the basal crop coefficient (K_{cb}) and thus the higher the share of transpiration. In case of bare soil, K_{cb} is zero and only evaporation takes place. On average, the sum of K_{cb} and the share for E_{max} ($K_{c\,max}$ - K_{cb}) is 1.11 (Fig. 5-4a). This means that the energy-

limited evapotranspiration of the test site is 11% higher than the reference crop evapotranspiration (ET_0), i.e., ET_{act} of short, green and well-watered grass.

This is quite an important observation, as it is not uncommon to use ET_0 as so called potential evapotranspiration, which then defines the upper limit for actual evapotranspiration in Hydrus (Šimůnek et al., 2013). In most cases this is a well working assumption. However, in cases with a high energy input, tall crops and almost permanent excess of water, e.g. through irrigation, actual evapotranspiration may easily exceed ET_0 (Kirkham, 2014; Rosenberg, 1974).

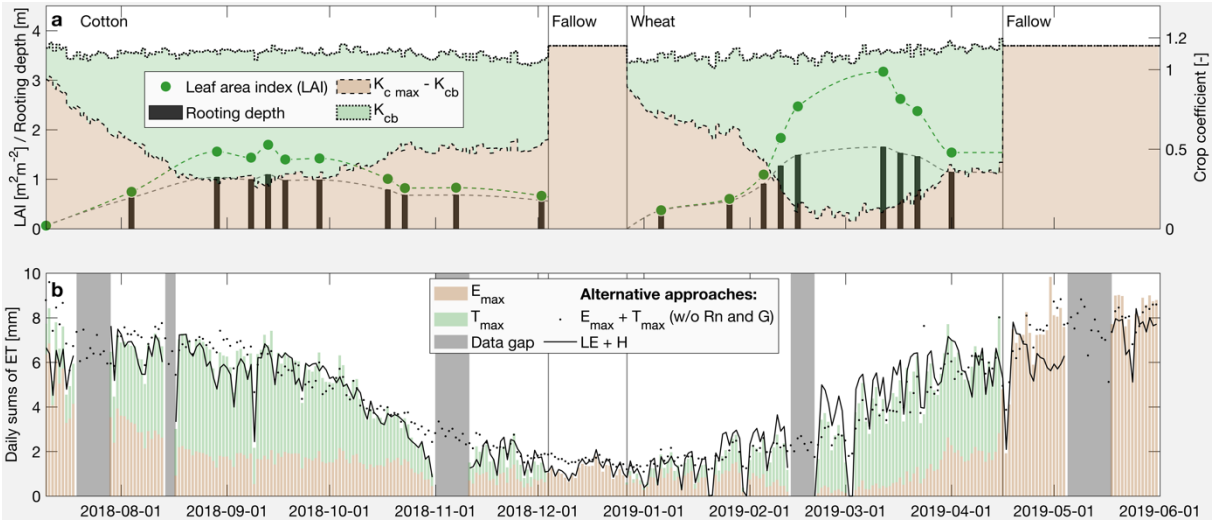

Fig. 5-4: (a) Temporal evolution of LAI, rooting depth and crop coefficient components. (b) Daily sums of energy-limited evaporation (E_{max}) and transpiration (T_{max}), and alternative estimates for energy limited evapotranspiration estimates.

Noteworthy findings also result from the comparison of the different possibilities to estimate evapotranspiration. For this study, energy-limited evaporation (E_{max}) and transpiration (T_{max}) estimates are used and derived from methods proposed in the FAO Irrigation and Drainage Paper No. 56 (Allen et al., 1998b) using energy balance data, i.e. Rn and G, from the monitoring station as well as routine weather data from the nearby weather station. Additionally, the energy-limited evapotranspiration is estimated with two alternative methods. One of them uses only energy balance data from the monitoring station and the other one uses only routine weather data. Results from the two alternative methods show a similar pattern as the approach presented here (Fig. 5-4b). The root mean square error (RMSE) of the FAO approach using only routine weather data and the approach using only energy balance data compared to the FAO approach based on both data sets are 0.73 mm and 0.69 mm, respectively. While the first mentioned alternative seems to slightly overestimate the energy-limited ET (mean error of +0.23 mm), the energy balance approach shows on average almost no difference (-0.04 mm). At first, the even better performance of the energy balance approach is somewhat

surprising, as it neglects any energy loss or input through sensible heat flux (H). However, the special conditions of the study area, i.e. almost constantly well-irrigated soil and relatively high temperatures, associated with low advection and low Bowen ratios, may explain this finding (McMahon et al., 2013; Priestley and Taylor, 1972). In this regard, it should also be noted that the deviation of LE + H related to the energy-limited ET increases during the first half of the last fallow period when the soil dries out (compare Fig. 5-3b and 5-4b). This supports the previously given explanation and likewise shows the limited validity of this alternative approach. Nevertheless, under the given conditions, i.e. irrigated agriculture in a semi-arid environment, LE + H could be used as a first estimate for the energy-limited ET. This approach is quite attractive because of its simplicity. It does not require any assumptions for the FAO Penman-Monteith method, nor is it necessary to compute crop coefficients.

First approximation of inflow

Daily soil moisture changes and energy limited evapotranspiration estimates constitute the base for the first approximation of inflow. Interpolation and subsequent integration of the observed soil moisture data (Fig. 5-3b) yield daily changes in soil moisture storage (Fig. 5-3c). Abrupt positive changes in soil moisture result either from precipitation or irrigation events and range from a few millimeters to almost 150 mm per day. More frequent, but less pronounced, are negative values of soil moisture storage changes representing water loss due to evapotranspiration and deep percolation. Here the maximum absolute rate is about 18 mm per day. The range of values resulting from the application of different interpolation schemes represents the uncertainty range.

Calculated first approximations of the daily inflow amounts for the different interpolation schemes are given in Table A 5-2 (Annex). Estimates for single inflow events show differences of up 14 mm and their relative cumulative uncertainty range is 9.5%.

Final estimation of inflow

To improve the estimation of inflow, in addition to soil moisture change in the first meter (dS_{1m}), estimates of ET_{act} and flux at 1 m depth ($flux_{1m}$) are required. These values and their uncertainties are derived from a series of forward simulations (Fig. 5-5a). For this, all possible combinations of the different initial inflow estimates, which are based on the different estimates of the soil moisture storage changes, and the a priori van Genuchten parameters (VGP) are used (Fig. 5-5b). The basis for the a priori parameter estimates is the grain size fractions and bulk densities of the three soil layers. These values and the resulting VGP are given in Table A 5-1 and A 5-3 (Annex), respectively. Not surprisingly, the derived initial set of ET_{act} and $flux_{1m}$ estimates show a rather wide range (Fig. 5-5a).

During the modeling period from 2018-08-16 to 2019-05-04, the mean initial ET_{act} and the mean initial $flux_{1m}$ are 3.5 and 0.8 mmd^{-1} with a relative uncertainty range of 64% and 246%, respectively. At first glance, these uncertainties seem to be quite large. However, these values are only used for inflow estimation, and compared to the relatively large soil moisture changes of up to almost 150 mmd^{-1} this first impression is somewhat relativized. Finally, equation 30 is applied to calculate three inflow time series using the mean, minimum and maximum values of dS, initial ET_{act}, and initial $flux_{1m}$, respectively. The final inflow estimates range from small events of only a few millimeters up to events of more than 150 mm (Tab. A 5-5).

Comparing the uncertainty range of the first approximation of inflow (introduced by the application of different interpolation schemes) and the final inflow estimates (based on both, interpolation and a priori soil parameter uncertainty) provides information about the sensitivity of the different interpolation methods and soil parameters. While the first approximation of the inflow shows a mean relative uncertainty of 9.5%, it increases to 23.8% for the final estimates (compare Tab. A 5-2 and A 5-5, Annex). This suggests that both sources of uncertainty are quite similarly sensitive.

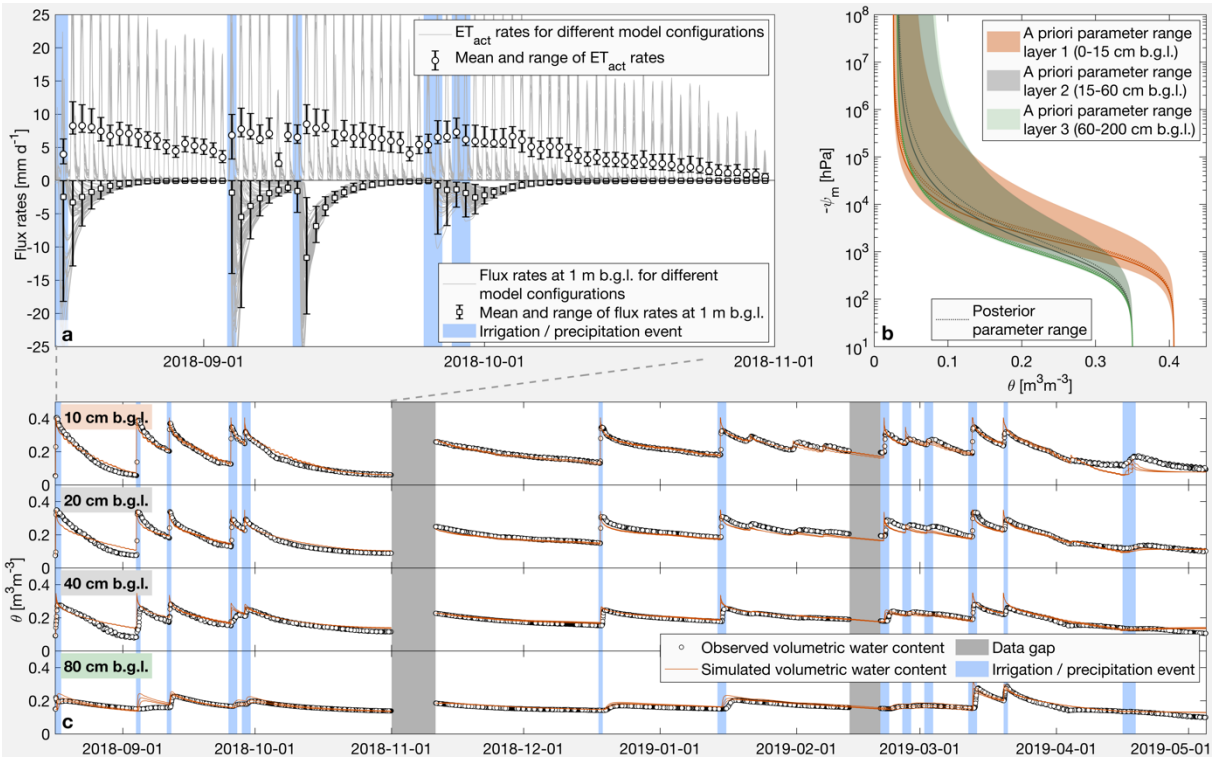

Fig. 5-5: (a) Exemplary data sets from the first modeling stage with first estimates of actual evapotranspiration and flux at 1 m b.g.l. (b) Soil water retention curves representing the a priori and posterior (optimized) van Genuchten parameter ranges of the three soil layers. (c) Simulated and observed volumetric water contents of the four sensor positions for the entire modeling period from 2018-08-16 to 2019-05-04.

Parameter optimization

The second stage is the VGP optimization. With the exception of the saturated water content (θ_s), the upper and lower parameter limits for optimization are defined by the a priori parameter range (Fig. 5-5b). θ_s of layer 1 is kept constant at the highest observed water content (θ_{obs}) of 40.6% recorded by the sensor at 10 cm b.g.l. θ_s of layer 2 is set to 35.0%, the highest observed values of the sensor at 20 cm b.g.l. Due to comparable soil properties of layer 2 and layer 3 and the difficulty of reaching saturation at greater depth, a value of 35.0% for θ_s of layer 3 is assumed. The calibration procedure is performed separately for the minimum, mean and maximum inflow estimates. This results in three different optimized parameter sets, representing the range of the posterior parameter uncertainties (Figure 5b). Values for the optimized VGP are given in Table A 5-4 (Annex). The simulated volumetric water contents with the best fitting parameter sets of the three inflow cases are quite similar and show fairly satisfactory fits to the observed values (Fig. 5-5c). The goodness-of-fit, expressed as root mean squared error, of the minimum, mean and maximum inflow case is 2.3%, 2.2% and 2.2% respectively.

Prognostic runs

Finally, the model is applied in a forward simulation using the three different optimized parameter sets to estimate ET_{act} and the flux in 2 m ($flux_{2m}$), which constitutes the bottom flux of the model, and their associated uncertainties (Fig. 5-6). The simulation with the parameters, resulting from the optimization using the mean inflow estimate, yields 769 mm and 297 mm of cumulative ET_{act} and $flux_{2m}$, respectively. These outflow components are balanced by a cumulative inflow of 946 mm. The difference of 120 mm results mainly from an unrecorded irrigation event during the first data gap and a soil moisture storage change over the modeling period. While the ET_{act} shows only a small uncertainty range of 2.1%, the uncertainties of the $flux_{2m}$ estimates are significantly larger with a range of about 72%. This is not a surprising result. The test site is always very well-watered and consequently ET_{act} is likely most of the time as high as the sum of E_{max} and T_{max} (Fig. 5-6). In order to fulfill continuity in the water balance, the uncertainty of the inflow is therefore mainly related to the uncertainty of $flux_{2m}$. Daily sums of simulated values of inflow, ET_{act} and $flux_{2m}$, as well as their associated uncertainty ranges are given in Table A 5-5 (Annex).

Due to a rather deep groundwater table of about 10 m b.g.l., a maximum rooting depth of 1.65 m and almost always well-watered conditions, one can expect a depth of the zero-flux plane of not more than 2 m b.g.l. Also, simulation results, i.e. fluxes at various observation points, suggest a maximum depth of the ZFP of 1.47 m b.g.l. during the modeling period. Consequently, the flow direction at 2 m depth is always downward and the flux at 2 m depth ($flux_{2m}$) can be considered as groundwater recharge.

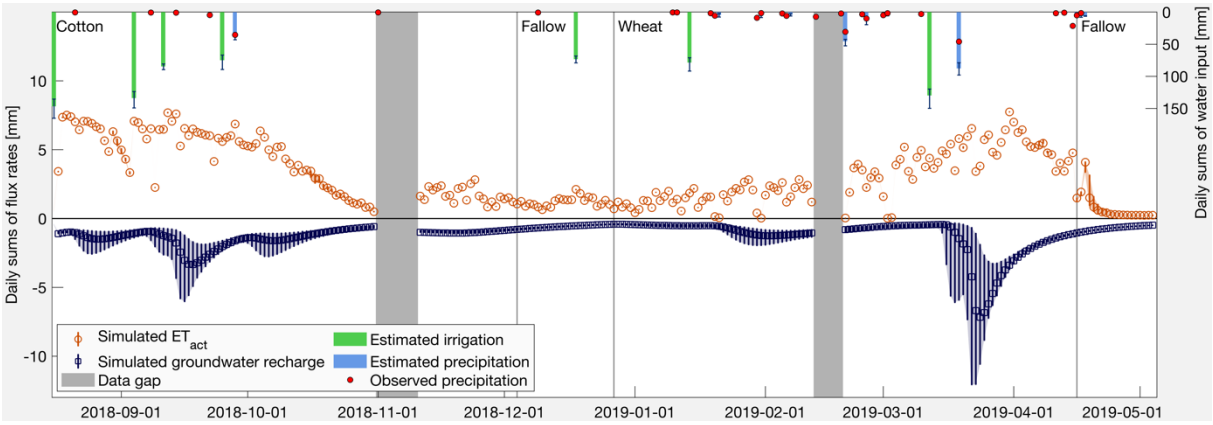

Fig. 5-6: Final inflow estimates and simulation results of actual evapotranspiration and groundwater recharge for the period from 2018-08-16 to 2019-05-04.

Comparison of results with observed data

From the nearby weather station, daily precipitation amounts are available for the modeling period. These data are used to identify precipitation events in the simulated inflow time series, i.e. inflow events that occur during a day or the following day when precipitation is recorded are attributed to precipitation. Thus, a comparison between measured and simulated precipitation is enabled. Generally, the measured precipitation pattern matches well with the one estimated from the water balance. Except for a few small precipitation events (< 5 mm) all precipitation events could be captured (Fig. 5-6). The reason for not detecting these small events is that low precipitation can be balanced out by evaporation during the day, i.e. no positive change in daily soil moisture storage is observed. Nevertheless, the sums of the measured precipitation are within the error range of those simulated during cotton and wheat cultivation (Tab. 5-1). The deviation of simulated (mean) and observed precipitation over the total simulation period is 7% (14 mm).

During the modeling period chosen in this study, mean simulated precipitation might account for only 23% of the total inflow, while irrigation accounts for 77%, illustrating the rather large blue water footprint of cotton and wheat production in the region. Similar values are reported by Ahmad et al. (2002), who analyzed the water balance of a cotton-wheat system of a comparable test field near Faisalabad from May 2000 to April 2001. For this period, they have measured a total precipitation and irrigation amount of 290 mm (26%) and 844 mm (74%), respectively.

Tab. 5-1: Seasonal sums of simulated and observed water balance components.

Period	Crop	Simulated					Observed
			ET_{act} [mm]	GWR [mm]	Irrigation [mm]	Precipitation [mm]	Precipitation [mm]
2018-08-16 to 2018-12-04	Cotton	min	407.3	94.3	406.8	32.2	42.3
		mean	411.6	132.0	440.2	36.7	
		max	413.2	186.5	493.3	43.1	
2018-12-04 to 2018-12-27	Fallow	min	27.8	12.3	68.5	0.0	0.7
		mean	27.9	13.4	73.4	0.0	
		max	28.0	14.4	79.0	0.0	
2018-12-27 to 2019-04-17	Wheat	min	308.7	90.4	190.9	141.4	154.1
		mean	309.8	138.9	208.4	168.3	
		max	310.6	209.5	241.7	205.4	
2019-04-17 to 2019-05-04	Fallow	min	9.4	11.9	0.0	9.7	6.6
		mean	12.7	12.2	0.0	12.5	
		max	16.9	12.9	0.0	14.6	
2018-08-16 to 2019-05-04	Total	min	753.2	208.9	666.2	183.3	203.7
		mean	762.1	296.5	722.0	217.5	
		max	768.6	423.3	814.1	263.1	

5.5 Conclusion

This part of the research presents a method for estimating water balance components with moderate measurement efforts. Focus lays on the specific requirements of irrigated agriculture in semi-arid and arid environments. A particular aspect is that the method does not require measurements of irrigation nor precipitation quantities to establish the water balance. This is quite useful as many irrigated areas lack the basic knowledge of these inflows. The final estimations of the actual evapotranspiration and groundwater recharge base on simulations with the numerical model Hydrus. This is also beneficial since models have predictive power and simulations could be performed to test different management scenarios, e.g. different irrigation practices or crop cycles.

Although the presented method of the inflow estimation could also be applied to solely rainfed systems, it can be reasonably assumed that precipitation can be measured more simply and with much lower uncertainties, e.g. with a rain gauge. However, it is different for irrigation. Theoretically, measurements are not complicated here either (simple flow meters would often be sufficient), but they would be needed for each field separately and farmers would have to keep accurate records. Moreover, irrigation water distribution over the field can vary considerably. This can lead to uncertainties if only one specific point is to be examined, as it is common e.g. in one-dimensional process analysis. Finally, the decision whether the presented approach is suitable depends on the research question and the available data. In this context, the two alternative methods for estimating energy limited evapotranspiration are also worth mentioning. If an accurate determination of evapotranspiration is not the primary goal, but only an estimation of irrigation or groundwater

recharge, one of the presented alternatives can also be applied. They require less data and the differences between the methods are quite small compared to irrigation amounts.

Moreover, this study could show some shortcomings in frequently applied assumptions such as using ET_0 as the upper limit for actual evapotranspiration or neglecting the ground heat flux in the energy balance. For most cases these assumptions might work and constitute valid simplifications. However, for irrigated agricultural systems with a high but variable energy input, as common in arid regions, they seem to be too much of a simplification and should be avoided.

For the study area, but also for other irrigation systems in arid environments, the complex interplay of different aspects such as waterlogging and salinity control, preservation of drinking water resources and reduction of the blue water footprint while ensuring agricultural productivity requires finely tuned management. A profound knowledge of the hydrological processes and a reliable quantification of the water balance components are essential for this.

6 Modelling climate change impacts in irrigated agricultural systems: Future yield declines despite intensification of irrigation

The previous chapters outlined the processes of model set-up and the complex calibration of the SWAT model. In addition, the elaboration of a framework to improve the estimation of water balance parameters to acquire more reliable validation data sets for modeling studies was described. Furthermore, it was explained how field data was collected which was used for the parameterization and validation of the SWAT and APSIM models.

After this careful set-up, calibration and validation, the models SWAT and APSIM can now be applied to address the main research question of how climate change will impact future agricultural water demand and productivity? In addition, it is investigated how structural model differences are impacting the simulated yield responses to changes in climate variables, and finally it is discussed which conclusion can be drawn from the findings of this study and how they can be used for a more sustainable future water management and a more sustainable productivity in this region.

6.1 Introduction

As mentioned in the introductory section (chapter 1), as part of the Indus river basin, the study region of the Lower Chenab Canal System can be considered a hot spot for the impact of climate change on water availability and agricultural productivity. Currently irrigation water in the region accounts for over 90% of the total water demand (Fischer et al., 2007). Significant climate induced changes in the upstream glacio-hydrology – the major water source for the Indus Basin - are threatening future water availability in the basin (Immerzeel et al., 2010); along with the rising temperatures that are generally projected to increase faster than on global average in the region (Saeed and Athar, 2018).

Under such conditions, water related adaptation strategies, such as increased irrigation amounts, and enhanced irrigation efficiency are possible solutions to cope with these challenges. The benefits of such adaptation measures have been studied for agricultural systems experiencing similar climate change pressures and have been suggested as possible actions (Elliott et al., 2014; Fader et al., 2016; Molden et al., 2010). Yet, sensitivities of crops to changes in temperature can be higher than those due to water availability changes (Lobell and Burke, 2008). Temperature induced stress on crop growth and productivity could counteract the potential of optimized water management for increased productivity (Lobell et al., 2015; Zaveri and Lobell, 2019).

It is therefore important to understand the role of temperature stress on crop growth and resulting plant water demand. Furthermore, improved knowledge about possible impacts of temperature and

water stress as well as their interlinkages on future crop growth will help defining adequate adaptation strategies. As mentioned above, in terms of adequate water availability for crop growths, especially in semi-arid regions, previous studies highlight that there is still very limited understanding of the potentials and limits of irrigation related climate change adaptation (Tack et al., 2017; Taraz, 2018); and that more research is needed to disentangle the effects of temperature and water stress related climate change impacts on agricultural yields (Carter *et al* 2016).

This study elaborates on how temperature stress controls agricultural productivity and plant water requirements in the study area of the intensively irrigated agricultural system in Pakistan's Punjab province. It suggests that the intuitive assumption, that increasing temperatures will inevitably lead to higher transpiration and thus to increasing irrigation demands, might not be a universal principle. This is shown by the application of two models from two different scientific disciplines. In order to tackle diversity in crop model parameterization, the hydrological SWAT model (Arnold et al., 2012) and the biophysical-crop modelling framework APSIM (Holzworth et al., 2014) are considered, to analyze climate change impacts on yield and water demand.

Numerous modeling studies regarding negative climate change impacts on yields and the potential of irrigation to mitigate these impacts exist. These studies, however, have been conducted using either hydrological models or crop models (Elliott et al., 2014). The combination of both model types is expected to allow a more detailed understanding of strengths and weaknesses of either model and thus, might result in a more reliable assessments of changes in future yield and water demand dynamics. Both models are used in an ensemble framework to analyze the climate change impacts on resulting crop growth over the study area. To this end, 9 climate model realizations are used; bias-corrected and downscaled to force both crop models under moderate (Representative Concentration Pathways - RCP 4.5) and high-end (RCP 8.5) future carbon emission scenarios. A careful modelling experiment is designed to analyze the impacts of increased temperature stress on future crop yields in connection to potential water stress. The final aim is to provide a better understanding on the interlinkages between temperature and water stress and to detect dominant drivers of declining (future) agricultural productivity - which could then aid in defining effective adaptation measures.

6.2 Material and Methods

In this study the focus s laid on analyzing the impacts of future climate change on summer crops, namely cotton, maize and rice, grown between May and October. The impact is evaluated based on changes in crop yield and relevant hydrologic and biophysical variables including evapotranspiration, irrigation demand, leaf-area growth, and biomass production (Fig. 3-1). Due to high summer

temperatures in the study region (mean daily Temperature > 30 °C), evaporative loss is highest during this time and changes in irrigation needs have a particularly strong impact on basin wide water demand. The selected crops represent high value crops with a wide distribution in the study area (Fig. 6-1A) and changes in yield will have significant economic impacts.

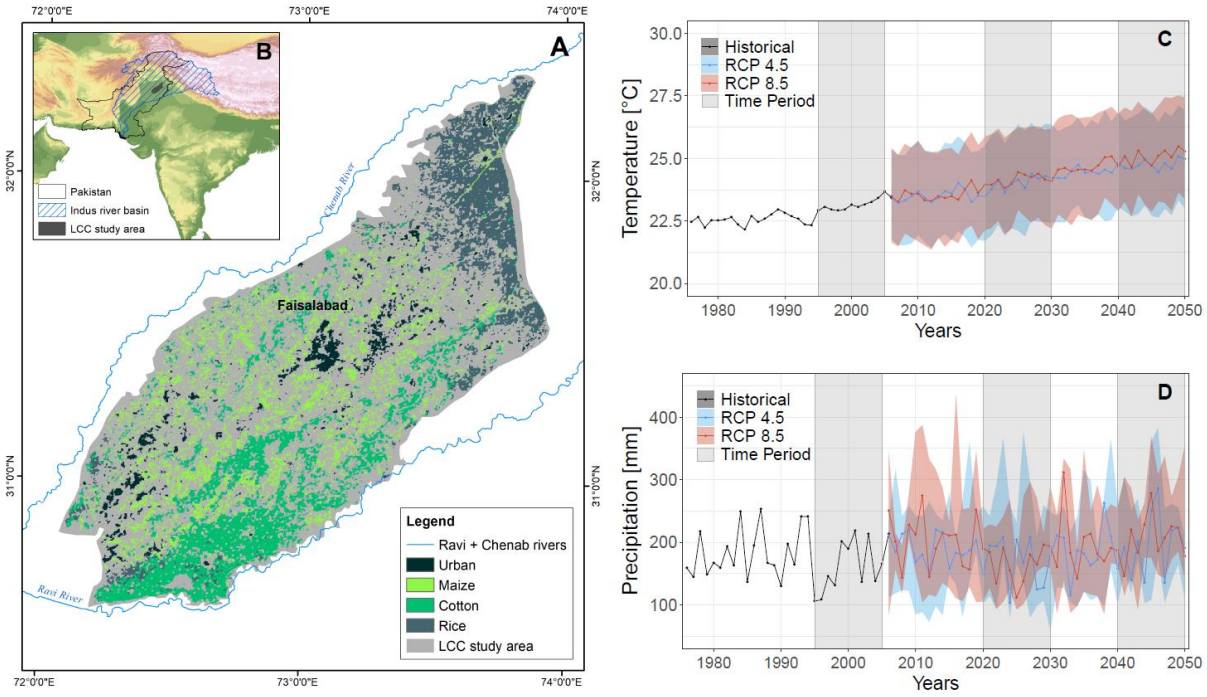

Fig. 6-1: LCC study area and spatial distribution of cotton, maize and rice growing regions (A, Land-use data from Awan et al., 2016). Lower Chenab Canal (LCC) study area, Pakistan, and the Indus River Basin (B). Mean annual temperature (C) and precipitation trends (D) of historical data (black line) and future climate projection of 9 CORDEX models (red and blue line – ensemble mean; colored uncertainty band span between 25th and 75th percentiles). Shaded grey areas (C and D) show the historical period (1996-2005) and future time periods of 2021-2030 and 2041-2050, examined in this study.

Models SWAT and APSIM

For the last past of the thesis the agro-hydrological SWAT model (Arnold et al., 1998) and the biophysical crop model APSIM (Holzworth et al., 2014) are applied. A detailed description of both models and their main strengths and differences can be found in chapter 3. As this chapter deals with the impact of climate change on agricultural water demand and productivity, a brief description of the models is given here again, especially with respect to differences in representing effects of changes in CO_2 concentrations.

The hydrological model SWAT (Soil & Water Assessment Tool) simulates the quantity and quality of water flow within catchments, incorporates detailed management strategies (e.g. irrigation schedule, planting schedule) and basic plant physiognomic stages, e.g. root development, leaf area

development, biomass change (Arnold et al., 2012; Gassman et al., 2014). Impacts of changing atmospheric CO_2 concentrations are accounted for in the estimation of potential evapotranspiration, affecting (i.e., reducing) plant water demand as well as in the estimation of plant radiation use efficiency, affecting (i.e., enhancing) the biomass production. To ensure correct and spatially differentiated parameterization, the model is calibrated following an automated and spatially distributed calibration approach (chapter 4 and Becker et al., 2019).

The Agricultural Production System Simulator (APSIM; Holzworth et al., 2014) is a biophysical crop modelling framework which simulates agricultural crop dynamics with respect to varying climatic and environmental conditions. Due to its modular approach, with individual sub-models for each crop type, it can account for plant specific reactions to climate change. For example, with individual models for cotton, rice, and maize it accounts for plant type specific carbon assimilation processes (C3 vs. C4-plants) and hence, differentiates between plant type reactions to increased atmospheric CO_2 levels.

The APSIM model parameterization for the study area was established (calibrated) following the guidelines given for the APSIM classic model (APSIM model documentation, 2021) for three crop specific modules for cotton, maize and rice. Like the SWAT model the APSIM model is run on a daily time scale, with daily climate input data. Yield estimates are taken at the time of harvest at the end of the growing season.

To allow comparison between the SWAT and the APSIM models, the soil and management parameter configurations from the calibrated SWAT model are adopted for the APSIM model. Soil parameters were furthermore verified through laboratory analysis of soil samples collected during a field campaign in the study region (chapter 5 and Schulz et al., 2021). Furthermore, a sensitivity analysis was conducted to analyze the effect of varying soil parameters on the APSIM simulated crop yields that further allowed to constrain appropriate parameters for the APSIM soil module.

Finally the modeled crop yields were compared and contrasted with observed data provided by the Agricultural Statistics of Pakistan, published by the Ministry of National Food Security & Research (MNFSR, 2021) (Fig. 6-2). Yield data for cotton, rice, and maize from the province of Punjab was taken for the years 2009-2013 and compared to simulated yield levels by SWAT and APSIM for the same period (mean of all years is shown in Fig. 6-2).

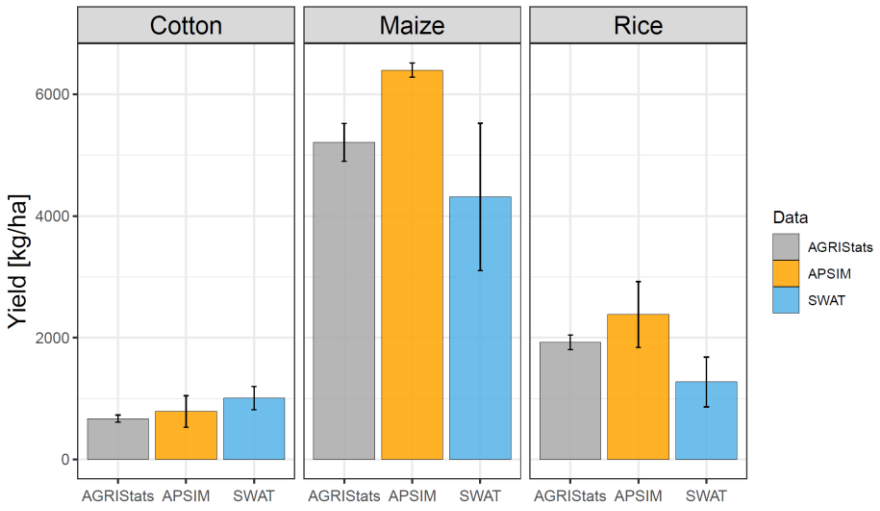

Fig. 6-2: Evaluation results of simulated yield simulations compared to observations; with the latter based on the AGRIStats = Agricultural Statistics of Pakistan. Bar heights show the mean of the years 2009-2013 and uncertainty bars show +/- one standard deviation.

Climate data sets

Daily Climate Forecast System Reanalysis data (CFSR; Saha *et al* 2010) are taken as historical reference climate data for a baseline period (1996-2005). The used data set encompasses temperature, precipitation, relative humidity, solar radiation, and wind speed. To ensure the accuracy of the baseline data set, the CFSR data is bias-corrected using climate records of three available local climate stations (see also chapter 3 for more details on the climate data pre-processing).

Climate projection datasets are taken from the Coordinated Regional Downscaling Experiment (CORDEX), which provides a suite of regional climate projections based on the Global Climate Models of the Coupled Model Intercomparison Project, Phase 5 (CMIP5; Taylor *et al* 2012). Medium (RCP 4.5) and high (RCP 8.5) greenhouse gas emission scenarios from the IPCC - Fifth Assessment Record (AR5) are considered; and the impacts in the near future (short; until 2030) and the mid future (medium; until 2050) are analyzed. The short-term time frame is selected to show the potential changes expected to occur in the coming next decade, and to show the necessity for immediate actions. The medium-term scenario is chosen to show the consequences of climate change at a time scale still relevant for today's population. Due to the capabilities of management and plants to adapt to changes in climate as well as long-term reactions of farming community to adapt to new environmental conditions, a long-term impact assessment is not included. For the short- and medium-term scenarios, it is assumed that factors such as plant genetics and management strategies remain constant and at a current level.

The projections of future CO_2 concentration are based on van Vuuren et al. (2011) and are assumed to be 420 ppm and 450ppm CO_2 for RCP 4.5 and RCP 8.5, respectively during the time period 2021-2030; and 470 and 520 ppm CO_2 for RCP 8.5 are projected for the time period 2041-2050.

6.3 Results and Discussions

Future climate trends in the LCC study area

The climate models project a strong increase in temperature over the study region, under the high-emission scenario RCP 8.5 as well as under the moderate emission scenario RCP 4.5 (Fig. 6-1C). For the summer season (May-October), the ensemble means predict an increase of 1.0 °C (±0.4°C) for RCP 4.5 and 1.0 °C (±0.3°C) for RCP 8.5 until 2030, compared to the historical period of 1996-2005. A warming of 1.6 °C (±0.5°C) and 1.8 °C (±0.5°C) is projected for RCP 4.5 and 8.5, respectively, until 2050 (Fig. 6-3A). Strong increases in temperature under both scenarios points towards higher pressure on agricultural production resulting from increased temperature stress on crop growth, especially during summer months (Fig. 6-3B). A high agreement between the climate model ensemble members regarding consistent increase in future temperature indicates that the future summer season warming in the LCC area can be projected with high confidence (Fig. 6-1C; Fig. 6-3A and 6-3B).

Precipitation projections, on the other hand, are highly uncertain and there is no clear trend in annual or monthly precipitation amounts (Fig. 6-1D, Fig. 6-3C and 6-3D). Future water availability in terms of precipitation projections over the study area is therefore difficult to predict. In this study, it is assumed that due to the constant irrigation activities in the LCC irrigation system, agricultural water availability is always assured, and plant water demand is met. Thus, impacts of changes in precipitation on the model results are small and water stress is kept low.

Scenarios that future water availability either by water abstractions from the river Chenab or from ground water resources can no longer meet irrigation demands are not analyzed in this study, as the focus lays on the effect of climate change impacts of agricultural productivity given enough water.

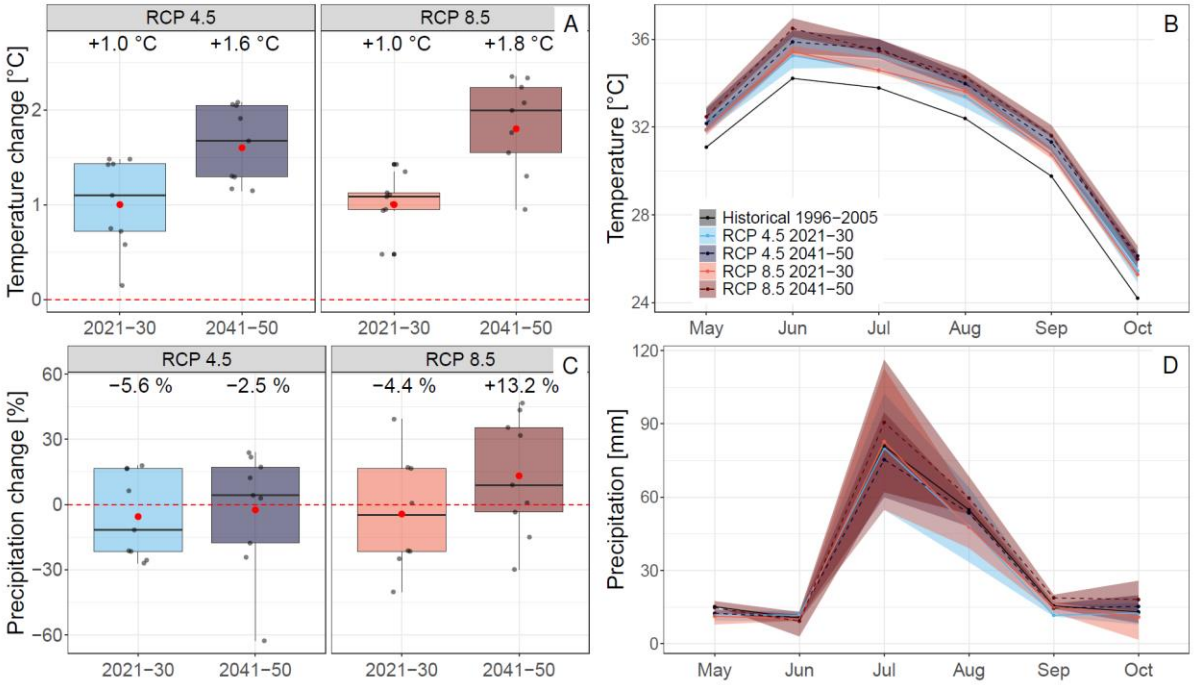

Fig. 6-3: Projected temperature and precipitation change during Kharif (summer) months, for selected time periods 2021-2030 and 2041-2050, with respect to historical data (1996-2005). Absolute seasonal temperature change (A) and absolute monthly temperature changes (B). Relative seasonal precipitation changes (C) and absolute monthly precipitation changes (D). Red dots and the displayed percentages show ensemble mean changes. Grey dots represent single ensemble members. Right panels show model ensemble uncertainty bands of 25th and 75th percentiles.

Declining yield levels under climate change

Both models show that climate change will lead to a substantial reduction of future yield levels in the study area. Under current CO_2 concentrations, mean yield levels are projected to decrease by up to -24% (±12%) under the high emission and mid-century scenario (Fig. 6-4A, light grey bar, RCP 8.5 2041-50). Despite their differences in predicted magnitudes of yield declines (SWAT: -32% (±12%) and APSIM: -16% (±2%)), the models agree in their trends (sign) and show increasing yield losses with increasing temperatures for all crop types (Fig. 6-4B, 6-4 C, 6-4D). Considering that water demand is assumed to be met, these results underline that the increasing temperature stress alone will have a strong negative effect on crop growth, which is in-line with findings of previous studies (Deryng et al., 2014; Saddique et al., 2020; Siebert and Ewert, 2014; Zhao et al., 2017).

Accounting for increasing CO_2-concentrations (Fig. 6-4, dark grey bars) dampens the negative impact of the temperature increase on yields, revealing the significant positive effect of higher CO_2 levels on agricultural productivity due higher photosynthesis rates, also known as CO_2-fertilization. For the short-term scenario (2021-2030), increasing CO_2-concentrations prevent the strong decline in simulated crop yields. This is generally in-agreement with previous studies showing this strong positive

effect of increasing CO_2 concentrations on plant growth and its ability to counteract plant growth limiting effects (Parry et al., 2004). Yet, the effectiveness of CO_2-fertilization is still a large source of uncertainty (Elliott et al., 2014; McGrath and Lobell, 2013). In the context of this study, uncertainty arises through the differences in representing CO_2-impacts on plant physiology by SWAT and APSIM. The hydrological SWAT model does not account for plant type specific impacts of CO_2 (e.g. different reactions of C3-plant and C4-plant) and might overestimates the positive effects of CO_2 (Wu et al., 2012). The APSIM crop models, on the other hand, consider plant specific impacts, e.g., the maize-model (Fig. 6-4C) correctly assumes maize-insensitivity to changing CO_2 effects (maize = C4-plant). In the case of cotton, which shows a lower yield reduction than rice and maize, the enhanced productivity under rising CO_2 levels even leads to an increasing yield (Fig. 6-4B). The sensitivities of rice and SWAT-maize yield to CO_2-concentrations are comparable, but their yield reductions due to temperature stress are too severe for increasing CO_2 emissions to compensate (Fig. 6-4D).

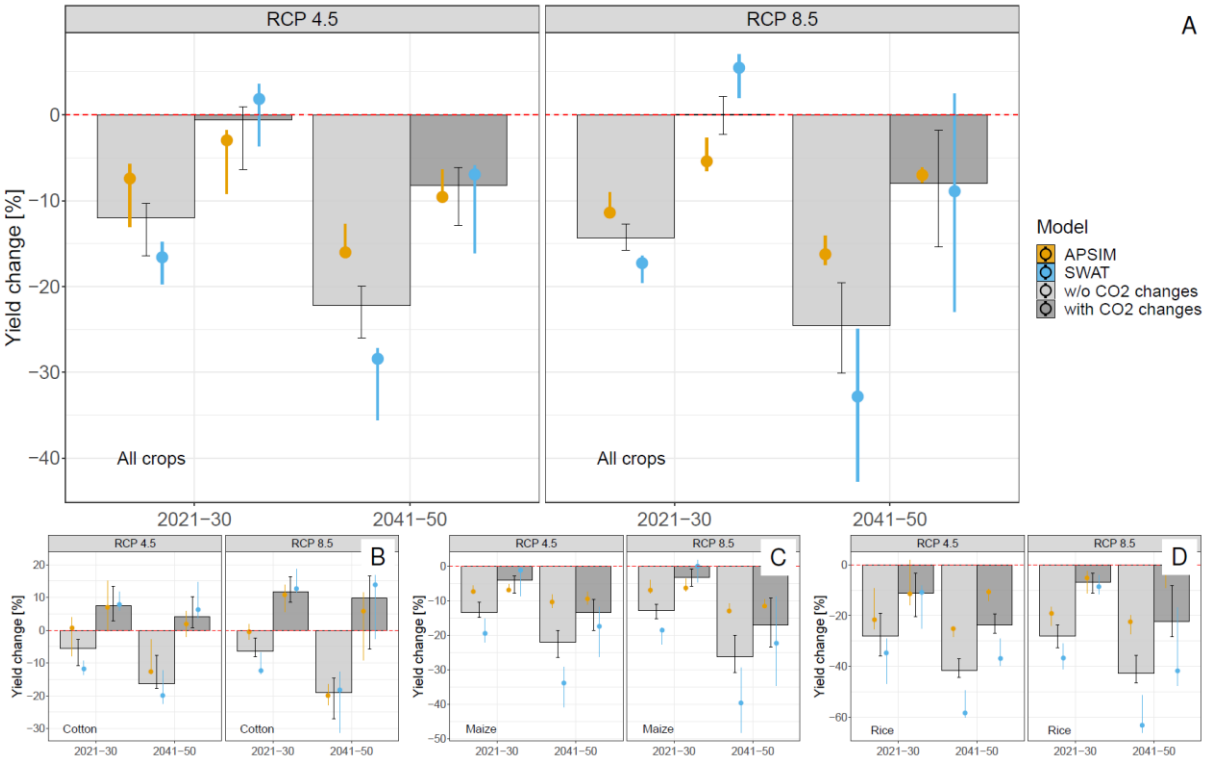

Fig. 6-4: Projected changes in future crop yield under the RCP 4.5 and RCP 8.5 scenario, neglecting (light grey bars) and considering (dark grey bars) the impact of CO_2 changes. Results are shown for all crops combined (A) as well as separately for cotton (B), maize (C) and rice (D). Filled bars show the model ensemble median and black error bars show the respective 25th and 75th percentiles of the model ensemble (SWAT and APSIM with nine climate models). Separate results for SWAT and APSIM models are shown as colored dots (median) and error lines (25th and 75th percentiles for the model ensemble of nine climate models).

Overall, APSIM results show declining yields even for the short-term future, indicating that elevated CO_2 concentrations are not able to compensate for reduced yield due to higher temperature stress.

Under further rising temperatures (2041-2050), both models project decline in crop yields (-8% (±9%), RCP 4.5 and -7% (±12%), RCP 8.5); and disclose that even with further elevated CO_2-concentrations and unlimited water availability climate change induced yield declines cannot be prevented. All estimated crop productivities show that yields are expected to benefit less from increasing CO_2 levels, as temperatures continue to rise (Fig. 6-4B).

Previous studies have indicated that increasing CO_2 improves water use efficiency by reducing plant transpiration which facilitates plant growth during dry/drought conditions (Wullschleger et al., 2002; Yoo et al., 2009). At the same time, it has been also reported that reduced plant transpiration leads to increased temperature stress, due to a reduced evaporative cooling effect (Siebert et al., 2014; Vanuytrecht et al., 2012). Both these effects are not covered presently by either of the models. As the strong increase in future temperature is projected under both RCPs and together with abundance of water due to irrigation, the positive effect of CO_2 on yield levels is most likely overestimated by both crop models. Recently, Wang et al., 2020 noted the positive effects of CO_2 tend to be overestimated by crop models based on their analysis of a global reduction in CO_2 fertilization effect on vegetation photosynthesis, which most models do not account for.

Future irrigation and evaporative demand

In the following, the reasons behind the estimated yield declines are discussed based on changes in irrigation demand, evapotranspiration, leaf area index and biomass productivity. Results presented here are averaged over the selected summer crops cotton, maize and rice. Crop specific results are presented in the supplementary material (Fig. A 6-1 and A 6-2, Annex).

Considering the significant temperature increase one would expect a strong increasing signal in plant water demand (Döll, 2002; Wada et al., 2013). Examining irrigation and evaporative demands in the study area, however, reveals that trends in future water demand do not align with projected temperature trends. Increasing water demands are surprisingly moderate and do not increase by more than 5% (average of both models; Fig. 6-5C). Against the expectation of a strong increase in irrigation needs under rising temperatures, both crop models show that average irrigation demands increase less under higher temperatures. Under both emission scenarios, a maximum increase is predicted for the moderate scenario (RCP 4.5, 2021-2030) while a minimum increase is predicted for the high-end emission scenario (RCP 8.5, 2041-2050). Figure 6-5 displays the results for APSIM and SWAT separately to reveal important differences in their simulation results. SWAT projects the lowest increase in water demand for the RCP 8.5 and mid-term future scenario (1±8%). Under elevated CO_2 concentrations (Fig.

6-5B), water demand even further reduces (-4±7%), which generally agrees with the effect of reduced plant water demand due to reduced stomatal conductance (Kimball et al., 2002).

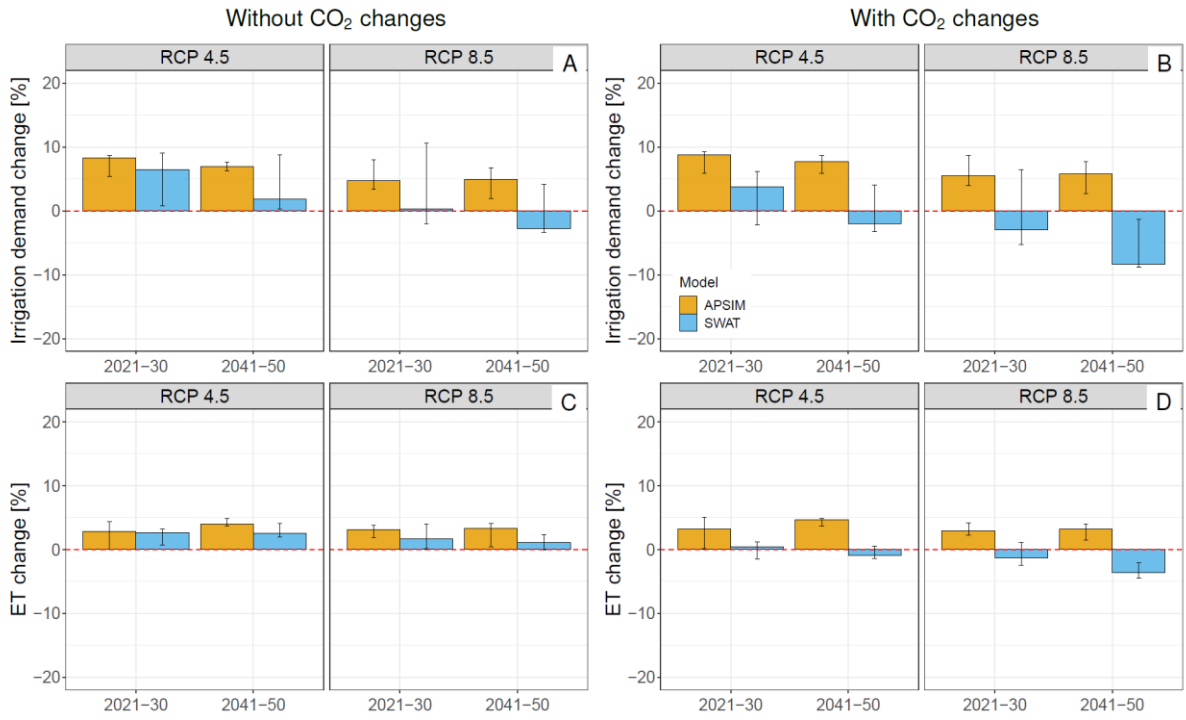

Fig. 6-5: Projections of future irrigation demand (A and B) and future ET rates (C and D). Changes under the baseline CO_2-scenario (A and C) and with increased CO_2-levels (B and D).

The APSIM model simulated irrigation demand appears insensitive to CO_2 changes, as irrigation demands remain constant regardless of changes in CO_2 levels (Fig. 6-5A vs. 6-5B). Yet, the significant increase in LAI (leaf area index) under elevated CO_2 levels (see below, Fig. 6-6B) and the negligible change in irrigation demand illustrates that the APSIM model likewise account for the positive CO_2 effects on water demand and show decreasing irrigation demands relative to leaf area growth.

The reason for the surprisingly low increase in irrigation demand can be explained by the low increase in actual evapotranspiration (Fig. 6-5C and 6-5D), which prevents irrigation demands to significantly increase. Despite the strong temperature rise, increases in ET are projected by both crop models to stay on average below 3% (±4%), and do not increase with higher temperatures, even under the assumption of unchanged CO_2 emissions.

Noting that water supply is guaranteed in both crop models, the low ET rates under rising temperatures cannot be related to water shortages and should be explained by ET controlling plant parameters, such as LAI and biomass production (as discussed below in the following section). The

limited changes in water demand also reveal that even if more water for intensified irrigation activity would be available, it would not help to reduce yield losses.

Future plant growth and agricultural productivity

The SWAT model estimates LAI development based on the influence of the predominant environmental stress factor (Neitsch et al., 2009), i.e. heat stress in this study. This results in a significant reduction in LAI by up to -27% (±6%) under the high-emission scenario (RCP 8.5, 2041-2050). The decreasing LAI trend clearly follows the increasing temperature trend, with highest LAI reductions under the RCP8.5 scenario (Fig. 6-6A) and confirms the LAI sensitivity towards temperature. In combination with the reduction of stomatal conductance, a significant decline in LAIs therefore seems to be one of the main reasons for the overall low ET rates simulated by the SWAT model under high temperatures (Fig. 6-5C). LAI calculations in SWAT do not account for CO_2 effects (Fig. 6-6A vs 6-6B), which leads to strong LAI decreases even under higher CO_2 concentrations (Fig. 6-6B) and to decreasing ET rates (Fig. 6-5D).

APSIM on the other hand, which does not account for a specific heat stress factor in parts of its LAI calculations, shows a clear LAI insensitivity to temperature (Fig. 6-6A and 6-6B). Yet, APSIM-LAI predictions show a notable sensitivity to CO_2-concentrations and increasing leaf growth under rising CO_2 levels. APSIM based simulated LAIs are projected to increase by up to 15% (±10%) under the high emission scenario, which explains why APSIM-ET rates do not decrease despite ET reducing CO_2-effects (Fig. 6-5D). Similar effects were described recently by Singh et al., 2020, revealing a strong increase in LAI due to CO_2 increases which can offset higher water use efficiency.

As the leaf area growth and temperature increase jointly control the evaporative demands and ultimately irrigation water needs, the differences in LAI projections underline the importance of model sensitivity with respect to temperature stress. These differences in the underlying model parameterizations between both models leads to two different conclusions. On the one hand, the SWAT model projects a decline in future plant growth, which is strong enough to reduce ET and irrigation demand -- this leads to the conclusion that irrigation intensification cannot help to mitigate future yield losses. APSIM on the other hand, forecast increasing leaf area growth and indicates that due to its (even if only moderately) rising irrigation demands, intensified irrigation is necessary to not further strengthen the predicted yield losses.

The apparent inconsistency in decreasing LAI and at the same time increasing biomass in SWAT under elevated CO_2 concentrations (Fig. 6-6B and 6-6D) can be explained by the sensitivity of biomass

production in SWAT to changes in CO_2. In SWAT, the biomass production is dependent on radiation use efficiency and available light for photosynthesis (see chapter 3.2). While the availability of light is dependent on LAI development, radiation use efficiency is positively affected by changes in CO_2-concentrations (Neitsch et al., 2009). Increasing CO_2 concentrations thus enhance biomass production. In this study, this biomass enhancing effect is stronger than the negative effect due to decreasing LAI (SWAT results Fig. 6-6D, RCP 4.5). Yet, for RCP 8.5 and a further temperature increase, this effect is dominated by a further reduction in LAI, leading to a reduction in biomass even under further elevated CO_2 concentrations (Fig. 6-6D).

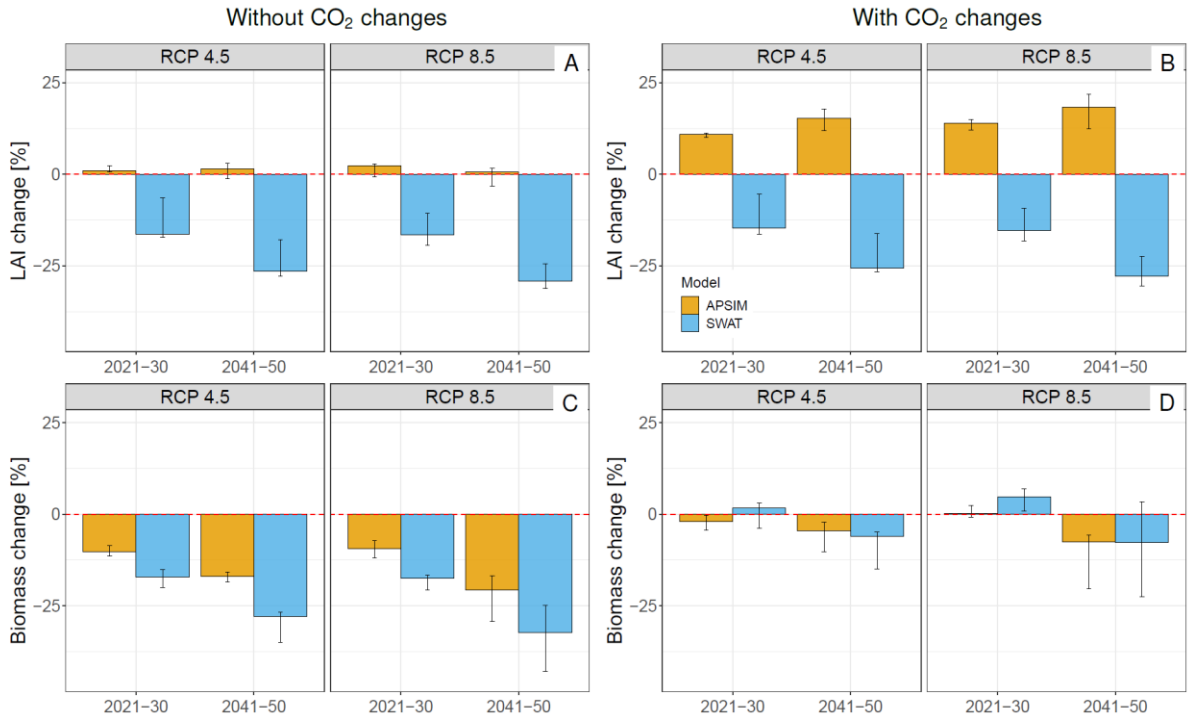

Fig. 6-6: Projections of future LAI changes (A and B) and future biomass changes (C and D). Changes under the baseline CO_2-scenario (A and C) and with increased atmospheric CO_2-levels (B and D).

Despite their differences in LAI estimation procedures, both models show that even if the increased future water demand is fulfilled, a substantial reduction in plant biomass (and thereafter yields) due to increasing temperatures is projected in future (Fig. 6-6C). To this end, both models show a good agreement in their predicting trends. Rising CO_2 levels might compensate negative temperature effects in the near future but already for the mid-century scenario (2041-2050), biomass is projected to decline despite further elevated CO_2 levels (Fig 6-6D).

The reason for the discrepancy between increasing LAI predictions and decreasing biomass estimates by APSIM, can be found in the way APSIM accounts for biomass partitioning processes. As a biophysical crop model, the APSIM model accounts for carbon assimilation in different plant parts (i.e. leaves,

stem, fruit). Leaf area can therefore remain constant or even increase while the overall biomass decreases (APSIM model documentation, 2021).

Recalling that both models assure a sufficient supply of irrigation water to meet changing water demands, the results reveal that temperature stress alone is responsible for the simulated yield declines in this study. It can therefore be concluded that increased water use has a strong limit in mitigating future yield losses. Intensification of irrigation might be able to mitigate yield declines in the near future, when positive CO_2 effects balance the harmful temperature effects and irrigation demands are still increasing (Fig. 6-5B). For the mid-century scenario however, when positive CO_2 effects are no longer sufficient and irrigation demand decrease, irrigation intensification will not be able to mitigate the projected yield losses.

It should be mentioned that these deductions are based on the average trends estimated for maize, cotton, and rice crops. Plant specific reactions should be considered, when impacts on individual crop types are the focus. The effects of climate change on each crop type showed that even though crop reactions differ, they agree in their overall responses to temperature stress and sensitivity to CO_2 (see Fig. A 6-1 and A 6-2, Annex). The exception to this general trend is the maize crop simulated by the APSIM model due its particular physiologies as a C4-plant.

6.4 Conclusion

The main finding of this study is that under the expected climate change scenarios a substantial reduction in summer crop yields is likely to occur in the study region, even though enough irrigation water is assumed to be available. It could be shown that plant development is dominantly controlled by temperature stress and that therefore the negative climate change impact on agricultural productivity cannot be mitigated by an intensification of irrigation.

Assuming a constantly satisfied plant water demand, the results indicate that in the intensively irrigated agricultural system, the limit of additional water as adaptation measure could be reached in the near future. The dominant future factor, likely causing a substantial yield decline, seems to be plant heat stress. Under these circumstances, temperature related adaptation strategies such as the selection of more heat resistant crops, or changes in crop planting schedules to avoid high temperature stress seem more suitable than water related adaptation measures.

The results contradict previous studies, which suggest that increased irrigation amounts can help to reduce crop heat sensitivity in such a way that it partially or even entirely offsets temperature induced yield reduction (Shaw et al., 2014; Tack et al., 2017; Zaveri and Lobell, 2019). However, these studies

also argue that yield gains from intensified irrigation have already slowed down in recent years and that the application of more water has its limits as a potential adaptation strategy to prevent harmful effects of rising temperatures.

Finally, by using two crop models from two different scientific disciplines, this study showed that while both models agree in their overall yield simulations, their predictions of future water demand and the capability of irrigation to counteract the dominating temperature stress can vary significantly. Hence, when using models as decision support systems for future water resources planning, it needs a careful examination of their respective model structures and especially their sensitivities with respect to temperature stress in order to draw the reliable conclusion about future irrigation demands.

7 Overall conclusions and main findings

In line with the two central objectives of this research, the main findings can be structured in two parts:

Main findings part 1: Set-up, calibration, and validation

The first part of this thesis assesses the suitability of using ET data for a spatially distributed model calibration of the agro-hydrological SWAT model. It gives an outlook on strengths and weaknesses of using remote sensing data for ET estimations and points out further research needs in this field. Furthermore, a framework is developed to acquire data of important water balance parameters using field observations in combination with numerical modeling. Main findings can be summarized as followed:

- The method of using spatially distributed and remote sensing derived ET data showed its advantages for the calibration of a large-scale hydrological model, in the heavily human impacted and intensively irrigated agricultural study region of the Lower Chenab Canal System. Yet, it also showed significant limitations in resolving the small-scale heterogeneity of the area.
- Hence, to use remote sensing ET data for model calibration, which is often the only spatially distributed data set available, a detailed assessment of the spatial variability represented by the "observed" data set (e.g., SEBAL) is necessary. For a small scale and highly divers agricultural setting with likewise diverse ET patterns, the preservation of the spatial heterogeneity of the "observed" (i.e., remote sensing) data set remains one of the main challenges.
- It could be demonstrated that the extraction of spatial ET data from a gridded remote-sensing based ET product, using the extent of SWAT model spatial extends (i.e., hydrological response units, HRUs), leads to averaged and nearly equal remote sensing ET values for all HRUs. In other words, the remote sensing ET data loses its heterogeneity due to an averaging of ET values over a larger (HRU-level) extend. The extracted time series from SEBAL data are therefore insufficiently representing spatial differences in ET patterns and are inhibiting satisfactory calibration results.
- For an improved model calibration in such an environment, a modified "observed" ET data set, which accounts for land-use class specific ET pattern is therefore desirable.
- The final calibration of SWAT using an ET data set which captures the spatial ET variability, showed the potential of an automated and spatially distributed calibration approach for a complex spatially distributed hydrological model.

- The research on alternative calibration strategies revealed once more the importance of data availability for model calibration and validation. In this regard, the developed framework to obtain data of central water balance components proved to be a possible way to get the valuable data for model calibration and validation.

- Even though it does not give spatially distributed information, the research on combining in-situ measuring and a modeling approach to estimate water balance parameter, showed how this approach can help to get reliable water balance estimates. Data obtained by this approach can be used as validation data in ungauged sites, such as the one selected for this thesis.

Main findings part 2: Model application - Impact of climate change on water demand and agricultural productivity

The final part of this thesis focuses on the assessment of climate change impacts on the water balance and agricultural productivity. It concentrates on the importance of temperature vs. water stress and elaborates on their implications for potential climate adaption strategies. Main findings are:

- Temperatures are projected to increase by approx. 1.6 °C until 2050, while precipitation projections are highly uncertain, and no clear future precipitation trend can be detected for the study region of the Lower Chenab Canal System.

- Even under the assumption of sufficient water, the model results of SWAT and APSIM revealed that yield will be significantly reduced in future due to increased plant temperature stress. It could be shown that in the intensively irrigated agricultural system, the limit of additional water as adaptation measure will certainly be reached soon. The dominant future factor, causing a substantial yield decline, seems to be plant heat stress.

- This is an important finding regarding water management in the area, as it shows the limitations of the resource “water” to relieve climate change impacts.

- The results contradict previous studies, which suggest that increased irrigation amounts can help to reduce crop heat sensitivity in such a way that it partially or even entirely offsets temperature induced yield reduction.

- Temperature stress related adaption strategies (e.g., more heat tolerant crops) or a regional crop shifting might under these circumstances be more important than increasing irrigation intensities.

- APSIM and SWAT differ in their results due to model structural differences. Especially the differences in mode equations which account for heat and water stress, are influencing the results on climate effects on plant productivity and yield. A careful assessment of the structural differences is needed to draw the right conclusion on potential measure to mitigate climate change impacts.

8 Outlook

The research undertaken in the scope of this thesis revealed that especially temperature stress is expected to significantly reduce future yield levels in the region of the Lower Chenab Canal System. An intensification of irrigation might fail as a measure to counteract climate change and to keep productivity levels high, because of severe negative impacts on plant growths due to temperature stress. Similar results regarding the effectiveness of irrigation are reported by (Lobell and Burke, 2008; Zaveri and Lobell, 2019), which show that under currently increasing temperatures yield levels decrease despite increased irrigation efforts. Yet other studies on agricultural systems experiencing similar environmental pressures, consider an intensification of irrigation as a possible action to mitigate climate change (Elliott et al., 2014; Fader et al., 2016; Molden et al., 2010).

This shows that the choice and the effectiveness of mitigation measures have to be seen in the local context and are controlled by the dominance of yield limiting stress factors (e.g. heat vs. water stress). The findings of this thesis show that contrary to expectations irrigation demand do not necessarily align with increasing temperatures. Based on the results of this thesis and for the respective region under study, it can be stated that heat stress is the dominant factor causing reductions in plant growth strong enough to even reduce plant water demand.

Consequently, measures to avoid extreme crop heat stress like the geographical shifting of crops to their “optimal growing areas” also entitled as “eco-agrological zones” could be a more effective solution than an increase in irrigation water supply. This aspect is important to consider, and it is already publicly discussed in Pakistan (Business Recorder, 2017), especially with respect to future climate change, under which these agro-ecological zones are expected to shift and affect water resources as well as productivity levels.

Another possible adaptation measure would be a shift to more heat resistant crops. Results of this modeling study show different sensitivities of crops to heat stress and accordingly less yield reduction of crops capable of coping with higher temperatures.

Nevertheless, it should be highlighted again, that one of the main assumptions of this modeling study is the constant availability of irrigation water. Only under this assumption heat stress could gain its dominant status. The study did not answer the question on how yield would change if irrigation water availability would reduce. Even if, due to intensive and often excessive ground water pumping, a sufficient irrigation supply can be assumed for the near future, in the long-term these resources are likely to diminish and increase the importance of water stress in this semi-arid and entirely irrigation dependent agricultural region.

Furthermore, no increasing frequency of heat waves or prolonged drought periods were considered. These will have a more detrimental effect on plant growth than gradually increasing trends (Dreesen et al., 2012) and can have a disproportionate impact on the ecosystem compared to the time span in which they happen (de Boeck et al., 2011). This shows again the importance of knowing the detailed impact of one or the other stressor (heat and drought) and their interactions.

Overall large knowledge gaps still exist on plant science as well as on plant model developing site in knowing and representing the interplay of heat and water stress on plant growth. Previous studies highlight that more research is needed to separate the effects of temperature and water stress related climate change impacts on agricultural yields (Carter *et al* 2016) to better understand which measures could help to mitigate negative climate change impacts. Further research should therefore be done on assessing the effects of heat and water stress on agricultural yields studying their potential synergistic, antagonistic or additive nature (Mahoorakashani, 2017).

The model comparison of APSIM and SWAT showed that their differences in accounting for the interplay of heat and water stress significantly influenced the results of plant productivity. As Jin et al. (2016) suggest, models should be able to coordinate the interaction of environmental stresses (especially heat and water stress). Future research questions for a better understanding of the interplay of heat and water stress could therefore be:

- What are the relative effects of temperature and water stress on plant productivity?
- What is the nature of their interplay and what does it tell us about potential adaption measures?
- Can a threshold of heat and water stress be defined which decides about the effectiveness of adaption measures to enhance plant productivity? E.g., until which heat stress level can irrigation still improve or maintain productivity?

Concludingly it can be stated that for the study area of the Lower Chenab Canal region, climate change impacts are posing a serious threat to future agricultural productivity. Based on the results of this thesis, heat stress affects will be strong enough to reduce plant growth, while water stress is expected to be less severe. This however is only true, if water demand can be met by surface water supply or groundwater pumping – an assumption which is made in this study, but which should be questioned in the long term. Future changes in discharge volumes of the glacier- and snowmelt driven rivers, over-

exploitation of ground water resources as well as increasing water demand of the growing population will put the water demand in the study area under additional pressure.

The results of this thesis suggest that to mitigate future climate change impacts the reductions of heat stress effects on crops should be prioritized in near future, while a more sustainable water management is unquestionable to continue to fulfill high water demands also in the long-term future.

9 References

Abbaspour, K., Vaghefi, S., Srinivasan, R., 2017. A Guideline for Successful Calibration and Uncertainty Analysis for Soil and Water Assessment: A Review of Papers from the 2016 International SWAT Conference. Water 10, 6. https://doi.org/10.3390/w10010006

Abbaspour, K.C., Rouholahnejad, E., Vaghefi, S., Srinivasan, R., Yang, H., Kløve, B., 2015. A continental-scale hydrology and water quality model for Europe: Calibration and uncertainty of a high-resolution large-scale SWAT model. J. Hydrol. 524, 733–752. https://doi.org/10.1016/j.jhydrol.2015.03.027

Ahmad, M.-D., Bastiaanssen, W.G.M., Feddes, R.A., 2002. Sustainable use of groundwater for irrigation: a numerical analysis of the subsoil water fluxes. Irrig. Drain. 51, 227–241. https://doi.org/10.1002/ird.59

Ahmad, M.D., Turral, H., Nazeer, A., 2009. Diagnosing irrigation performance and water productivity through satellite remote sensing and secondary data in a large irrigation system of Pakistan. Agric. Water Manag. 96, 551–564. https://doi.org/10.1016/j.agwat.2008.09.017

Allen, R.G., Pereira, L.S., Howell, T.A., Jensen, M.E., 2011. Evapotranspiration information reporting: I. Factors governing measurement accuracy. Agric. Water Manag. 98, 899–920. https://doi.org/10.1016/j.agwat.2010.12.015

Allen, R.G., Pereira, L.S., Raes, D., Smith, M., 1998a. Crop evapotranspiration - Guidelines for computing crop water requirements - FAO Irrigation and drainage paper 56. FAO - Food Agric. Organ. U. N.

Allen, R.G., Pereira, L.S., Raes, D., Smith, M., 1998b. FAO Irrigation and Drainage Paper No. 56: Crop Evapotranspiration. Rome.

APSIM, Crop Module Documentation. https://www.apsim.info/documentation/model-documentation/ (last accessed: 2021-03-14).

Arnold, J.G., D. N. Moriasi, P. W. Gassman, K. C. Abbaspour, M. J. White, R. Srinivasan, C. Santhi, R. D. Harmel, A. van Griensven, M. W. Van Liew, N. Kannan, M. K. Jha, 2012. SWAT: Model Use, Calibration, and Validation. Trans. ASABE 55, 1491–1508. https://doi.org/10.13031/2013.42256

Arnold, J.G., Srinivasan, R., Muttiah, R.S., Williams, J.R., 1998. Large Area Hydrologic Modeling and Assessment Part I: Model Development1. JAWRA J. Am. Water Resour. Assoc. 34, 73–89. https://doi.org/10.1111/j.1752-1688.1998.tb05961.x

Awan, U.K., Ismaeel, A., 2014. A new technique to map groundwater recharge in irrigated areas using a SWAT model under changing climate. J. Hydrol. 519, 1368–1382. https://doi.org/10.1016/j.jhydrol.2014.08.049

Awan, U.K., Liaqat, U.W., Choi, M., Ismaeel, A., 2016. A SWAT modeling approach to assess the impact of climate change on consumptive water use in Lower Chenab Canal area of Indus basin. Hydrol. Res. 47, 1025–1037. https://doi.org/10.2166/nh.2016.102

Bastiaanssen, W.G.M., Bandara, K.M.P.S., 2001. Evaporative depletion assessments for irrigated watersheds in Sri Lanka 15.

Bastiaanssen, W.G.M., Cheema, M.J.M., Immerzeel, W.W., Miltenburg, I.J., Pelgrum, H., 2012. Surface energy balance and actual evapotranspiration of the transboundary Indus Basin estimated from satellite measurements and the ETLook model. Water Resour. Res. 48. https://doi.org/10.1029/2011WR010482

Bastiaanssen, W.G.M., Menenti, M., Feddes, R.A., Holtslag, A.A.M., 1998a. A remote sensing surface energy balance algorithm for land (SEBAL). 1. Formulation. J. Hydrol. 212–213, 198–212. https://doi.org/10.1016/S0022-1694(98)00253-4

Bastiaanssen, W.G.M., Pelgrum, H., Wang, J., Ma, Y., Moreno, J.F., Roerink, G.J., 1998b. A remote sensing surface energy balance algorithm for land (SEBAL) 2. Validation. J. Hydrol. 17.

Becker, R., Koppa, A., Schulz, S., Usman, M., aus der Beek, T., Schüth, C., 2019. Spatially distributed model calibration of a highly managed hydrological system using remote sensing-derived ET data. J. Hydrol. 577, 123944. https://doi.org/10.1016/j.jhydrol.2019.123944

Behrangi, A., Khakbaz, B., Vrugt, J.A., Duan, Q., Sorooshian, S., 2008. Comment on "Dynamically dimensioned search algorithm for computationally efficient watershed model calibration" by Bryan A. Tolson and Christine A. Shoemaker. Water Resour. Res. 44. https://doi.org/10.1029/2007WR006429

Bolch, T., 2019. Past and Future Glacier Changes in the Indus River Basin, in: Indus River Basin. Elsevier, pp. 85–97. https://doi.org/10.1016/B978-0-12-812782-7.00004-7

Bouman, B.A.M., Kropff, M.J., Toung, T.P., Wopereis, M.C.S., Ten Berge, H.F.M., Van Laar, H.H., 2001. ORYZA2000: Modeling Lowland Rice. International Rice Research Institute, and Wageningen University and Research Centre, Los Banos, Philippines and Wageningen, Netherlands.

Brocca, L., Ciabatta, L., Massari, C., Moramarco, T., Hahn, S., Hasenauer, S., Kidd, R., Dorigo, W., Wagner, W., Levizzani, V., 2014. Soil as a natural rain gauge: Estimating global rainfall from satellite soil moisture data. J. Geophys. Res. Atmospheres 119, 5128–5141. https://doi.org/10.1002/2014JD021489

Brocca, L., Massari, C., Ciabatta, L., Moramarco, T., Penna, D., Zuecco, G., Pianezzola, L., Borga, M., Matgen, P., Martínez-Fernández, J., 2015. Rainfall estimation from in situ soil moisture observations at several sites in Europe: an evaluation of the SM2RAIN algorithm. J. Hydrol. Hydromech. 63, 201–209. https://doi.org/10.1515/johh-2015-0016

Brocca, L., Moramarco, T., Melone, F., Wagner, W., 2013. A new method for rainfall estimation through soil moisture observations. Geophys. Res. Lett. 40, 853–858. https://doi.org/10.1002/grl.50173

Brocca, L., Tarpanelli, A., Filippucci, P., Dorigo, W., Zaussinger, F., Gruber, A., Fernández-Prieto, D., 2018. How much water is used for irrigation? A new approach exploiting coarse resolution satellite soil moisture products. Int. J. Appl. Earth Obs. Geoinformation 73, 752–766. https://doi.org/10.1016/j.jag.2018.08.023

Business Recorder, 2017. Climate Change: Government redesigning agro-ecological zones. August 17th, 2017. https://fp.brecorder.com/2017/08/20170817209733/ (last accessed: 2021-03-24)

Campbell, G.S., Norman, J.M., 1998. An Introduction to Environmental Biophysics. Springer New York, New York, NY. https://doi.org/10.1007/978-1-4612-1626-1

Campbell Scientific, 2018. Instruction Manual CS650 and CS655 Water Content Reflectometers.

Campo, L., Caparrini, F., Castelli, F., 2006. Use of multi-platform, multi-temporal remote-sensing data for calibration of a distributed hydrological model: an application in the Arno basin, Italy. Hydrol. Process. 20, 2693–2712. https://doi.org/10.1002/hyp.6061

Carter, E.K., Melkonian, J., Riha, S.J., Shaw, S.B., 2016. Separating heat stress from moisture stress: analyzing yield response to high temperature in irrigated maize. Environ. Res. Lett. 11, 094012. https://doi.org/10.1088/1748-9326/11/9/094012

Chung, S.-O., Horton, R., 1987. Soil heat and water flow with a partial surface mulch. Water Resour. Res. 23, 2175–2186. https://doi.org/10.1029/WR023i012p02175

Clevers, J., 1989. Application of a weighted infrared-red vegetation index for estimating leaf Area Index by Correcting for Soil Moisture. Remote Sens. Environ. 29, 25–37. https://doi.org/10.1016/0034-4257(89)90076-X

Clevers, J., Kooistra, L., van den Brande, M., 2017. Using Sentinel-2 Data for Retrieving LAI and Leaf and Canopy Chlorophyll Content of a Potato Crop. Remote Sens. 9, 405. https://doi.org/10.3390/rs9050405

CORDEX, Coordinated Regional Climate Downscaling Experiment [WWW Document]. URL https://cordex.org/ (accessed 4.15.20).

Dari, J., Brocca, L., Quintana-Seguí, P., Escorihuela, M.J., Stefan, V., Morbidelli, R., 2020. Exploiting High-Resolution Remote Sensing Soil Moisture to Estimate Irrigation Water Amounts over a Mediterranean Region. Remote Sens. 12, 2593. https://doi.org/10.3390/rs12162593

Dechmi, F., Burguete, J., Skhiri, A., 2012. SWAT application in intensive irrigation systems: Model modification, calibration and validation. J. Hydrol. 470–471, 227–238. https://doi.org/10.1016/j.jhydrol.2012.08.055

Deihimfard, R., Eyni-Nargeseh, H., Mokhtassi-Bidgoli, A., 2018. Effect of Future Climate Change on Wheat Yield and Water Use Efficiency Under Semi-arid Conditions as Predicted by APSIM-Wheat Model. Int. J. Plant Prod. 12, 115–125. https://doi.org/10.1007/s42106-018-0012-4

Deryng, D., Conway, D., Ramankutty, N., Price, J., Warren, R., 2014. Global crop yield response to extreme heat stress under multiple climate change futures. Environ. Res. Lett. 9, 034011. https://doi.org/10.1088/1748-9326/9/3/034011

Doherty, J., 2015. Calibration and Uncertainty Analysis for Complex Environmental Models. Watermark Numerical Computing, Brisbane.

Döll, P., 2002. Impact of Climate Change and Variability on Irrigation Requirements: A Global Perspective. Clim. Change 54, 269–293. https://doi.org/10.1023/A:1016124032231

Droogers, P., Bastiaanssen, W.G.M., Beyazgül, M., Kayam, Y., Kite, G.W., Murray-Rust, H., 2000. Distributed agro-hydrological modeling of an irrigation system in western Turkey. Agric. Water Manag. 43, 183–202. https://doi.org/10.1016/S0378-3774(99)00055-4

Duan, Q., Sorooshian, S., Gupta, V.K., 1994. Optimal use of the SCE-UA global optimization method for calibrating watershed models. J. Hydrol. 158, 265–284. https://doi.org/10.1016/0022-1694(94)90057-4

Duan, Q.Y., Gupta, V.K., Sorooshian, S., 1993. Shuffled complex evolution approach for effective and efficient global minimization. J. Optim. Theory Appl. 76, 501–521. https://doi.org/10.1007/BF00939380

Eckstein, D., Hutfils, M.-L., Winges, M., Germanwatch, 2018. Global Climate Risk Index 2019 Who Suffers Most From Extreme Weather Events? Weather-related Loss Events in 2017 and 1998 to 2017.

Elliott, J., Deryng, D., Müller, C., Frieler, K., Konzmann, M., Gerten, D., Glotter, M., Flörke, M., Wada, Y., Best, N., Eisner, S., Fekete, B.M., Folberth, C., Foster, I., Gosling, S.N., Haddeland, I., Khabarov, N., Ludwig, F., Masaki, Y., Olin, S., Rosenzweig, C., Ruane, A.C., Satoh, Y., Schmid, E., Stacke, T., Tang, Q., Wisser, D., 2014. Constraints and potentials of future irrigation water availability on agricultural production under climate change. Proc. Natl. Acad. Sci. 111, 3239–3244. https://doi.org/10.1073/pnas.1222474110

Ershadi, A., McCabe, M.F., Evans, J.P., Walker, J.P., 2013. Effects of spatial aggregation on the multi-scale estimation of evapotranspiration. Remote Sens. Environ. 131, 51–62. https://doi.org/10.1016/j.rse.2012.12.007

Fader, M., Shi, S., von Bloh, W., Bondeau, A., Cramer, W., 2016. Mediterranean irrigation under climate change: more efficient irrigation needed to compensate for increases in irrigation water requirements. Hydrol. Earth Syst. Sci. 20, 953–973. https://doi.org/10.5194/hess-20-953-2016

Fatichi, S., Vivoni, E.R., Ogden, F.L., Ivanov, V.Y., Mirus, B., Gochis, D., Downer, C.W., Camporese, M., Davison, J.H., Ebel, B., Jones, N., Kim, J., Mascaro, G., Niswonger, R., Restrepo, P., Rigon, R., Shen, C., Sulis, M., Tarboton, D., 2016. An overview of current applications, challenges, and future trends in distributed process-based models in hydrology. J. Hydrol. 537, 45–60. https://doi.org/10.1016/j.jhydrol.2016.03.026

Feddes, R.A., Kowalik, P., Kolinska-Malinka, K., Zaradny, H., 1976. Simulation of field water uptake by plants using a soil water dependent root extraction function. J. Hydrol. 31, 13–26. https://doi.org/10.1016/0022-1694(76)90017-2

Filippucci, P., Tarpanelli, A., Massari, C., Serafini, A., Strati, V., Alberi, M., Raptis, K.G.C., Mantovani, F., Brocca, L., 2020. Soil moisture as a potential variable for tracking and quantifying irrigation: A case study with proximal gamma-ray spectroscopy data. Adv. Water Resour. 136, 103502. https://doi.org/10.1016/j.advwatres.2019.103502

Fischer, G., Tubiello, F.N., van Velthuizen, H., Wiberg, D.A., 2007. Climate change impacts on irrigation water requirements: Effects of mitigation, 1990–2080. Technol. Forecast. Soc. Change 74, 1083–1107. https://doi.org/10.1016/j.techfore.2006.05.021

Forkutsa, I., Sommer, R., Shirokova, Y.I., Lamers, J.P.A., Kienzler, K., Tischbein, B., Martius, C., Vlek, P.L.G., 2009. Modeling irrigated cotton with shallow groundwater in the Aral Sea Basin of Uzbekistan: I. Water dynamics. Irrig. Sci. 27, 331–346. https://doi.org/10.1007/s00271-009-0148-1

Fraga, I., Cea, L., Puertas, J., 2019. Effect of rainfall uncertainty on the performance of physically based rainfall-runoff models. Hydrol. Process. 33, 160–173. https://doi.org/10.1002/hyp.13319

Gao, X., Chen, X., Biggs, T., Yao, H., 2018. Separating Wet and Dry Years to Improve Calibration of SWAT in Barrett Watershed, Southern California. Water 10, 274. https://doi.org/10.3390/w10030274

Gassman, P.W., Sadeghi, A.M., Srinivasan, R., 2014. Applications of the SWAT Model Special Section: Overview and Insights. J. Environ. Qual. 8.

Gudmundsson, L., Bremnes, J.B., Haugen, J.E., Engen-Skaugen, T., 2012. Technical Note: Downscaling RCM precipitation to the station scale using statistical transformations. A comparison of methods. Hydrol. Earth Syst. Sci. 16, 3383–3390. https://doi.org/10.5194/hess-16-3383-2012

Gupta, H.V., Kling, H., Yilmaz, K.K., Martinez, G.F., 2009. Decomposition of the mean squared error and NSE performance criteria: Implications for improving hydrological modelling. J. Hydrol. 377, 80–91. https://doi.org/10.1016/j.jhydrol.2009.08.003

Gupta, H.V., Sorooshian, S., Yapo, P.O., 1998. Toward improved calibration of hydrologic models: Multiple and noncommensurable measures of information. Water Resour. Res. 34, 751–763. https://doi.org/10.1029/97WR03495

Habib, Z., 2004. Scope for Reallocation of River Waters for Agriculture in the Indus Basin. École nationale du génie rural, des eaux et des forêts.

Hanjra, M.A., Qureshi, M.E., 2010. Global water crisis and future food security in an era of climate change. Food Policy 35, 365–377. https://doi.org/10.1016/j.foodpol.2010.05.006
Hanks, R.J., 1992. Applied Soil Physics, Advanced Series in Agricultural Sciences. Springer New York, New York, NY. https://doi.org/10.1007/978-1-4612-2938-4
Hansen, N., 2006. The CMA Evolution Strategy: A Comparing Review, in: Lozano, J.A., Larrañaga, P., Inza, I., Bengoetxea, E. (Eds.), Towards a New Evolutionary Computation. Springer Berlin Heidelberg, Berlin, Heidelberg, pp. 75–102. https://doi.org/10.1007/3-540-32494-1_4
Hartmann, D.L., 2016. Global Physical Climatology, 2nd ed. Elsevier Science, Amsterdam.
Healy, R.W., 2010. Estimating Groundwater Recharge. Cambridge University Press, New York.
Hearn, A.B., 1994. OZCOT: A simulation model for cotton crop management. Agric. Syst. 44, 257–299. https://doi.org/10.1016/0308-521X(94)90223-3
Henderson-Sellers, B., 1984. A new formula for latent heat of vaporization of water as a function of temperature. Q. J. R. Meteorol. Soc. 110, 1186–1190. https://doi.org/10.1002/qj.49711046626
Holzworth, D.P., Huth, N.I., deVoil, P.G., Zurcher, E.J., Herrmann, N.I., McLean, G., Chenu, K., van Oosterom, E.J., Snow, V., Murphy, C., Moore, A.D., Brown, H., Whish, J.P.M., Verrall, S., Fainges, J., Bell, L.W., Peake, A.S., Poulton, P.L., Hochman, Z., Thorburn, P.J., Gaydon, D.S., Dalgliesh, N.P., Rodriguez, D., Cox, H., Chapman, S., Doherty, A., Teixeira, E., Sharp, J., Cichota, R., Vogeler, I., Li, F.Y., Wang, E., Hammer, G.L., Robertson, M.J., Dimes, J.P., Whitbread, A.M., Hunt, J., van Rees, H., McClelland, T., Carberry, P.S., Hargreaves, J.N.G., MacLeod, N., McDonald, C., Harsdorf, J., Wedgwood, S., Keating, B.A., 2014. APSIM – Evolution towards a new generation of agricultural systems simulation. Environ. Model. Softw. 62, 327–350. https://doi.org/10.1016/j.envsoft.2014.07.009
Huss, M., Hock, R., 2018. Global-scale hydrological response to future glacier mass loss. Nat. Clim. Change 8, 135–140. https://doi.org/10.1038/s41558-017-0049-x
Immerzeel, W.W., Droogers, P., 2008. Calibration of a distributed hydrological model based on satellite evapotranspiration. J. Hydrol. 349, 411–424. https://doi.org/10.1016/j.jhydrol.2007.11.017
Immerzeel, W.W., van Beek, L.P.H., Bierkens, M.F.P., 2010. Climate Change Will Affect the Asian Water Towers. Science 328, 1382–1385. https://doi.org/10.1126/science.1183188
IPCC, 2019, Shukla, P.R., Skea, J., Calvo Buendia, E., Masson-Delmotte, V., Pörtner, H.-O., Roberts, D.C., Zhai, P., Slade, R., Connors, S., van Diemen, R., Ferrat, M., Haughey, E., Luz, S., Neogi, S., Pathak, M., Petzold, J., Portugal Pereira, J., Vyas, P., Huntley, E., Kissick, K., Belkacemi, M., Malley, J., n.d. Climate Change and Land: an IPCC special report on climate change, desertification, land degradation, sustainable land management, food security, and greenhouse gas fluxes in terrestrial ecosystems.
Jiang, Y., Xu, X., Huang, Q., Huo, Z., Huang, G., 2015. Assessment of irrigation performance and water productivity in irrigated areas of the middle Heihe River basin using a distributed agro-hydrological model. Agric. Water Manag. 147, 67–81. https://doi.org/10.1016/j.agwat.2014.08.003
Jin, Z., Zhuang, Q., Tan, Z., Dukes, J.S., Zheng, B., Melillo, J.M., 2016. Do maize models capture the impacts of heat and drought stresses on yield? Using algorithm ensembles to identify successful approaches. Glob. Change Biol. 22, 3112–3126. https://doi.org/10.1111/gcb.13376
Jones, C.A., Kiniry, J.R., 1986. CERES-Maize: A simulation model of maize growth and development. Texas A&M University Press, College Station.
Khan, M.A., Khan, J.A., Ali, Z., Ahmad, I., Ahmad, M.N., 2016. The challenge of climate change and policy response in Pakistan. Environ. Earth Sci. 75, 412. https://doi.org/10.1007/s12665-015-5127-7
Kimball, B.A., Kobayashi, K., Bindi, M., 2002. Responses of agricultural crops to free air CO2 enrichment. Adv. Agron. 77, 293–361.
Kirkham, M.B., 2014. Principles of soil and plant water relations, 2nd ed. Elsevier, Oxford.
Kling, H., Fuchs, M., Paulin, M., 2012. Runoff conditions in the upper Danube basin under an ensemble of climate change scenarios. J. Hydrol. 424–425, 264–277. https://doi.org/10.1016/j.jhydrol.2012.01.011
Kottek, M., Grieser, J., Beck, C., Rudolf, B., Rubel, F., 2006. World Map of the Köppen-Geiger climate classification updated. Meteorol. Z. 15, 259–263. https://doi.org/10.1127/0941-2948/2006/0130
Kulkarni, A.V., Karyakarte, Y., 2014. Observed changes in Himalayan glaciers. Curr. Sci. 106, 8.
Lankford, B., 2006. Localising irrigation efficiency. Irrig. Drain. 55, 345–362. https://doi.org/10.1002/ird.270

Legates, D.R., McCabe, G.J., 1999. Evaluating the use of "goodness-of-fit" Measures in hydrologic and hydroclimatic model validation. Water Resour. Res. 35, 233–241. https://doi.org/10.1029/1998WR900018
Li, Y., Grimaldi, S., Pauwels, V.R.N., Walker, J.P., 2018. Hydrologic model calibration using remotely sensed soil moisture and discharge measurements: The impact on predictions at gauged and ungauged locations. J. Hydrol. 557, 897–909. https://doi.org/10.1016/j.jhydrol.2018.01.013
Liaqat, U.W., Choi, M., Awan, U.K., 2015. Spatio-temporal distribution of actual evapotranspiration in the Indus Basin Irrigation System. Hydrol. Process. 29, 2613–2627. https://doi.org/10.1002/hyp.10401
Lin, F.-R., Wu, N.-J., Tu, C.-H., Tsay, T.-K., 2017. Automatic Calibration of an Unsteady River Flow Model by Using Dynamically Dimensioned Search Algorithm [WWW Document]. Math. Probl. Eng. https://doi.org/10.1155/2017/7919324
Liu, L., Zhu, Y., Tang, L., Cao, W., Wang, E., 2013. Impacts of climate changes, soil nutrients, variety types and management practices on rice yield in East China: A case study in the Taihu region. Field Crops Res. 149, 40–48. https://doi.org/10.1016/j.fcr.2013.04.022
Lobell, D.B., Burke, M.B., 2008. Why are agricultural impacts of climate change so uncertain? The importance of temperature relative to precipitation. Environ. Res. Lett. 3, 034007. https://doi.org/10.1088/1748-9326/3/3/034007
Lopez Lopez, P., Sutanudjaja, E., Schellekens, J., Sterk, G., Bierkens, M., 2017. Calibration of a large-scale hydrological model using satellite-based soil moisture and evapotranspiration products. Hydrol. Earth Syst. Sci. Discuss. 1–39. https://doi.org/10.5194/hess-2017-16
Louis, J., Debaecker, V., Pflug, B., Main-Knorn, M., Bieniarz, J., Mueller-Wilm, U., Cadau, E., Gascon, F., 2016. SENTINEL-2 SEN2COR: L2A Processor for Users, in: ESA Living Planet Symposium. Prague, pp. 1–8.
Lutz, A.F., Immerzeel, W.W., Shrestha, A.B., Bierkens, M.F.P., 2014. Consistent increase in High Asia's runoff due to increasing glacier melt and precipitation. Nat. Clim. Change 4, 587–592. https://doi.org/10.1038/nclimate2237
Madsen, H., 2003. Parameter estimation in distributed hydrological catchment modelling using automatic calibration with multiple objectives. Adv. Water Resour. 26, 205–216. https://doi.org/10.1016/S0309-1708(02)00092-1
Matott, LS., 2017. OSTRICH: an Optimization Software Tool, Documentation and User's Guide, Version 17.12.19. 79 pages, University at Buffalo Center for Computational Research, www.eng.buffalo.edu/~lsmatott/Ostrich/OstrichMain.html.
McCabe, M.F., Wood, E.F., 2006. Scale influences on the remote estimation of evapotranspiration using multiple satellite sensors. Remote Sens. Environ. 105, 271–285. https://doi.org/10.1016/j.rse.2006.07.006
McGrath, J.M., Lobell, D.B., 2013. Regional disparities in the CO2 fertilization effect and implications for crop yields. Environ. Res. Lett. 8, 014054. https://doi.org/10.1088/1748-9326/8/1/014054
McMahon, T.A., Peel, M.C., Lowe, L., Srikanthan, R., McVicar, T.R., 2013. Estimating actual, potential, reference crop and pan evaporation using standard meteorological data: a pragmatic synthesis. Hydrol. Earth Syst. Sci. 17, 1331–1363. https://doi.org/10.5194/hess-17-1331-2013
Mekonnen, M.M., Hoekstra, A.Y., 2011. The green, blue and grey water footprint of crops and derived crop products. Hydrol. Earth Syst. Sci. 15, 1577–1600. https://doi.org/10.5194/hess-15-1577-2011
MNFSR, Pakistan Ministry of National Food Security & Research, http://www.mnfsr.gov.pk/pubDetails.aspx (last accessed: 2021-03-14)
Molden, D., Oweis, T., Steduto, P., Bindraban, P., Hanjra, M.A., Kijne, J., 2010. Improving agricultural water productivity: Between optimism and caution. Agric. Water Manag. 97, 528–535. https://doi.org/10.1016/j.agwat.2009.03.023
Narain, V., 2008. Warabandi as a sociotechnical system for canal water allocation: opportunities and challenges for reform. Water Policy 10, 409–422. https://doi.org/10.2166/wp.2008.057
Neitsch, S.L., Arnold, J.G., Kiniry, J.R., Williams, J.R., 2009. Soil and Water Assessment Tool. Theoretical Documentation. Version 2009.
Oxfam, 2009. Climate change, poverty and environmental crisis in the disaster prone areas of Pakistan.
Parry, M.L., Rosenzweig, C., Iglesias, A., Livermore, M., Fischer, G., 2004. Effects of climate change on global food production under SRES emissions and socio-economic scenarios. Glob. Environ. Change 14, 53–67. https://doi.org/10.1016/j.gloenvcha.2003.10.008
Peters-Lidard, C.D., Mocko, D.M., Garcia, M., Santanello, J.A., Tischler, M.A., Moran, M.S., Wu, Y., 2008. Role of precipitation uncertainty in the estimation of hydrologic soil properties using remotely

sensed soil moisture in a semiarid environment. Water Resour. Res. 44. https://doi.org/10.1029/2007WR005884
Priestley, C.H.B., Taylor, R.J., 1972. On the Assessment of Surface Heat Flux and Evaporation Using Large-Scale Parameters. Mon. Weather Rev. 100, 81–92. https://doi.org/10.1175/1520-0493(1972)100<0081:OTAOSH>2.3.CO;2
Qureshi, A.S., 2011. Water Management in the Indus Basin in Pakistan: Challenges and Opportunities. Mt. Res. Dev. 31, 252–260. https://doi.org/10.1659/MRD-JOURNAL-D-11-00019.1
Qureshi, A.S., McCornick, P.G., Sarwar, A., Sharma, B.R., 2010. Challenges and Prospects of Sustainable Groundwater Management in the Indus Basin, Pakistan. Water Resour. Manag. 24, 1551–1569. https://doi.org/10.1007/s11269-009-9513-3
Qureshi, S.K., Hussain, Z., 1994. An Assessment of Warabandi (Irrigation Rotation) in Pakistan: A Preliminary Analysis. Pak. Dev. Rev. 33, 12.
Rajib, A., Evenson, G.R., Golden, H.E., Lane, C.R., 2018. Hydrologic model predictability improves with spatially explicit calibration using remotely sensed evapotranspiration and biophysical parameters. J. Hydrol. 567, 668–683. https://doi.org/10.1016/j.jhydrol.2018.10.024
Rientjes, T.H.M., Muthuwatta, L.P., Bos, M.G., Booij, M.J., Bhatti, H.A., 2013. Multi-variable calibration of a semi-distributed hydrological model using streamflow data and satellite-based evapotranspiration. J. Hydrol. 505, 276–290. https://doi.org/10.1016/j.jhydrol.2013.10.006
Rosenberg, N.J., 1974. Microclimate: The Biological Environment. Wiley, New York.
Rosenzweig, C., Elliott, J., Deryng, D., Ruane, A.C., Müller, C., Arneth, A., Boote, K.J., Folberth, C., Glotter, M., Khabarov, N., Neumann, K., Piontek, F., Pugh, T.A.M., Schmid, E., Stehfest, E., Yang, H., Jones, J.W., 2014. Assessing agricultural risks of climate change in the 21st century in a global gridded crop model intercomparison. Proc. Natl. Acad. Sci. 111, 3268–3273. https://doi.org/10.1073/pnas.1222463110
Saddique, Q., Khan, M.I., Habib ur Rahman, M., Jiatun, X., Waseem, M., Gaiser, T., Mohsin Waqas, M., Ahmad, I., Chong, L., Cai, H., 2020. Effects of Elevated Air Temperature and CO2 on Maize Production and Water Use Efficiency under Future Climate Change Scenarios in Shaanxi Province, China. Atmosphere 11, 843. https://doi.org/10.3390/atmos11080843
Saeed, F., Athar, H., 2018. Assessment of simulated and projected climate change in Pakistan using IPCC AR4-based AOGCMs. Theor. Appl. Climatol. 134, 967–980. https://doi.org/10.1007/s00704-017-2320-5
Saha, S., Moorthi, S., Pan, H.-L., Wu, X., Wang, Jiande, Nadiga, S., Tripp, P., Kistler, R., Woollen, J., Behringer, D., Liu, H., Stokes, D., Grumbine, R., Gayno, G., Wang, Jun, Hou, Y.-T., Chuang, H., Juang, H.-M.H., Sela, J., Iredell, M., Treadon, R., Kleist, D., Van Delst, P., Keyser, D., Derber, J., Ek, M., Meng, J., Wei, H., Yang, R., Lord, S., van den Dool, H., Kumar, A., Wang, W., Long, C., Chelliah, M., Xue, Y., Huang, B., Schemm, J.-K., Ebisuzaki, W., Lin, R., Xie, P., Chen, M., Zhou, S., Higgins, W., Zou, C.-Z., Liu, Q., Chen, Y., Han, Y., Cucurull, L., Reynolds, R.W., Rutledge, G., Goldberg, M., 2010. The NCEP Climate Forecast System Reanalysis. Bull. Am. Meteorol. Soc. 91, 1015–1058. https://doi.org/10.1175/2010BAMS3001.1
Schaap, M.G., Leij, F.J., van Genuchten, M.Th., 2001. rosetta : a computer program for estimating soil hydraulic parameters with hierarchical pedotransfer functions. J. Hydrol. 251, 163–176. https://doi.org/10.1016/S0022-1694(01)00466-8
Schewe, J., Heinke, J., Gerten, D., Haddeland, I., Arnell, N.W., Clark, D.B., Dankers, R., Eisner, S., Fekete, B.M., Colón-González, F.J., Gosling, S.N., Kim, H., Liu, X., Masaki, Y., Portmann, F.T., Satoh, Y., Stacke, T., Tang, Q., Wada, Y., Wisser, D., Albrecht, T., Frieler, K., Piontek, F., Warszawski, L., Kabat, P., 2014. Multimodel assessment of water scarcity under climate change. Proc. Natl. Acad. Sci. 111, 3245–3250. https://doi.org/10.1073/pnas.1222460110
Schulz, S., Becker, R., Richard-Cerda, J.C., Usman, M.O., Beek, T. aus der, Merz, R., Schüth, C., 2020. Energy balance and soil moisture data of an agricultural test field in Faisalabad, Pakistan. PANGAEA: https://doi.pangeaea.de/10.1594/PANGAEA.921389
Schulz, S., Becker, R., Richard-Cerda, J.C., Usman, M., Beek, T., Merz, R., Schüth, C., 2021. Estimating water balance components in irrigated agriculture using a combined approach of soil moisture and energy balance monitoring, and numerical modeling. Hydrol. Process. https://doi.org/10.1002/hyp.14077
Shaw, S.B., Mehta, D., Riha, S.J., 2014. Using simple data experiments to explore the influence of non-temperature controls on maize yields in the mid-West and Great Plains. Clim. Change 122, 747–755. https://doi.org/10.1007/s10584-014-1062-y
Siebert, S., Ewert, F., 2014. Future crop production threatened by extreme heat. Environ. Res. Lett. 9, 041001. https://doi.org/10.1088/1748-9326/9/4/041001

Siebert, S., Ewert, F., Eyshi Rezaei, E., Kage, H., Graß, R., 2014. Impact of heat stress on crop yield—on the importance of considering canopy temperature. Environ. Res. Lett. 9, 044012. https://doi.org/10.1088/1748-9326/9/4/044012

Šimůnek, J., Šejna, M., Saito, H., Sakai, M., van Genuchten, M.Th., 2013. The HYDRUS-1D Software Package for Simulating the One-Dimensional Movement of Water, Heat, and Multiple Solutes in Variably-Saturated Media, 4.17. ed. Department of Environmental Sciences University of California Riverside, Riverside.

Šimůnek, J., van Genuchten, M.Th., Šejna, M., 2008. Development and Applications of the HYDRUS and STANMOD Software Packages and Related Codes. Vadose Zone J. 7, 587–600. https://doi.org/10.2136/vzj2007.0077

Singh, A., Kumar, S., Akula, S., Lawrence, D.M., Lombardozzi, D.L., 2020. Plant Growth Nullifies the Effect of Increased Water-Use Efficiency on Streamflow Under Elevated CO2 in the Southeastern United States. Geophys. Res. Lett. 10.

Singh Vijay P., Woolhiser David A., 2002. Mathematical Modeling of Watershed Hydrology. J. Hydrol. Eng. 7, 270–292. https://doi.org/10.1061/(ASCE)1084-0699(2002)7:4(270)

Sorooshian, S., Duan, Q., Gupta, V.K., 1993. Calibration of rainfall-runoff models: Application of global optimization to the Sacramento Soil Moisture Accounting Model. Water Resour. Res. 29, 1185–1194. https://doi.org/10.1029/92WR02617

Tack, J., Barkley, A., Hendricks, N., 2017. Irrigation offsets wheat yield reductions from warming temperatures. Environ. Res. Lett. 12, 114027. https://doi.org/10.1088/1748-9326/aa8d27

Taraz, V., 2018. Can farmers adapt to higher temperatures? Evidence from India. World Dev. 112, 205–219. https://doi.org/10.1016/j.worlddev.2018.08.006

Taylor, K.E., Stouffer, R.J., Meehl, G.A., 2012. An Overview of CMIP5 and the Experiment Design. Bull. Am. Meteorol. Soc. 93, 485–498. https://doi.org/10.1175/BAMS-D-11-00094.1

Taylor, S.A., Ashcroft, G.L., 1972. Physical Edaphology: The Physics of Irrigated and Nonirrigated Soils. W.H. Freeman, New York.

Teutschbein, C., Seibert, J., 2012. Bias correction of regional climate model simulations for hydrological climate-change impact studies: Review and evaluation of different methods. J. Hydrol. 456–457, 12–29. https://doi.org/10.1016/j.jhydrol.2012.05.052

Tobin, K.J., Bennett, M.E., 2017. Constraining SWAT Calibration with Remotely Sensed Evapotranspiration Data. JAWRA J. Am. Water Resour. Assoc. 53, 593–604. https://doi.org/10.1111/1752-1688.12516

Tolson, B.A., Shoemaker, C.A., 2007. Dynamically dimensioned search algorithm for computationally efficient watershed model calibration. Water Resour. Res. 43. https://doi.org/10.1029/2005WR004723

Troutman, B.M., 1983. Runoff prediction errors and bias in parameter estimation induced by spatial variability of precipitation. Water Resour. Res. 19, 791–810. https://doi.org/10.1029/WR019i003p00791

Ullah, S., 2017. Climate Change Impact on Agriculture of Pakistan- A Leading Agent to Food Security. Int. J. Environ. Sci. 4.

Usman, M., Liedl, R., Awan, U.K., 2015a. Spatio-temporal estimation of consumptive water use for assessment of irrigation system performance and management of water resources in irrigated Indus Basin, Pakistan. J. Hydrol. 525, 26–41. https://doi.org/10.1016/j.jhydrol.2015.03.031

Usman, M., Liedl, R., Kavousi, A., 2015b. Estimation of distributed seasonal net recharge by modern satellite data in irrigated agricultural regions of Pakistan. Environ. Earth Sci. 74, 1463–1486. https://doi.org/10.1007/s12665-015-4139-7

Usman, M., Reimann, T., Liedl, R., Abbas, A., Conrad, C., Saleem, S., Usman, M., Reimann, T., Liedl, R., Abbas, A., Conrad, C., Saleem, S., 2018. Inverse Parametrization of a Regional Groundwater Flow Model with the Aid of Modelling and GIS: Test and Application of Different Approaches. ISPRS Int. J. Geo-Inf. 7, 22. https://doi.org/10.3390/ijgi7010022

van Genuchten, M.Th., 1980. A Closed-form Equation for Predicting the Hydraulic Conductivity of Unsaturated Soils. Soil Sci. Soc. Am. J. 44, 892–898. https://doi.org/10.2136/sssaj1980.03615995004400050002x

van Griensven, A., Meixner, T., Grunwald, S., Bishop, T., Diluzio, M., Srinivasan, R., 2006. A global sensitivity analysis tool for the parameters of multi-variable catchment models. J. Hydrol. 324, 10–23. https://doi.org/10.1016/j.jhydrol.2005.09.008

van Griensven, A. van, Bauwens, W., 2003. Multiobjective autocalibration for semidistributed water quality models. Water Resour. Res. 39. https://doi.org/10.1029/2003WR002284

van Vuuren, D.P., Edmonds, J., Kainuma, M., Riahi, K., Thomson, A., Hibbard, K., Hurtt, G.C., Kram, T., Krey, V., Lamarque, J.-F., Masui, T., Meinshausen, M., Nakicenovic, N., Smith, S.J., Rose, S.K., 2011. The representative concentration pathways: an overview. Clim. Change 109, 5–31. https://doi.org/10.1007/s10584-011-0148-z

Vanuytrecht, E., Raes, D., Willems, P., Geerts, S., 2012. Quantifying field-scale effects of elevated carbon dioxide concentration on crops. Clim. Res. 54, 35–47. https://doi.org/10.3354/cr01096

Vrugt, J.A., Gupta, H.V., Bouten, W., Sorooshian, S., 2003. A Shuffled Complex Evolution Metropolis algorithm for optimization and uncertainty assessment of hydrologic model parameters: Efficient method for estimating parameter uncertainty. Water Resour. Res. 39. https://doi.org/10.1029/2002WR001642

Wada, Y., Wisser, D., Eisner, S., Flörke, M., Gerten, D., Haddeland, I., Hanasaki, N., Masaki, Y., Portmann, F.T., Stacke, T., Tessler, Z., Schewe, J., 2013. Multimodel projections and uncertainties of irrigation water demand under climate change: Irrigation demand under climate change. Geophys. Res. Lett. 40, 4626–4632. https://doi.org/10.1002/grl.50686

Wang, K., Dickinson, R.E., 2012. A review of global terrestrial evapotranspiration: Observation, modeling, climatology, and climatic variability. Rev. Geophys. 50. https://doi.org/10.1029/2011RG000373

Wang, X., Zhang, J., Shahid, S., Guan, E., Wu, Y., Gao, J., He, R., 2016. Adaptation to climate change impacts on water demand. Mitig. Adapt. Strateg. Glob. Change 21, 81–99. https://doi.org/10.1007/s11027-014-9571-6

Wang, Y.Q., Xiong, Y.J., Qiu, G.Y., Zhang, Q.T., 2016. Is scale really a challenge in evapotranspiration estimation? A multi-scale study in the Heihe oasis using thermal remote sensing and the three-temperature model. Agric. For. Meteorol. 230–231, 128–141. https://doi.org/10.1016/j.agrformet.2016.03.012

Wesseling, J.G., 1991. Meerjarige simulatie van grondwaterstroming voor verschillende bodemprofielen, grondwatertrappen en gewassen met het model SWATRE. Wageningen.

Williams, A., White, N., Mushtaq, S., Cockfield, G., Power, B., Kouadio, L., 2015. Quantifying the response of cotton production in eastern Australia to climate change. Clim. Change 129, 183–196. https://doi.org/10.1007/s10584-014-1305-y

Wisser, D., Frolking, S., Douglas, E.M., Fekete, B.M., Vörösmarty, C.J., Schumann, A.H., 2008. Global irrigation water demand: Variability and uncertainties arising from agricultural and climate data sets. Geophys. Res. Lett. 35, L24408. https://doi.org/10.1029/2008GL035296

Wongkaew, A., Saito, H., Fujimaki, H., Šimůnek, J., 2018. Numerical analysis of soil water dynamics in a soil column with an artificial capillary barrier growing leaf vegetables. Soil Use Manag. 34, 206–215. https://doi.org/10.1111/sum.12423

Wu, Y., Liu, S., Abdul-Aziz, O.I., 2012. Hydrological effects of the increased CO2 and climate change in the Upper Mississippi River Basin using a modified SWAT. Clim. Change 110, 977–1003. https://doi.org/10.1007/s10584-011-0087-8

Wullschleger, S.D., Tschaplinski, T.J., Norby, R.J., 2002. Plant water relations at elevated CO_2 - implications for water-limited environments: Interactions between elevated CO_2 and drought. Plant Cell Environ. 25, 319–331. https://doi.org/10.1046/j.1365-3040.2002.00796.x

Yoo, C.Y., Pence, H.E., Hasegawa, P.M., Mickelbart, M.V., 2009. Regulation of Transpiration to Improve Crop Water Use. Crit. Rev. Plant Sci. 28, 410–431. https://doi.org/10.1080/07352680903173175

Zambrano-Bigiarini, M., Rojas, R., 2013. A model-independent Particle Swarm Optimisation software for model calibration. Environ. Model. Softw. 43, 5–25. https://doi.org/10.1016/j.envsoft.2013.01.004

Zaveri, E., Lobell, D., 2019. The role of irrigation in changing wheat yields and heat sensitivity in India. Nat. Commun. 10. https://doi.org/10.1038/s41467-019-12183-9

Zhang, X., Srinivasan, R., Zhao, K., Liew, M.V., 2008. Evaluation of global optimization algorithms for parameter calibration of a computationally intensive hydrologic model. Hydrol. Process. 23, 430–441. https://doi.org/10.1002/hyp.7152

Zhang, Y., Schaap, M.G., 2017. Weighted recalibration of the Rosetta pedotransfer model with improved estimates of hydraulic parameter distributions and summary statistics (Rosetta3). J. Hydrol. 547, 39–53. https://doi.org/10.1016/j.jhydrol.2017.01.004

Zhao, C., Liu, B., Piao, S., Wang, X., Lobell, D.B., Huang, Y., Huang, M., Yao, Y., Bassu, S., Ciais, P., Durand, J.-L., Elliott, J., Ewert, F., Janssens, I.A., Li, T., Lin, E., Liu, Q., Martre, P., Müller, C., Peng, S., Peñuelas, J., Ruane, A.C., Wallach, D., Wang, T., Wu, D., Liu, Z., Zhu, Y., Zhu, Z., Asseng, S., 2017.

Temperature increase reduces global yields of major crops in four independent estimates. Proc. Natl. Acad. Sci. 114, 9326–9331. https://doi.org/10.1073/pnas.1701762114
Zink, M., Mai, J., Cuntz, M., Samaniego, L., 2018. Conditioning a Hydrologic Model Using Patterns of Remotely Sensed Land Surface Temperature. Water Resour. Res. 54, 2976–2998. https://doi.org/10.1002/2017WR021346

10 Annex

10.1 Annex – Chapter 4

A 4-1 – Monthly correction factors for each land-use type; for land-use class descriptions see Fig. 4-1

Month	FOCO	WHCO	WHMZ	FOFO	WHFA	WHRI	FOFA	SUGR	WHFO
Jan	1.38	1.29	1.29	1.38	1.29	1.29	1.38	0.34	1.29
Feb	1.04	0.96	0.96	1.04	0.96	0.96	1.04	1	0.96
Mar	1.31	1.17	1.17	1.31	1.17	1.17	1.31	0.53	1.17
Apr	0.48	0.35	0.35	0.48	0.35	0.35	0.48	2.17	0.35
May	0.5	0.5	0.4	0.4	0.2	1	0.2	1.5	0.4
Jun	0.73	0.73	0.77	0.77	0.2	1.42	0.2	1.61	0.77
Jul	0.82	0.82	1.02	1.02	0.2	1.09	0.2	1.16	1.02
Aug	0.7	0.7	1.08	1.08	0.2	1.08	0.2	1.07	1.08
Sep	0.56	0.56	1.22	1.22	0.2	1.27	0.2	1.27	1.22
Oct	0.33	0.33	0.75	0.75	0.2	1.26	0.2	1.66	0.75
Nov	0.44	0.97	0.97	0.44	0.97	0.97	0.44	1.59	0.97
Dec	0.86	1.05	1.05	0.86	1.05	1.05	0.86	1.09	1.05

A 4-2 – New parameter ranges from best calibration runs, yielding a KGE of 0.4, for all land-use classes used in calibration. The range of parameter values shows the spread of calibrated values for all HRUs of each respective land use or soil class.

#	Parameter name	Land-use /Soil Class	Unit	Range		
				1st quantile	mean	3rd quantile
1	EPCO	Fodder-Cotton	-	0.90	0.90	0.90
2	EPCO	Fodder-Fallow	-	0.99	0.99	0.99
3	EPCO	Fodder-Fodder	-	0.91	0.91	0.91
4	EPCO	Sugarcane	-	0.02	0.02	0.02
5	EPCO	Wheat-Cotton	-	0.91	0.91	0.91
6	EPCO	Wheat-Fallow	-	0.04	0.04	0.04
7	EPCO	Wheat-Fodder	-	0.91	0.91	0.91
8	EPCO	Wheat-Maize	-	0.99	0.99	0.99
9	EPCO	Wheat-Rice	-	0.83	0.83	0.83
10	CN2	Fodder-Cotton	-	69	69	69
11	CN2	Fodder-Fallow	-	41	41	41
12	CN2	Fodder-Fodder	-	68	69	71
13	CN2	Sugarcane	-	71	70	71
14	CN2	Wheat-Cotton	-	42	45	49
15	CN2	Wheat-Fallow	-	33	35	36
16	CN2	Wheat-Fodder	-	74	74	74
17	CN2	Wheat-Maize	-	65	65	65
18	CN2	Wheat-Rice	-	44	46	44
19	SOL_AWC	Farida (loam)	mm H_2O/mm soil	0.065	0.066	0.067
20	SOL_AWC	Jhang (fine-sandy loam)	mm H_2O/mm soil	0.045	0.045	0.045
21	SOL_AWC	Buchiana (clay loam)	mm H_2O/mm soil	0.061	0.063	0.064
22	SOL_AWC	Chuharcana (loamy sand)	mm H_2O/mm soil	0.054	0.045	0.045
23	GW_DELAY	Fodder-Cotton	days	236	295	375
24	GW_DELAY	Fodder-Fallow	days	229	306	348
25	GW_DELAY	Fodder-Fodder	days	164	210	266

26	GW_DELAY	Sugarcane	days	248	256	292
27	GW_DELAY	Wheat-Cotton	days	38	39	47
28	GW_DELAY	Wheat-Fallow	days	356	404	496
29	GW_DELAY	Wheat-Fodder	days	192	244	289
30	GW_DELAY	Wheat-Maize	days	17	37	45
31	GW_DELAY	Wheat-Rice	days	198	214	204
32	SOL_K1	Farida (loam)	mm/h	374	374	374
33	SOL_K1	Jhang (fine-sandy loam)	mm/h	470	470	470
34	SOL_K1	Buchiana (clay loam)	mm/h	389	389	389
35	SOL_K1	Chuharcana (loamy sand)	mm/h	480	480	480
36	SOL_K2	Farida (loam)	mm/h	50	50	50
37	SOL_K2	Jhang (fine-sandy loam)	mm/h	86	86	86
38	SOL_K2	Buchiana (clay loam)	mm/h	52	52	53
39	SOL_K2	Chuharcana (loamy sand)	mm/h	64	64	64
40	SOL_K3	Farida (loam)	mm/h	4.8	4.8	4.8
41	SOL_K3	Jhang (fine-sandy loam)	mm/h	26	26	30
43	SOL_K3	Buchiana (clay loam)	mm/h	15	15	15
44	SOL_K3	Chuharcana (loamy sand)	mm/h	45	45	45

10.2 Annex – Chapter 5

A 5-1 – Measured soil texture and bulk density

	Sand [%]	Silt [%]	Clay [%]	Bulk density [g cm-3]
Layer 1 (0-15 cm)	46.8	51.5	1.6	1.45
Layer 2 (15-60 cm)	54.9	39.5	5.6	1.61
Layer 3 (60-200 cm)	56.1	39.0	4.9	1.59

A 5-2 – First approximation of inflow estimates

	First approximation of inflow [mm]					Range [mm]
Date	linear	makina	nearest	pchip	spline	
2018-08-16	149.34	146.26	138.47	145.65	148.31	10.87
2018-09-04	133.17	135.11	126.53	134.02	127.58	8.58
2018-09-11	83.39	83.79	81.02	83.50	83.60	2.77
2018-09-25	73.22	72.55	68.88	72.76	83.29	14.41
2018-09-28	31.11	30.91	31.85	30.85	33.16	2.31
2018-09-18	72.55	72.40	68.93	72.13	74.82	5.89
2019-01-14	73.93	73.71	71.86	73.85	72.22	2.06
2019-01-21	2.94	2.95	1.96	3.36	4.98	3.03
2019-01-31	7.30	6.58	5.11	7.13	1.43	5.87
2019-02-07	4.14	4.66	3.44	4.34	2.98	1.69
2019-02-19	45.55	45.74	44.77	45.50	48.67	3.90
2019-02-25	12.73	13.03	13.28	12.76	14.58	1.85
2019-03-02	3.64	3.20	2.04	3.67	2.97	1.64
2019-03-12	120.99	118.67	118.23	120.37	129.12	10.89
2019-03-19	73.50	72.55	71.51	74.52	73.48	3.02
2019-04-16	7.34	5.89	6.40	7.43	5.31	2.12
2019-04-17	8.07	6.79	6.62	7.09	4.04	4.04
2019-04-18	6.61	6.54	6.13	6.23	6.28	0.48

A 5-3 – Van Genuchten Parameter estimates with standard deviation (σ) derived by the Rosetta model using soil texture and bulk density information.

	θr [%]	σ [%]	θs [%]	σ [%]	α [cm^{-1}]	σ [cm^{-1}]	n [cm^{-1}]	σ [cm^{-1}]	Ks [cm d^{-1}]	σ [cm d^{-1}]
Layer 1 (0-15 cm)	5.2	1.3	36.3	1.9	0.009	0.14*	1.6	0.026*	51.7	0.23*
Layer 2 (15-60 cm)	5.5	1.2	33.9	1.4	0.013	0.11*	1.5	0.018*	24.9	0.14*
Layer 3 (60-200 cm)	5.5	1.2	34.1	1.4	0.014	0.11*	1.5	0.019*	28.6	0.14*

* log10-transformed

A 5-4 – Optimized van Genuchten Parameter using CMAES (Covariance Matrix Adaptation Evolution Strategy) and RMSE (root mean squared error) of simulated and observed volumetric water content.

		θr [%]	θs [%]	α [cm^{-1}]	n [cm^{-1}]	Ks [cm d^{-1}]	RMSE [%]
Maximum	Layer 1 (0-15 cm)	2.6	40.6	0.0011	1.71	40.6	2.25
	Layer 2 (15-60 cm)	3.2	35.0	0.0017	1.49	19.5	
	Layer 3 (60-200 cm)	3.1	35.0	0.0021	1.60	22.4	
Mean	Layer 1 (0-15 cm)	2.6	40.6	0.0010	1.67	40.5	2.15
	Layer 2 (15-60 cm)	3.2	35.0	0.0016	1.46	19.5	

	Layer 3 (60-200 cm)	3.1	35.0	0.0020	1.60	22.4	
	Layer 1 (0-15 cm)	2.6	40.6	0.0010	1.65	35.2	
Minimum	Layer 2 (15-60 cm)	3.2	35.0	0.0016	1.44	17.0	2.17
	Layer 3 (60-200 cm)	3.1	35.0	0.0018	1.60	19.5	

A 5-5 – Daily sums of simulated water balance components inflow, actual evapotranpiration (ET_{act}) and downward flux at 2 mbgl ($Flux_{2m}$)

	Inflow [mm]			ET_{act} [mm]			$Flux_{2m}$ [mm]		
Date	min	mean	max	min	mean	max	min	mean	max
2018-08-16	135.37	146.72	165.27	0.50	0.56	0.60	0.37	0.43	0.43
2018-08-17	-	-	-	3.39	3.43	3.43	0.96	1.10	1.11
2018-08-18	-	-	-	7.34	7.36	7.36	0.92	1.05	1.05
2018-08-19	-	-	-	7.50	7.52	7.51	0.88	1.00	1.03
2018-08-20	-	-	-	7.39	7.40	7.40	0.84	0.98	1.14
2018-08-21	-	-	-	7.01	7.03	7.03	0.82	1.02	1.52
2018-08-22	-	-	-	6.43	6.44	6.45	0.81	1.13	2.00
2018-08-23	-	-	-	7.06	7.08	7.09	0.83	1.26	2.36
2018-08-24	-	-	-	7.04	7.06	7.07	0.85	1.38	2.55
2018-08-25	-	-	-	6.89	6.91	6.93	0.88	1.45	2.59
2018-08-26	-	-	-	6.66	6.67	6.69	0.91	1.49	2.52
2018-08-27	-	-	-	6.50	6.52	6.54	0.92	1.49	2.41
2018-08-28	-	-	-	5.64	5.66	5.68	0.93	1.47	2.27
2018-08-29	-	-	-	4.84	4.87	4.89	0.93	1.42	2.13
2018-08-30	-	-	-	6.15	6.32	6.36	0.91	1.37	1.99
2018-08-31	-	-	-	5.29	5.66	5.79	0.90	1.31	1.85
2018-09-01	-	-	-	4.76	4.99	5.08	0.87	1.25	1.73
2018-09-02	-	-	-	4.16	4.31	4.38	0.85	1.19	1.61
2018-09-03	-	-	-	3.23	3.34	3.40	0.82	1.13	1.51
2018-09-04	123.73	133.88	149.26	7.02	7.07	7.06	0.79	1.07	1.41
2018-09-05	-	-	-	6.94	6.97	6.96	0.77	1.02	1.32
2018-09-06	-	-	-	6.50	6.51	6.51	0.74	0.97	1.25
2018-09-07	-	-	-	5.77	5.78	5.77	0.71	0.93	1.29
2018-09-08	-	-	-	6.52	6.53	6.53	0.68	0.93	1.60
2018-09-09	-	-	-	2.25	2.26	2.25	0.67	1.00	2.06
2018-09-10	-	-	-	6.44	6.46	6.46	0.68	1.12	2.44
2018-09-11	80.79	84.66	89.52	6.45	6.48	6.37	0.70	1.24	2.65
2018-09-12	-	-	-	7.67	7.69	7.67	0.73	1.34	2.71
2018-09-13	-	-	-	7.06	7.07	7.05	0.76	1.44	2.98
2018-09-14	-	-	-	7.59	7.60	7.59	0.82	1.77	4.35
2018-09-15	-	-	-	5.27	5.27	5.26	0.95	2.43	5.83
2018-09-16	-	-	-	6.54	6.55	6.54	1.20	3.03	6.04
2018-09-17	-	-	-	6.02	6.03	6.02	1.46	3.32	5.60
2018-09-18	-	-	-	6.50	6.51	6.51	1.68	3.34	4.94
2018-09-19	-	-	-	6.26	6.27	6.27	1.80	3.21	4.32
2018-09-20	-	-	-	6.18	6.18	6.19	1.85	3.02	3.88
2018-09-21	-	-	-	6.06	6.07	6.08	1.85	2.81	3.49
2018-09-22	-	-	-	6.01	6.02	6.02	1.80	2.59	3.15
2018-09-23	-	-	-	4.15	4.15	4.16	1.74	2.39	2.86
2018-09-24	-	-	-	5.83	5.84	5.85	1.66	2.20	2.60
2018-09-25	66.91	74.98	89.29	5.58	5.60	5.59	1.58	2.03	2.37
2018-09-26	-	-	-	5.85	5.89	5.91	1.49	1.88	2.17
2018-09-27	-	-	-	6.00	6.02	6.03	1.41	1.74	1.99
2018-09-28	32.18	36.68	43.06	6.81	6.87	6.86	1.33	1.62	1.85
2018-09-29	-	-	-	5.56	5.60	5.61	1.26	1.52	1.75
2018-09-30	-	-	-	5.32	5.35	5.36	1.19	1.44	1.73

2018-10-01	-	-	-	5.25	5.28	5.28	1.14	1.39	1.80
2018-10-02	-	-	-	5.17	5.19	5.19	1.10	1.38	2.02
2018-10-03	-	-	-	5.43	5.45	5.45	1.07	1.42	2.34
2018-10-04	-	-	-	6.35	6.37	6.37	1.06	1.48	2.61
2018-10-05	-	-	-	5.89	5.91	5.92	1.06	1.55	2.76
2018-10-06	-	-	-	4.98	5.00	5.01	1.06	1.59	2.78
2018-10-07	-	-	-	4.49	4.50	4.52	1.06	1.61	2.72
2018-10-08	-	-	-	5.18	5.20	5.21	1.06	1.60	2.60
2018-10-09	-	-	-	5.22	5.23	5.24	1.05	1.57	2.46
2018-10-10	-	-	-	4.32	4.33	4.34	1.04	1.52	2.31
2018-10-11	-	-	-	3.98	3.99	4.01	1.02	1.47	2.16
2018-10-12	-	-	-	3.36	3.38	3.39	0.99	1.40	2.02
2018-10-13	-	-	-	3.86	3.87	3.89	0.96	1.34	1.89
2018-10-14	-	-	-	3.42	3.44	3.45	0.93	1.28	1.76
2018-10-15	-	-	-	3.49	3.52	3.54	0.90	1.21	1.65
2018-10-16	-	-	-	2.99	3.45	3.47	0.87	1.15	1.54
2018-10-17	-	-	-	2.57	2.93	3.16	0.84	1.10	1.45
2018-10-18	-	-	-	2.63	2.90	3.07	0.81	1.04	1.36
2018-10-19	-	-	-	2.19	2.38	2.49	0.78	0.99	1.28
2018-10-20	-	-	-	2.09	2.22	2.32	0.75	0.95	1.21
2018-10-21	-	-	-	1.93	2.06	2.13	0.72	0.90	1.14
2018-10-22	-	-	-	1.60	1.70	1.76	0.69	0.86	1.08
2018-10-23	-	-	-	1.70	1.79	1.84	0.67	0.82	1.03
2018-10-24	-	-	-	1.52	1.59	1.64	0.64	0.79	0.98
2018-10-25	-	-	-	1.24	1.31	1.35	0.62	0.75	0.93
2018-10-26	-	-	-	1.10	1.15	1.19	0.60	0.72	0.88
2018-10-27	-	-	-	1.00	1.05	1.08	0.58	0.69	0.84
2018-10-28	-	-	-	1.10	1.14	1.19	0.56	0.66	0.81
2018-10-29	-	-	-	0.76	0.81	0.84	0.54	0.64	0.77
2018-10-30	-	-	-	0.79	0.84	0.86	0.52	0.61	0.74
2018-10-31	-	-	-	0.48	0.50	0.52	0.50	0.59	0.71
2018-11-01	-	-	-	-	-	-	-	-	-
2018-11-02	-	-	-	-	-	-	-	-	-
2018-11-03	-	-	-	-	-	-	-	-	-
2018-11-04	-	-	-	-	-	-	-	-	-
2018-11-05	-	-	-	-	-	-	-	-	-
2018-11-06	-	-	-	-	-	-	-	-	-
2018-11-07	-	-	-	-	-	-	-	-	-
2018-11-08	-	-	-	-	-	-	-	-	-
2018-11-09	-	-	-	-	-	-	-	-	-
2018-11-10	-	-	-	-	-	-	-	-	-
2018-11-11	-	-	-	1.62	1.64	1.64	0.87	1.00	1.00
2018-11-12	-	-	-	1.37	1.38	1.38	0.87	1.01	1.01
2018-11-13	-	-	-	2.32	2.33	2.32	0.88	1.02	1.02
2018-11-14	-	-	-	2.07	2.08	2.07	0.89	1.02	1.02
2018-11-15	-	-	-	2.25	2.26	2.26	0.89	1.03	1.03
2018-11-16	-	-	-	2.37	2.38	2.37	0.90	1.04	1.04
2018-11-17	-	-	-	1.61	1.62	1.61	0.90	1.05	1.06
2018-11-18	-	-	-	1.70	1.70	1.70	0.91	1.05	1.07
2018-11-19	-	-	-	1.11	1.11	1.11	0.91	1.06	1.08
2018-11-20	-	-	-	2.17	2.18	2.18	0.91	1.06	1.09
2018-11-21	-	-	-	2.28	2.29	2.28	0.90	1.05	1.09
2018-11-22	-	-	-	1.33	1.33	1.33	0.90	1.04	1.08
2018-11-23	-	-	-	2.53	2.53	2.53	0.89	1.03	1.08
2018-11-24	-	-	-	2.82	2.83	2.83	0.88	1.01	1.07
2018-11-25	-	-	-	1.64	1.65	1.64	0.86	1.00	1.05
2018-11-26	-	-	-	1.43	1.43	1.43	0.85	0.97	1.03
2018-11-27	-	-	-	0.83	0.83	0.83	0.83	0.95	1.01
2018-11-28	-	-	-	1.22	1.22	1.22	0.82	0.93	0.99

2018-11-29	-	-	-	0.88	0.88	0.88	0.80	0.91	0.97
2018-11-30	-	-	-	1.57	1.57	1.57	0.78	0.88	0.94
2018-12-01	-	-	-	1.42	1.42	1.42	0.76	0.86	0.92
2018-12-02	-	-	-	1.51	1.52	1.52	0.74	0.83	0.89
2018-12-03	-	-	-	1.21	1.21	1.21	0.72	0.81	0.87
2018-12-04	-	-	-	1.06	1.06	1.05	0.71	0.79	0.85
2018-12-05	-	-	-	1.25	1.25	1.25	0.69	0.77	0.82
2018-12-06	-	-	-	0.89	0.89	0.89	0.67	0.74	0.80
2018-12-07	-	-	-	1.08	1.08	1.08	0.65	0.72	0.78
2018-12-08	-	-	-	1.01	1.01	1.01	0.64	0.70	0.75
2018-12-09	-	-	-	0.83	0.84	0.83	0.62	0.68	0.73
2018-12-10	-	-	-	0.64	0.64	0.64	0.60	0.66	0.71
2018-12-11	-	-	-	0.93	0.93	0.93	0.59	0.64	0.69
2018-12-12	-	-	-	0.82	0.82	0.82	0.57	0.62	0.67
2018-12-13	-	-	-	1.29	1.29	1.29	0.56	0.60	0.65
2018-12-14	-	-	-	1.45	1.46	1.45	0.54	0.59	0.63
2018-12-15	-	-	-	1.37	1.38	1.37	0.53	0.57	0.61
2018-12-16	-	-	-	1.35	1.35	1.35	0.51	0.55	0.60
2018-12-17	-	-	-	1.37	1.37	1.37	0.50	0.54	0.58
2018-12-18	68.49	73.39	79.04	2.09	2.12	2.12	0.49	0.52	0.56
2018-12-19	-	-	-	1.81	1.83	1.83	0.47	0.51	0.55
2018-12-20	-	-	-	1.29	1.31	1.30	0.46	0.49	0.53
2018-12-21	-	-	-	1.56	1.57	1.56	0.45	0.48	0.52
2018-12-22	-	-	-	1.50	1.51	1.51	0.44	0.47	0.50
2018-12-23	-	-	-	0.88	0.89	0.89	0.42	0.45	0.49
2018-12-24	-	-	-	1.03	1.04	1.04	0.41	0.44	0.47
2018-12-25	-	-	-	1.31	1.32	1.32	0.40	0.43	0.46
2018-12-26	-	-	-	1.02	1.02	1.02	0.39	0.42	0.45
2018-12-27	-	-	-	0.70	0.70	0.70	0.39	0.42	0.45
2018-12-28	-	-	-	1.21	1.22	1.21	0.38	0.41	0.45
2018-12-29	-	-	-	0.82	0.83	0.83	0.38	0.41	0.46
2018-12-30	-	-	-	1.07	1.07	1.07	0.37	0.42	0.47
2018-12-31	-	-	-	0.78	0.79	0.78	0.37	0.43	0.48
2019-01-01	-	-	-	0.42	0.43	0.43	0.38	0.44	0.50
2019-01-02	-	-	-	0.66	0.67	0.66	0.38	0.45	0.51
2019-01-03	-	-	-	1.31	1.32	1.31	0.38	0.46	0.53
2019-01-04	-	-	-	1.28	1.28	1.28	0.39	0.47	0.55
2019-01-05	-	-	-	0.79	0.79	0.79	0.39	0.48	0.56
2019-01-06	-	-	-	1.90	1.91	1.90	0.40	0.49	0.58
2019-01-07	-	-	-	1.30	1.30	1.30	0.40	0.49	0.59
2019-01-08	-	-	-	1.60	1.60	1.60	0.41	0.50	0.60
2019-01-09	-	-	-	1.99	1.99	1.99	0.41	0.51	0.61
2019-01-10	-	-	-	1.15	1.15	1.15	0.41	0.51	0.61
2019-01-11	-	-	-	1.40	1.40	1.40	0.42	0.52	0.62
2019-01-12	-	-	-	0.54	0.55	0.54	0.42	0.52	0.62
2019-01-13	-	-	-	1.51	1.51	1.51	0.42	0.52	0.63
2019-01-14	71.10	78.56	91.78	1.84	1.86	1.81	0.42	0.53	0.63
2019-01-15	-	-	-	2.15	2.19	2.19	0.42	0.52	0.63
2019-01-16	-	-	-	0.79	0.81	0.81	0.42	0.52	0.62
2019-01-17	-	-	-	1.27	1.29	1.28	0.42	0.52	0.62
2019-01-18	-	-	-	1.56	1.57	1.57	0.42	0.52	0.61
2019-01-19	-	-	-	1.57	1.58	1.57	0.42	0.51	0.63
2019-01-20	-	-	-	0.14	0.15	0.15	0.42	0.52	0.68
2019-01-21	1.98	4.70	7.81	0.05	0.06	0.06	0.43	0.55	0.80
2019-01-22	-	-	-	1.71	1.74	1.74	0.44	0.60	0.97
2019-01-23	-	-	-	1.25	1.27	1.28	0.46	0.67	1.18
2019-01-24	-	-	-	1.91	1.93	1.93	0.49	0.75	1.38
2019-01-25	-	-	-	2.17	2.19	2.20	0.52	0.85	1.56
2019-01-26	-	-	-	2.08	2.09	2.09	0.57	0.94	1.71

2019-01-27	-	-	-	2.65	2.66	2.66	0.61	1.02	1.82
2019-01-28	-	-	-	2.82	2.83	2.83	0.66	1.09	1.90
2019-01-29	-	-	-	2.06	2.07	2.08	0.70	1.15	1.95
2019-01-30	-	-	-	0.40	0.40	0.41	0.74	1.20	1.96
2019-01-31	1.63	6.21	8.54	0.02	0.03	0.04	0.77	1.23	1.95
2019-02-01	-	-	-	1.67	1.70	1.71	0.80	1.25	1.92
2019-02-02	-	-	-	2.35	2.39	2.40	0.82	1.25	1.88
2019-02-03	-	-	-	2.22	2.25	2.26	0.84	1.25	1.83
2019-02-04	-	-	-	2.01	2.04	2.04	0.85	1.24	1.77
2019-02-05	-	-	-	2.59	2.61	2.62	0.85	1.22	1.71
2019-02-06	-	-	-	1.18	1.19	1.19	0.85	1.20	1.66
2019-02-07	2.60	4.12	6.02	1.56	1.58	1.60	0.85	1.18	1.60
2019-02-08	-	-	-	2.23	2.25	2.26	0.84	1.15	1.55
2019-02-09	-	-	-	2.81	2.84	2.85	0.84	1.13	1.50
2019-02-10	-	-	-	2.15	2.17	2.18	0.83	1.10	1.45
2019-02-11	-	-	-	2.41	2.42	2.43	0.81	1.07	1.40
2019-02-12	-	-	-	1.20	1.20	1.21	0.80	1.04	1.35
2019-02-13	-	-	-	-	-	-	-	-	-
2019-02-14	-	-	-	-	-	-	-	-	-
2019-02-15	-	-	-	-	-	-	-	-	-
2019-02-16	-	-	-	-	-	-	-	-	-
2019-02-17	-	-	-	-	-	-	-	-	-
2019-02-18	-	-	-	-	-	-	-	-	-
2019-02-19	-	-	-	-	-	-	-	-	-
2019-02-20	42.55	45.49	52.60	0.04	0.04	0.04	0.65	0.80	0.99
2019-02-21	-	-	-	1.87	1.90	1.92	0.63	0.77	0.96
2019-02-22	-	-	-	3.64	3.68	3.69	0.61	0.75	0.92
2019-02-23	-	-	-	3.91	3.95	3.97	0.59	0.72	0.88
2019-02-24	-	-	-	3.50	3.53	3.54	0.57	0.69	0.85
2019-02-25	10.19	13.03	19.67	2.21	2.25	2.30	0.55	0.67	0.81
2019-02-26	-	-	-	2.92	2.98	3.04	0.53	0.64	0.78
2019-02-27	-	-	-	3.36	3.40	3.45	0.52	0.62	0.75
2019-02-28	-	-	-	2.90	2.94	2.97	0.50	0.59	0.73
2019-03-01	-	-	-	1.57	1.59	1.61	0.48	0.57	0.70
2019-03-02	2.16	4.09	5.79	0.02	0.02	0.03	0.46	0.55	0.69
2019-03-03	-	-	-	0.06	0.07	0.08	0.45	0.54	0.67
2019-03-04	-	-	-	3.86	3.89	3.91	0.43	0.52	0.66
2019-03-05	-	-	-	4.27	4.30	4.33	0.42	0.51	0.66
2019-03-06	-	-	-	5.16	5.19	5.21	0.41	0.50	0.66
2019-03-07	-	-	-	3.41	3.43	3.44	0.40	0.49	0.67
2019-03-08	-	-	-	2.83	2.84	2.85	0.39	0.48	0.67
2019-03-09	-	-	-	4.43	4.45	4.46	0.37	0.47	0.67
2019-03-10	-	-	-	4.94	4.95	4.97	0.36	0.47	0.68
2019-03-11	-	-	-	3.74	3.76	3.76	0.35	0.46	0.68
2019-03-12	119.82	129.84	149.93	4.38	4.38	4.39	0.34	0.45	0.68
2019-03-13	-	-	-	3.62	3.65	3.62	0.34	0.44	0.67
2019-03-14	-	-	-	4.07	4.08	4.07	0.33	0.43	0.67
2019-03-15	-	-	-	4.91	4.92	4.91	0.32	0.43	1.05
2019-03-16	-	-	-	4.68	4.69	4.68	0.31	0.45	3.35
2019-03-17	-	-	-	5.40	5.41	5.40	0.30	0.62	5.63
2019-03-18	-	-	-	3.47	3.47	3.47	0.31	0.99	6.10
2019-03-19	78.84	87.66	98.01	5.80	5.81	5.80	0.35	1.46	5.93
2019-03-20	-	-	-	5.11	5.16	5.09	0.41	1.85	5.53
2019-03-21	-	-	-	5.95	5.97	5.95	0.50	2.25	7.35
2019-03-22	-	-	-	6.54	6.55	6.53	0.65	4.23	12.08
2019-03-23	-	-	-	3.42	3.42	3.41	1.08	6.69	12.04
2019-03-24	-	-	-	3.81	3.81	3.80	1.88	7.17	10.58
2019-03-25	-	-	-	5.73	5.73	5.72	2.65	6.84	8.85
2019-03-26	-	-	-	6.07	6.07	6.06	3.10	6.20	7.24

2019-03-27	-	-	-	4.82	4.82	4.81	3.26	5.44	6.31
2019-03-28	-	-	-	4.60	4.60	4.59	3.23	4.68	5.61
2019-03-29	-	-	-	5.53	5.53	5.52	3.10	4.14	4.92
2019-03-30	-	-	-	6.44	6.44	6.44	2.94	3.74	4.27
2019-03-31	-	-	-	7.73	7.75	7.74	2.76	3.39	3.70
2019-04-01	-	-	-	7.02	7.01	7.02	2.58	3.07	3.31
2019-04-02	-	-	-	6.25	6.25	6.24	2.40	2.81	3.01
2019-04-03	-	-	-	6.44	6.45	6.44	2.24	2.57	2.75
2019-04-04	-	-	-	5.58	5.58	5.59	2.08	2.36	2.52
2019-04-05	-	-	-	5.21	5.23	5.22	1.94	2.17	2.31
2019-04-06	-	-	-	5.15	5.16	5.16	1.81	2.01	2.13
2019-04-07	-	-	-	5.30	5.33	5.02	1.69	1.86	1.97
2019-04-08	-	-	-	5.45	5.48	5.25	1.59	1.73	1.83
2019-04-09	-	-	-	4.78	4.78	4.65	1.49	1.61	1.70
2019-04-10	-	-	-	4.63	4.65	4.56	1.40	1.50	1.59
2019-04-11	-	-	-	3.42	3.43	3.39	1.32	1.41	1.49
2019-04-12	-	-	-	4.02	4.03	4.00	1.25	1.32	1.40
2019-04-13	-	-	-	3.42	3.44	3.42	1.18	1.25	1.32
2019-04-14	-	-	-	4.15	4.18	4.17	1.11	1.17	1.24
2019-04-15	-	-	-	4.74	4.78	4.77	1.05	1.11	1.17
2019-04-16	1.49	3.01	6.97	1.25	1.49	1.50	1.00	1.05	1.10
2019-04-17	3.91	6.41	8.09	1.65	1.93	1.92	0.95	0.99	1.04
2019-04-18	5.81	6.06	6.55	3.36	4.09	4.12	0.90	0.93	0.99
2019-04-19	-	-	-	0.94	1.51	3.16	0.85	0.89	0.93
2019-04-20	-	-	-	0.50	0.84	1.60	0.81	0.84	0.89
2019-04-21	-	-	-	0.36	0.60	1.04	0.77	0.80	0.84
2019-04-22	-	-	-	0.29	0.47	0.75	0.74	0.76	0.80
2019-04-23	-	-	-	0.27	0.42	0.63	0.70	0.72	0.76
2019-04-24	-	-	-	0.21	0.32	0.48	0.67	0.69	0.73
2019-04-25	-	-	-	0.19	0.30	0.42	0.64	0.66	0.70
2019-04-26	-	-	-	0.19	0.28	0.39	0.62	0.63	0.67
2019-04-27	-	-	-	0.18	0.26	0.35	0.59	0.61	0.64
2019-04-28	-	-	-	0.18	0.25	0.32	0.57	0.59	0.62
2019-04-29	-	-	-	0.17	0.24	0.30	0.55	0.56	0.60
2019-04-30	-	-	-	0.17	0.24	0.30	0.53	0.54	0.57
2019-05-01	-	-	-	0.18	0.24	0.28	0.52	0.53	0.56
2019-05-02	-	-	-	0.18	0.23	0.28	0.50	0.51	0.54
2019-05-03	-	-	-	0.19	0.24	0.27	0.48	0.49	0.52
2019-05-04	-	-	-	0.19	0.24	0.26	0.47	0.48	0.50

10.3 Annex – Chapter 6

A 6-1 – Simulated biomass changes for cotton maize, and rice

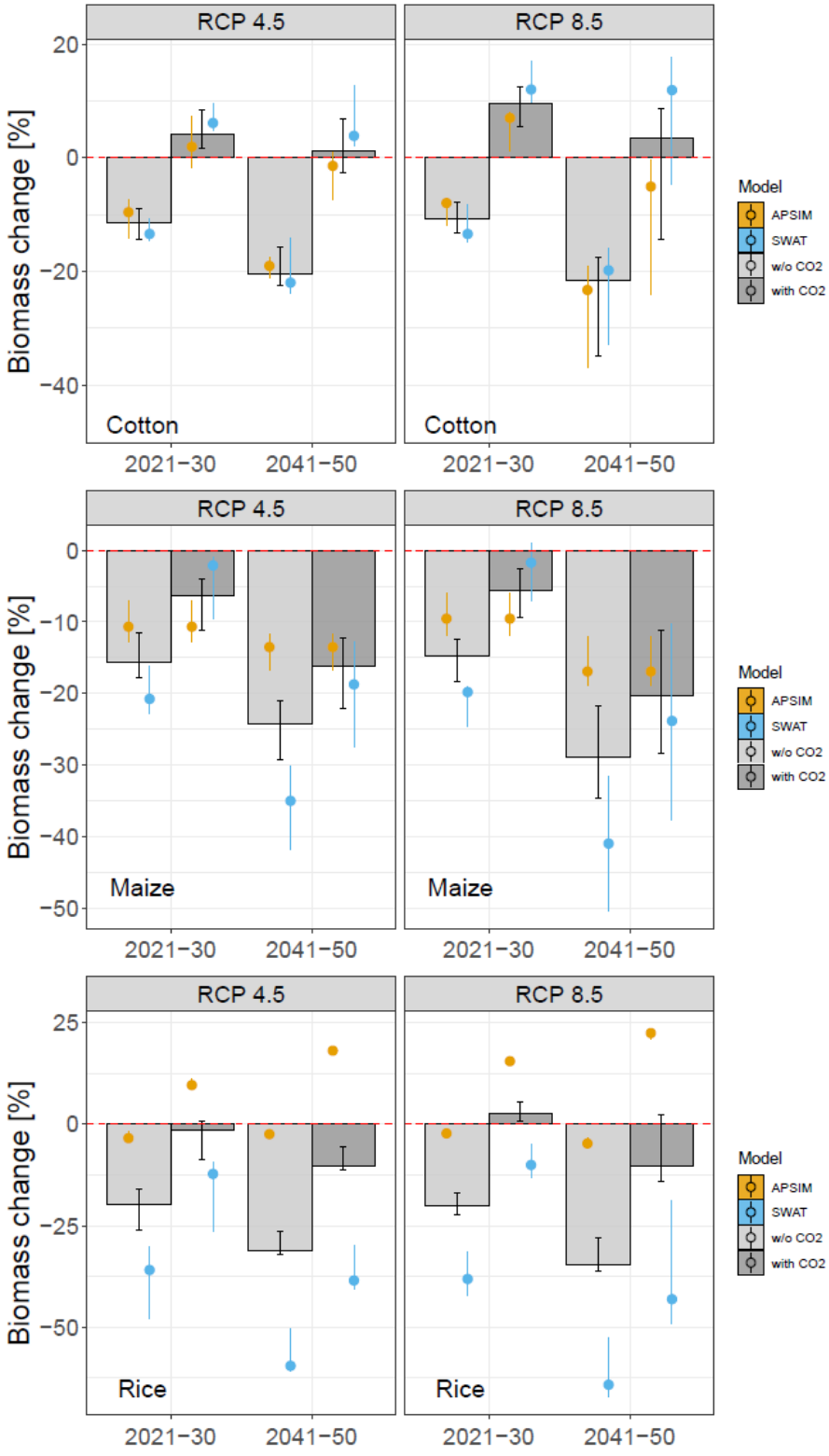

A 6-2 – Simulated changes in irrigation demand, ET, and LAI showing mean changes per model and for ach crop type